Los Alamos National Laboratory is operated by the University of California for the United States Department of Energy under contract W-7405-ENG-36.

Numerical Solutions of the Fokker-Planck Charged Particle Transport Equation

Los Alamos
Los Alamos National Laboratory
Los Alamos, New Mexico 87545

This thesis was accepted by the University of Michigan, Ann Arbor, Michigan, Department of Nuclear Engineering in partial fulfillment of the requirements for the degree of Doctor of Philosophy. It is the independent work of the author and has not been edited by the Technical Information staff.

LA-8985-T
Thesis

UC-32
Issued: September 1981

Numerical Solutions of The Fokker-Planck Charged Particle Transport Equation

Antonio Andrade

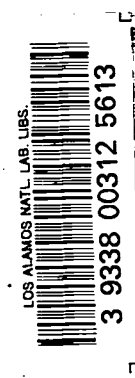

Los Alamos National Laboratory
Los Alamos, New Mexico 87545

TABLE OF CONTENTS

LIST OF FIGURES

Figure

LIST OF APPENDICES

Appendix

NUMERICAL SOLUTIONS OF THE FOKKER-PLANCK CHARGED PARTICLE TRANSPORT EQUATION

by

Antonio Andrade

ABSTRACT

In this work, two numerical methods are developed to solve the Fokker-Planck charged particle transport equation by simple and efficient means, and without approximation to the collision term. The first of these methods demonstrates that the kinetic transport equation can be integrated to yield the time dependent distribution function of test particles $f_a(r,\underline{v},t)$ in a fully implicit manner by a combination of S_n methodology with a matrix factorization technique. It is shown that the full three dimensional velocity space dependence along with the radial configuration space dependence of the distribution function can be obtained as a function of time by this method if all of the phase space variables are treated as discrete. In order to illustrate this technique, the energy deposited by fast ions to geometrically spherical and cylindrical field-free Maxwellian D-T plasmas is calculated. The results are shown to be in good agreement with those previously published.

The second technique that is developed is an implicit Monte Carlo method which is suitable for transport problems in field-free and externally magnetized plasmas. Here the transport of test particles in background Maxwellian plasmas is based on probabilities derivable from the FP equation, such as the expected time for deflection and the expected time of energy exchange. It is shown that this technique is comparable in efficiency to the first method discussed above since large samples of particles are not necessary because self-consistent fields are not calculated. This technique is illustrated by again calculating the energy deposited by fast ions to

a background plasma. The results for problems in the field-free transport case are compared to those obtained by the first method and are found to be in good agreement. Since this is a particle pushing method, the tracks left by the test particles as they transport through the background plasma can be followed in scatter plots. Similarly, the way in which the orbits of test particles deteriorate as they transport in a magnetized plasma can also be followed in time and the energy deposition profiles for each of the background species can be compared to those obtained in the field-free case. It is also shown that a treatment of Coulomb-nuclear scattering, a process which becomes important in the analysis of transport in high temperature plasmas, can be succesfully incorporated within the framework of this implicit Monte Carlo method.

CHAPTER I

INTRODUCTION

In the study of charged particle transport in plasmas, numerical techniques for solving the Fokker-Planck equation have been developed which closely parallel those used in neutron transport. This was a natural step in the development of solution methods in charged particle transport (CPT) in view of the fact that the theory and methods of neutron transport have been well developed[1,2]. Moreover, since much of the pioneering work in CPT was carried out in conjunction with the on-going effort to build controlled fusion devices, the early methodologies developed to solve the transport equation were made more applicable to those machines. In the well known analysis of transport in mirror machines by Killeen, et al[3] for example, the calculations of spatial changes along the magnetic field are based on an assumption that the distribution function of ions remain approximately constant along a guiding center orbit; an assumption which is sufficiently accurate and more appropriate for low density mirror confinement systems.

Other authors have used expansion methods[4,5] or diffusion theory techniques[6] to solve the transport equation. The diffusion techniques require that sequential moments of the transport equation be taken so as to generate a coupled set of equations, and further require that a prescription for closing that set be given. The transport problem is then reduced to the solution of that set.

In other methods[7,8], the differencing and multigrouping techniques of neutronics are directly applied to yield solutions to the CPT equation by standard algorithms. In all of the methods

mentioned above however, the Fokker-Planck collision term is usually approximated in some fashion. The diffusion techniques, for example, usually include only a treatment of collisional slowing down without velocity space dispersion ("straight-line slowing down"). The S_n techniques of Ref. 7 are also applied to a Boltzmann-like equation in which only straight-line slowing down is considered in a deceleration term. As will be shown in this work the exclusion of velocity space dispersion may lead to very inaccurate results.

Recently, some researchers have attempted to solve the Fokker-Planck (FP) equation without recourse to approximations. This was done by either reformulating the FP collision term into a form which matches the structure of a standard neutronics code[9] such that existing computer programs can be used directly for CPT, or by deriving cross sections[10] which siumlate the slowing down of ions to be used in existing neutronics codes. The drawbacks that were found to these approaches were that the large computer codes were cumbersome to modify or as in the case of Ref. 9, the existing code structure forced a semi-implicit differencing of the collision term which subsequently led to long computer runs.

In this work, two numerical methods are developed to solve the Fokker-Planck charged particle transport equation by simple and efficient means, and without approximation to the collision term. The first of these methods demonstrates that the kinetic transport equation can be integrated to yield the time dependent distribution function of test particles $f_a(r,v,t)$ in a fully implicit manner by a combination of S_n methodology with a matrix factorization technique. It is shown that the full three dimensional velocity space dependence along with the radial configuration space dependence of the distribution function can be obtained as a function of time by this method if all of the phase space variables are treated as discrete. In order to illustrate this technique, the energy deposited by fast ions to geometrically spherical and cylindrical field-free Maxwellian D-T plasmas is calculated. The results are shown to be in good agreement with those published in Ref. 9.

The second technique that is developed is an implicit Monte Carlo method which is suitable for transport problems in field-free and externally magnetized plasmas. Here the transport of test particles in background Maxwellian plasmas is based on probabilities derivable from the FP equation, such as the expected time for deflection and the expected time of energy exchange. It is shown that this technique is comparable in efficiency to the first method discussed above since large samples of particles are not necessary because self-consistent fields are not calculated. This technique is illustrated by again calculating the energy deposited by fast ions to a background plasma. The results for problems in the field-free transport case are compared to those obtained by the first method and are found to be in good agreement. Since this is a particle pushing method, the tracks left by the test particles as they transport through the background plasma can be followed in scatter plots. Similarly, the way in which the orbits of test particles deteriorate as they transport in a magnetized plasma can also be followed in time and the energy deposition profiles for each of the background species can be compared to those obtained in the field-free case.

In Chapter II, the form of the transport equation to be solved is developed. It is shown that by some simple tensor analysis, the FP collision term can be written in a divergence form for which the vector components in velocity space contain no third derivatives for all geometries. This makes its form convenient for finite difference analysis of any type since it would otherwise be difficult to numerically compute third derivatives of functions. Chapter III describes the S_n and matrix factorization techniques of the method used to integrate the FP transport equation for the time dependent distribution function and in Chapter IV the Monte Carlo technique for transport problems in field-free and magnetized plasmas is developed in detail. Further, in Chapter IV a means by which large angle (Coulomb-Nuclear) scattering can be treated is demonstrated. All quantities to be used herein will have MKS units while temperatures will be given in keV.

REFERENCES

1. G.I. Bell and S. Glasstone, "Nuclear Reactor Theory", Van Nostrand Reinhold, New York, 1970.

2. J.J. Duderstadt and W.R. Martin, "Transport Theory", John Wiley and Sons, New York, 1979.

3. J. Killeen and K.D. Marx, "Methods of Computational Physics", Vol. 9, Academic Press, New York, 1969.

4. J. Killeen, A.A. Mirin, and M.E. Rensińk, "Methods of Computational Physics", Vol. 16, Academic Press, New York, 1976.

5. P.A. Haldy and J. Ligou, Nucl. Fusion 17(1977), 1225.

6. E.G. Corman, W.E. Loewe, G.E. Cooper and A.M. Winslow, Nucl. Fusion 15(1975), 377.

7. M.J. Antal and C. Lee, J. of Comp. Phys. 20(1976), 298; M.J. Antal and C. Lee, Nucl. Sci. Eng. 64(1977), 379.

8. P.A. Haldy and J. Ligou, Nucl. Sci. Eng. 74(1980), 178.

9. T.A. Mehlhorn and J.J. Duderstadt, J. of Comp. Phys. 38(1980), 86; T.A. Mehlhorn, PhD dissertation (The University of Michigan, 1978).

10. J.E. Morel, personal communication, Sandia Laboratories (1979).

CHAPTER II

THE FOKKER-PLANCK TRANSPORT EQUATION

The kinetic equation which characterizes the transport of charged particles in a plasma as they suffer collisions which result in their deflection by small angles has come to be known as the Fokker-Planck transport equation and is given by

$$\frac{\partial f_a(\underline{r},\underline{v},t)}{\partial t} + \underline{v} \cdot \frac{\partial f_a}{\partial \underline{r}} + \frac{\underline{F}^{ext}}{m_a} \cdot \frac{\partial f_a}{\partial \underline{v}} - \frac{1}{m_a} \frac{\partial \langle \phi \rangle}{\partial \underline{r}} \cdot \frac{\partial f_a}{\partial \underline{v}} = \left(\frac{\partial f_a}{\partial t} \right)_c \qquad (2\text{-}1)$$

where

$$\left(\frac{\partial f_a}{\partial t} \right)_c = -\sum_b \{ \nabla_{\underline{v}} \cdot (f_a \langle \Delta \underline{v} \rangle) - \frac{1}{2} \nabla_{\underline{v}} \nabla_{\underline{v}} : (f_a \langle \Delta \underline{v} \Delta \underline{v} \rangle) \} \qquad (2\text{-}2)$$

is the collision term of the equation. $\langle \phi \rangle$ is the average electrostatic potential at $\underline{r}$ produced by the particles at other positions while $\underline{F}^{ext}$ is the force experienced by the plasma particles at $\underline{r}$ due to externally applied electromagnetic fields. Eq.(1-1), therefore, is an equation for the time evolution of the one particle distribution function of particles of species 'a', as this distribution is affected by internal and external forces and as it is affected by collisions with plasma particles of all species 'b' within a given system, including collisions among its own species 'a'.

Rosenbluth, MacDonald, and Judd[1] first formulated the averages $\langle \Delta \underline{v} \rangle$ and $\langle \Delta \underline{v} \Delta \underline{v} \rangle$ in Eq. (2-2) in terms of the potential-like functions $h_{ab}(\underline{v})$ and $g_{ab}(\underline{v})$ as

$$\langle \Delta \underline{v} \rangle = \Gamma_{ab} \nabla_{\underline{v}} h_{ab}(\underline{v}) \tag{2-3}$$

$$\langle \Delta \underline{v} \Delta \underline{v} \rangle = \Gamma_{ab} \nabla_{\underline{v}} \nabla_{\underline{v}} g_{ab}(\underline{v}) \tag{2-4}$$

where

$$h_{ab}(\underline{v}) = \frac{A_a + A_b}{A_b} Z_b^2 \int d\underline{u}\ f_b(\underline{r},\underline{u},t) |\underline{v}-\underline{u}|^{-1} \tag{2-5}$$

and

$$g_{ab}(\underline{v}) = Z_b^2 \int d\underline{u}\ f_b(\underline{r},\underline{u},t)\ |\underline{v}-\underline{u}| \ . \tag{2-6}$$

Here $\Gamma_{ab} = (Z_a^2 e^4/4\pi m_a^2 \epsilon_o^2) \ln\Lambda$ and $\ln\Lambda = \ln(\lambda_d/b_o)$ where λ_d is the Debye length $[\sum_b n_b Z_b e^2/kT_b \epsilon_o]^{-1/2}$ and b_o is the impact parameter for scattering at 90^o which is equal to $Z_a Z_b e^2/4\pi\epsilon_o \mu_{ab} V^2$. Defining the integrals in Eqs. (2-5) and (2-6) as

$$L_b(\underline{v}) = \int d\underline{u}\ f_b(\underline{r},\underline{u},t)\ |\underline{v}-\underline{u}|^{-1} \tag{2-7}$$

$$K_b(\underline{b}) = \int d\underline{u}\ f_b(\underline{r},\underline{u},t)\ |\underline{v}-\underline{u}| \tag{2-8}$$

the potential-like relationship between Eqs. (2-5) and (2-6) is easily shown with

$$\nabla^2_{\underline{v}} K_b(v) = 2L_b(v) \tag{2-9}$$

and

$$\nabla^2_{\underline{v}} L_b(\underline{v}) = -4\pi f_b(\underline{r},\underline{v},t) \ . \tag{2-10}$$

In this work, the effects of internal forces on the evolution of f_a will not be considered so that $<\phi>$ in Eq. (2-1) can effectively be set equal to zero.

A Formulation of the Collision Term in Terms of the Riemann-Christoffel Tensor

In Ref. 1, it is shown that the collision term can be written in covarient form by first noting that $\Gamma_{ab}^{-1}<\Delta\underline{v}>$ and $\Gamma_{ab}^{-1}<\Delta\underline{v}\,\Delta\underline{v}>$ transform like a contravarient vector and tensor respectively. The subsequent tensor extension of Eq. (2-2) is then given as

$$\frac{\partial f_a}{\partial t}\Big)_c = -\sum_b \Gamma_{ab}\left\{(f_a T_{ab}^{\mu})_{,\mu} - \frac{1}{2}(f_a S_{ab}^{\mu\nu})_{,\mu\nu}\right\} \tag{2-11}$$

where

$$T_{ab}^{\mu} = a^{\mu\nu} h_{ab,\nu} \tag{2-12}$$

and

$$S_{ab}^{\mu\nu} = a^{\mu\omega} a^{\nu\tau} g_{ab,\omega\tau} \tag{2-13}$$

and where the relationships between $K_b(\underline{v})$ and $L_b(\underline{v})$, i.e. Eqs. (2-9) and (2-10) are now given as

$$a^{\alpha\beta}K_{b,\alpha\beta} = 2L_b \tag{2-14}$$

$$a^{\alpha\beta}L_{b,\alpha\beta} = -4\pi f_b \ . \tag{2-15}$$

Here the subscripts ,i indicate covarient differentiation with respect to the i^{th} component while the superscripts indicate either a particular vector component or a tensor element. $a^{\mu\nu}$ is the inverse of the metric tensor $a_{\mu\nu}$ which defines the space of interest.

For finite difference numerical analysis, it is naturally more convenient to use a divergence form for the collision term such as

$$\frac{\partial f_a}{\partial t}\Big)_c = -J^i_{,i}. \tag{2-16}$$

From Eq. (2-11), it can be seen that the components J^i are given by

$$J^i = \sum_b \Gamma_{ab}\left\{f_a T^i_{ab} - \frac{1}{2}(f_a S^{ji}_{ab})_{,j}\right\} \ . \tag{2-17}$$

Eq. (2-16) will be called the Landau-Fokker-Planck collision term since Landau[2] first formulated a kinetic equation for small angle Coulomb scattering in this divergence form.

The analytic evaluation of the components J^i for simple velocity space geometries is straightforward but the second term of Eq. (2-17) gives rise to terms which contain third derivatives of the function $K_b(\underline{v})$, which are difficult to approximate numerically. It is easy to show that for say, a spherical velocity space in which the background distribution functions are either fully isotropic or only azimuthally symmetric, these third derivatives can be eliminated from the components J^i by making use of the relations given in Eqs. (2-14) and (2-15).

In the course of this work it was found that the third derivatives could be eliminated in any geometry and for distributions in a general state, by tensorially reformulating the collision term as follows.

Using Eqs. (2-5),(2-6),(2-12), and (2-13) and by using the definitions of the functions $K_b(\underline{v})$ and $L_b(\underline{v})$ given in Eqs. (2-7) and (2-8), Eq. (2-17) can be written in the form

$$J^i = \sum_b \Gamma_{ab} Z_b^2 \left\{ \frac{A_a + A_b}{A_b} f_a a^{i\alpha} L_{b,\alpha} - \frac{1}{2} (f_a a^{i\alpha} a^{j\beta} K_{b,\alpha\beta})_{,j} \right\} \qquad (2\text{-}18)$$

or since the covarient derivatives of the inverse metric tensors are equal to zero, it can further be simplified to

$$J^i = \sum \Gamma_{ab} Z_b^2 \left\{ \frac{A_a + A_b}{A_b} f_a a^{i\alpha} L_{b,\alpha} - \frac{1}{2} a^{i\alpha} a^{j\beta} (f_a K_{b,\alpha\beta})_{,j} \right\} . \qquad (2\text{-}19)$$

The second term of Eq. (2-19) can be expanded as

$$(f_a K_{b,\alpha\beta})_{,j} = f_{a,j} K_{b,\beta\alpha} + f_a K_{b,\beta\alpha j} \qquad (2\text{-}20)$$

since $K_b(\underline{v})$ is a scaler invariant. The Riemann-Christoffel tensor $R^{\gamma}_{.\beta\alpha j}$ is defined as[3]

$$R^{\gamma}_{.\beta\alpha j} K_{b,\gamma} = K_{b,\beta\alpha j} - K_{b,\beta j\alpha} \qquad (2\text{-}21)$$

and is a tensor of rank 4 which does not depend on the choice of the vector $K_{b,\gamma}$. It can be computed as

$$R^{\gamma}_{.\beta\alpha j} = \partial_{\alpha}\{\gamma,\beta j\} - \partial_{j}\{\gamma,\beta\alpha\}$$

$$+ \{\gamma,js\}\{s,\beta j\} - \{\gamma,\alpha s\}\{s,\beta\alpha\} \qquad (2\text{-}22)$$

where the symbols { } are the Christoffel symbols of the second kind. With this definition Eq. (2-20) can be replaced as

$$(f_a K_{b,\alpha\beta})_{,j} = f_{a,j} K_{b,\beta\alpha} + f_a[K_{b,\beta j\alpha} + R^{\gamma}_{.\beta\alpha j} K_{b,\gamma}] \qquad (2\text{-}23)$$

and Eq. (2-19) can then be rewritten as

$$J^i = \sum_b \Gamma_{ab} Z_b^2 \{\frac{A_a + A_b}{A_b} f_a a^{i\alpha} L_{b,\alpha} - \frac{1}{2} a^{i\alpha} a^{j\beta}[f_{a,j} K_{b,\beta\alpha}$$

$$+ f_a K_{b,\beta j\alpha} + f_a R^{\gamma}_{.\beta\alpha j} K_{b,\gamma}]\} . \qquad (2\text{-}24)$$

Consider the second term of Eq. (2-24) which will be called term II. Using $(f_a K_{b,\beta j})_{,\alpha} = f_{a,\alpha} K_{b,\beta j} + f_a K_{b,\beta j\alpha}$, term II becomes

$$II = \frac{1}{2}[a^{i\alpha} a^{j\beta} f_{a,j} K_{b,\beta\alpha} + a^{i\alpha} a^{j\beta} (f_a K_{b,\beta j})_{,\alpha}$$

$$- a^{i\alpha} a^{j\beta} f_{a,\alpha} K_{b,\beta j} + a^{i\alpha} a^{j\beta} f_a R^{\gamma}_{.\beta\alpha j} K_{b,\gamma}] . \qquad (2\text{-}25)$$

By changing the dummy indices in the second term of Eq. (2-25) and then using the Poisson-like relation given in Eq. (2-14), II becomes

$$II = \frac{1}{2}[a^{i\alpha}a^{j\beta}f_{a,j}K_{b,\beta\alpha} + 2a^{ij}f_aL_{b,j} + a^{ij}a^{\alpha\beta}K_{b,\alpha\beta}f_{a,j} -$$

$$a^{i\alpha}a^{j\beta}f_{a,\alpha}K_{b,\beta j} + a^{i\alpha}a^{j\beta}f_aR^{\gamma}_{.\beta\alpha j}K_{b,\gamma}] \quad . \qquad (2\text{-}26)$$

By changing dummy indices again, it is seen that the third and fourth terms will cancel and that two $L_{b,\alpha}$ terms will also cancel when Eq. (2-26) is substituted back into Eq. (2-24) so that the collision term will now take the form $\left(\frac{\partial f_a}{\partial t}\right)_c = -J^i_{;i}$ as before but with

$$J^i = \sum_b \Gamma_{ab}Z_b^2\{\frac{A_a}{A_b}f_aa^{i\alpha}L_{b,\alpha} -$$

$$\frac{1}{2}a^{i\alpha}a^{j\beta}[f_{a,j}K_{b,\beta\alpha} + f_aR^{\gamma}_{.\beta\alpha j}K_{b,\gamma}]\} \quad . \qquad (2\text{-}27)$$

It is to be noted that Eq. (2-27) will involve only the second derivatives of the function $K^b(\underline{v})$ making it satisfactory for numerical analysis in any geometry, and that it also simplifies the analytic evaluation of the components J^i.

In the chapter to follow, a spherical velocity space is chosen for the example problems which demonstrate the numerical methods developed there. This choice is made because of the convenience of determining whether a plasma is Maxwellized in terms of only one variable, the magnitude of the velocity $|\underline{v}|$. In Appendix A, the components J^i are evaluated analytically for a spherical velocity space by using Eq. (2-27).

A Scaling of the Fokker-Planck Equation

It is often convenient in numerical work to scale the variables of interest in order to avoid using large numbers. In a laser fusion pellet plasma, for example, it is not uncommon to encounter particle densities on the order of $10^{28}/m^3$. Although many different scaling systems can be applied to the Fokker-Planck equation, here it is chosen to scale densities, velocities, and time as

$$\tilde{n} = \frac{n}{N_o} \qquad \tilde{v} = \frac{v}{C_o} \qquad \tilde{t} = \frac{t}{\tau_o} \tag{2-28}$$

where N_o and τ_o are chosen to suit the problem at hand and where C_o is defined to be $(2kT_o/m_o)^{1/2}$. k is Boltzmann's constant, T_o is a standard kinetic temperature and m_o is the mass corresponding to 1 AMU. With these scalings the scaled distribution function is related to the unscaled distribution by

$$\tilde{f} = fC_o^3/n_o \ . \tag{2-29}$$

By further defining the scaled length as $\tilde{r} = r/C_o\tau_o$ and the scaled acceleration by $\tilde{a} = a\tau_o/C_o$ and then substituting the relations of Eq. (2-28) into Eq. (2-1), it is found that the Fokker-Planck transport equation retains its original form if the traditional Γ_{ab} is replaced by $\Gamma_{ab}N_o\tau_o/C_o^3$. The final working form of the Fokker-Planck equation is then given by

$$\frac{\partial f_a(\underline{r},\underline{v},t)}{\partial t} + \underline{v}\cdot\frac{\partial f_a}{\partial \underline{r}} + \underline{a}^{ext}\cdot\frac{\partial f_a}{\partial \underline{v}} = -\nabla_{\underline{v}}\cdot\underline{J} \tag{2-30}$$

where

$$J^i = \sum_b \Gamma_{ab} \frac{N_o \tau_o Z_b^2}{C_o^3} \left\{ \frac{A_a}{A_b} f_a a^{i\alpha} L_{b,\alpha} \right.$$

$$\left. - \frac{1}{2} a^{i\alpha} a^{j\beta} \left[f_{a,j} K_{b,\beta\alpha} + f_a R^{\gamma}_{.\beta\alpha j} K_{b,\gamma} \right] \right\} \qquad (2\text{-}31)$$

and where the barred scaling notation has now been dropped since it is understood that this is a scaled equation.

REFERENCES

1. M.N. Rosenbluth, W.M. MacDonald, and D.L. Judd, Phys. Rev. 107 (1957),1.

2. L. Landau, Phys. Z. Sowjet. 10(1936),154.

3. B. Spain, "Tensor Calculus", Interscience, New York, 1960.

CHAPTER III

CHARGED PARTICLE TRANSPORT IN A FIELD-FREE PLASMA: AN INTEGRATION OF THE FOKKER-PLANCK TRANSPORT EQUATION

Solution For A Spherical Plasma

A symmetric, field-free, spherical plasma configuration is a particularly simple system in which new techniques for solving the transport equation can be tested. Since results of benchmark calculations in this type of system exist in abundance[1], comparisons can easily be made.

To this end, consider the time evolution of a distribution $f_a(r,v,\mu,t)$ of test particles in a fully symmetric state in a spherical configuration space and in a spherical velocity space in which the distribution function will only be constrained to be azimuthally symmetric. In Appendices A and B the charged particle transport equation, Eq. (2-30), is developed for these geometries as

$$\frac{\partial f_a(r,v,\mu,t)}{\partial t} + \frac{v\mu}{r^2}\frac{\partial}{\partial r}(r^2 f_a) + \frac{v}{r}\frac{\partial}{\partial \mu}[(1-\mu^2)f_a] = \frac{\partial f_a}{\partial t}\Big)_c \qquad (3\text{-}1)$$

where

$$\frac{\partial f_a}{\partial t}\Big)_c = -\{\frac{1}{v^2}\frac{\partial}{\partial v}v^2 J^v + \frac{\partial}{\partial \mu}J^\mu\} \qquad (3\text{-}2)$$

and

$$J^v = \sum_b \Gamma_{ab} \frac{N_o \tau_o Z_b^2}{C_o^3} \left\{ \frac{A_a}{A_b} f_a \frac{\partial L_b}{\partial v} - \frac{1}{2} \left[\frac{\partial f_a}{\partial v} \frac{\partial^2 K_b}{\partial v^2} \right] \right\} \tag{3-3}$$

$$J^\mu = \sum_b \frac{N_o \tau_o Z_b^2}{C_o^3} \left\{ -\frac{(1-\mu^2)}{2v^2} \left[\frac{1}{v} \frac{\partial f_a}{\partial \mu} \frac{\partial K_b}{\partial v} \right] \right\} . \tag{3-4}$$

Here the functions K_b and L_b of the background distributions f_b will remain isotropic for all time and the sums over the species 'b' will not include the species 'a' so that the treatment of Eq. (3-1) will become fully linear. The background Maxwellian distribution functions in scaled variables have the form

$$f_b(u) = \frac{n_b}{\pi^{3/2} v_{ob}^3} \exp(-u^2/v_{ob}^2) \tag{3-5}$$

where $v_{ob} = (T_b/A_b)^{1/2}$.

With the definitions of K_b and L_b given by Eqs. (2-7) and (2-8), the derivatives in J^v and J^μ can be computed as

$$\frac{\partial L_b}{\partial v} = -\frac{4\pi}{v^2} \int_0^v u^2 f_b(u) du \tag{3-6}$$

$$\frac{\partial K_b}{\partial v} = 4\pi \int_0^v \left(u^2 - \frac{u^4}{3v^2} \right) f_b(u) du + 4\pi \int_v^\infty \frac{2uv}{3} f_b(u) du \tag{3-7}$$

$$\frac{\partial^2 K_b}{\partial v^2} = 4\pi\int_0^v \frac{2u^4}{3v^3} f_b(u)du + 4\pi\int_v^\infty \frac{2}{3} u f_b(u)du \ . \qquad (3\text{-}8)$$

Defining the standard integrals in Eqs. (3-6)-(3-8) as

$$H_{b1}(v) = \int_v^\infty u f_b du \qquad (3\text{-}9)$$

$$H_{b2}(v) = \int_0^v u^2 f_b du \qquad (3\text{-}10)$$

$$H_{b3}(v) = \int_0^v u^4 f_b du \ , \qquad (3\text{-}11)$$

it is seen that the Landau-Fokker-Planck components can then be rewritten as

$$J^v = -4\pi\sum_b \Gamma_{ab} \frac{N_o \tau_o Z_b^2}{C_o^3} \left\{ \frac{A_a}{A_b} f_a \frac{H_{b2}(v)}{v^2} \right.$$

$$\left. + \frac{1}{3}\frac{\partial f_a}{\partial v}\left(\frac{H_{b3}(v)}{v^3} + H_{b1}(v) \right) \right\} \qquad (3\text{-}12)$$

and

$$J^\mu = -4\pi\sum_b \Gamma_{ab} \frac{N_o \tau_o Z_b^2}{C_o^3} \left\{ \frac{(1-\mu^2)}{2v^3}\frac{\partial f_a}{\partial \mu} \times \right.$$

$$\left. \left(H_{b2}(v) - \frac{H_{b3}(v)}{3v^2} + \frac{2v}{3} H_{b1}(v) \right) \right\} \ . \qquad (3\text{-}13)$$

Since the background distributions are Maxwellian, the integrals H_{b1}, H_{b2}, and H_{b3} are easily evaluated as

$$H_{b1}(v) = \frac{n_b}{2\pi^{3/2}v_{ob}}\exp(-v^2/v_{ob}^2) \tag{3-14}$$

$$H_{b2}(v) = \frac{n_b}{\pi^{3/2}}\left[\frac{\pi^{1/2}}{4}\mathrm{erf}(v/v_{ob}) - \frac{v}{2v_{ob}}\exp(-v^2/v_{ob}^2)\right. \tag{3-15}$$

$$H_{b3}(v) = \frac{n_b v_{ob}^2}{2\pi^{3/2}}\left[\frac{3\pi^{1/2}}{4}\mathrm{erf}(v/v_{ob}) - \frac{v}{v_{ob}}\left(\frac{3}{2} + \frac{v^2}{v_{ob}^2}\right)\exp(-v^2/v_{ob}^2)\right]. \tag{3-16}$$

The Difference Approximation

Equation (3-1) can be solved by a direct finite difference method which is similar in many repects to the S_n technique used in neutron transport. In this method the angular dependence of the distribution function is not expanded via a complete set of functions but rather is treated as discrete. The way in which the methodology presented in this chapter varies from the standard S_n method is in the treatment of the collision physics. Here the collision effects will be solved for separate from the streaming effects.

An operator κ which will discretize all of the arguments of $f_a(r,v,\mu,t)$ through the transport equation is

$$\kappa = \frac{1}{\beta}\int_{t_s}^{t_{s+1}} dt \int_{r_{i-1/2}}^{r_{i+1/2}} r^2 dr \int_{v_{g-1/2}}^{v_{g+1/2}} v^2 dv \int_{\mu_{n-1/2}}^{\mu_{n+1/2}} d\mu \tag{3-17}$$

where $\beta = \Delta t_s(\Delta r_i^3/3)(\Delta v_g^3/3)\Delta\mu_n$ and $\Delta t_s = t_{s+1} - t_s$, $\Delta r_i^3/3 = (r_{i+1/2}^3 - r_{i-1/2}^3)/3$, $\Delta v_g^3/3 = (v_{g+1/2}^3 - v_{g-1/2}^3)/3$, $\Delta\mu_n = \mu_{n+1/2} - \mu_{n-1/2}$. In this analysis the intervals on a mesh will be centered at integer values of the indices s,i,g and n and the distribution function f_a will always be defined at $t = t_{s+1}$ i.e., implicitly, unless specified by a subscript to be otherwise.

Applying the operator κ to Eq. (3-1) yields the difference approximation

$$\frac{f(r_i,v_g,\mu_n,t_{s+1}) - f_s}{\Delta t_s} + \frac{\mu_n \Delta v_g^4/4}{V_i \Delta v_g^3/3}\left[A_{i+1/2}f_{i+1/2} - A_{i-1/2}f_{i-1/2}\right]$$

$$+ \frac{\Delta v_g^4/4}{V_i \Delta\mu_n \Delta v_g^3/3}\left[\alpha_{n+1/2}f_{n+1/2} - \alpha_{n-1/2}f_{n-1/2}\right]$$

$$= -\left\{\frac{1}{\Delta v_g^3/3}\left[v_{g+1/2}^2 J_{g+1/2}^v - v_{g-1/2}^2 J_{g-1/2}^v\right]\right.$$

$$\left. + \frac{1}{\Delta\mu_n}\left[J_{n+1/2}^\mu - J_{n-1/2}^\mu\right]\right\} \qquad (3\text{-}18)$$

where $V_i = \Delta r_i^3/3$, $A_{i+1/2} = r_{i+1/2}^2$, and where the angular streaming term has been differenced as in the S_n methodology of neutronics[2] in order to preserve conservation of particles for finite sized intervals $\Delta\mu_n$. The subscript 'a' of the test distribution has been dropped since it is understood that this is an equation for f_a.

By using the definitions

$$B_g = A_a \sum_b \Gamma_{ab} \frac{N_o \tau_o Z_b^2}{C_o^3 A_b} H_{b2}(v_g) \tag{3-19}$$

$$C_g = \frac{1}{3} \sum_b \Gamma_{ab} \frac{N_o \tau_o}{C_o^3} Z_b^2 \left(\frac{H_{b3}(v_g)}{v_g} + v_g^2 H_{b1}(v_g) \right) \tag{3-20}$$

$$D_g = \sum_b \Gamma_{ab} \frac{N_o \tau_o Z_b^2}{C_o^3 v_g^3} \left(H_{b2}(v_g) - \frac{1}{3v_g^2} H_{b3}(v_g) + \frac{2}{3} v_g H_{b1}(v_g) \right) \tag{3-21}$$

in Eqs. (3-12) and (3-13), the components of $\underline{J}$ in the collision term of the difference approximation become

$$J^v_{g+1/2} = -\frac{4\pi}{v^2_{g+1/2}} \left\{ B_{g+1/2} f_{g+1/2} + C_{g+1/2} \left(\frac{f_{g+1} - f_g}{\Delta v_{g+1/2}} \right) \right\} \tag{3-22}$$

$$J^v_{g-1/2} = -\frac{4\pi}{v^2_{g-1/2}} \left\{ B_{g-1/2} f_{g-1/2} + C_{g-1/2} \left(\frac{f_g - f_{g-1}}{\Delta v_{g-1/2}} \right) \right\} \tag{3-23}$$

$$J^\mu_{n+1/2} = -2\pi D_g \left\{ (1-\mu^2_{n+1/2}) \frac{f_{n+1} - f_n}{\Delta \mu_{n+1/2}} \right\} \tag{3-24}$$

$$J^\mu_{n-1/2} = -2\pi D_g \left\{ (1-\mu^2_{n-1/2}) \frac{f_n - f_{n-1}}{\Delta \mu_{n-1/2}} \right\} . \tag{3-25}$$

The velocity grid interval edge values $f_{g\pm1/2}$ in the $J^v_{g\pm1/2}$

components can be related to the centered values f_g by the interpolating relations of Chang and Cooper[3] as

$$f_{g+1/2} = (1 - \delta_{g+1/2})f_{g+1} + \delta_{g+1/2}f_g \tag{3-26}$$

$$f_{g-1/2} = (1 - \delta_{g-1/2})f_g + \delta_{g-1/2}f_{g-1} \tag{3-27}$$

where

$$\delta_{g\pm1/2} = \frac{1}{\omega_{g\pm1/2}} - \frac{1}{[\exp(\omega_{g\pm1/2}) - 1]} \tag{3-28}$$

and

$$\omega_{g\pm1/2} = \frac{\Delta v_g B_{g\pm1/2}}{C_{g\pm1/2}} \quad . \tag{3-29}$$

By using these relations in Eqs. (3-22) and (3-23), the collision term of Eq. (3-18) can be rewritten as the sum of two terms as

$$\tilde{q} = \tilde{q}^v + \tilde{q}^\mu \tag{3-30}$$

where

$$\begin{aligned}\tilde{q}^v = \frac{4\pi}{\Delta_g^3/3}\{ & f_{g-1}\left[\frac{C_{g-1/2}}{\Delta v_{g-1/2}} - B_{g-1/2}\delta_{g-1/2}\right] \\ & + f_g\left[B_{g+1/2}\delta_{g+1/2} - B_{g-1/2}(1 - \delta_{g-1/2}) - \frac{C_{g-1/2}}{\Delta v_{g-1/2}} - \frac{C_{g+1/2}}{\Delta v_{g+1/2}}\right] \\ & + f_{g+1}\left[B_{g+1/2}(1 - \delta_{g+1/2}) + \frac{C_{g+1/2}}{\Delta v_{g+1/2}}\right]\}\end{aligned} \tag{3-31}$$

and

$$\tilde{q}^{\mu} = \frac{2\pi}{\Delta\mu_n} D_g \left\{ f_{n-1} \frac{(1 - \mu_{n-1/2}^2)}{\Delta\mu_{n-1/2}} \right.$$

$$- f_n \left[\frac{(1 - \mu_{n+1/2}^2)}{\Delta\mu_{n+1/2}} + \frac{(1 - \mu_{n-1/2}^2)}{\Delta\mu_{n-1/2}} \right]$$

$$\left. + f_{n+1} \frac{(1 - \mu_{n+1/2}^2)}{\Delta\mu_{n+1/2}} \right\} . \qquad (3\text{-}32)$$

Note that $\tilde{q}$ is a sum of two 3-point difference terms.

By further defining the quantities

$$\xi = \frac{\Delta v_g^4/4}{V_i \Delta v_g^3/3} \qquad (3\text{-}33)$$

$$\Lambda = \mu_n \Delta\mu_n \left[A_{i+1/2} f_{i+1/2} - A_{i-1/2} f_{i-1/2} \right]$$

$$+ \left[\alpha_{n+1/2} f_{n+1/2} - \alpha_{n-1/2} f_{n-1/2} \right] \qquad (3\text{-}34)$$

and the combining Eqs. (3-30) and (3-18), it is seen that the transport equation can be written in the simple form

$$f - \tilde{q}\Delta t_s = f_s - \frac{\xi\Lambda\Delta t_s}{\Delta\mu_n} . \qquad (3\text{-}35)$$

In this equation , it is seen that the collision terms are now on the

L.H.S. while the streaming terms have been separated off into the R.H.S. This formulation suggests that a splitting procedure may be used to solve for the effects of collisions and streaming on the distribution separately and then combined in some self-consistent fashion to yield an updated distribution.

Solution of the Difference Approximation by Consistent Splitting with Matrix Factorization

Eq. (3-35) can be split into two, separate fully implicit equations of the form

$$\left[f - \tilde{q}\Delta t\right]^* = \left[f_s - \frac{\xi\Lambda\Delta t_s}{\Delta\mu_n}\right]_{t=t_s} \tag{3-36}$$

and

$$f + \frac{\xi\Lambda\Delta t_s}{\Delta\mu_n} = \tilde{q}^*\Delta t_s + f_s \ . \tag{3-37}$$

Here Eq. (3-36) is seen to be an equation which modifies the distribution function f for collision effects while using the streaming terms as a constant known source term evaluated with quantities defined at the previous time step while Eq. (3-37) is an equation which corrects f for streaming and uses the result f^* of Eq. (3-36) as $\tilde{q}^* = \tilde{q}(f^*)$ as a constant. When Eqs. (3-36) and (3-37) are solved together within a given time step, the distribution function $f(r_i, v_g, \mu_n, t_{s+1})$ is then determined for all i,g, and n.

Consider first Eq. (3-36) and recall that $\tilde{q}$ was defined as the sum of two 3-point terms in Eqs. (3-30)-(3-32). As such, Eq. (3-36) resembles the differenced 2-dimensional Poisson equation which has the form

$$E^{lk}_{ng}\psi_{lk} + G^{lk}_{ng}\psi_{lk} = S_{ng} \tag{3-38}$$

$$l = n-1,n,n+1$$

$$k = g-1,g,g+1$$

where the matrices $\underline{\underline{E}}$ and $\underline{\underline{G}}$ contain the coefficients of the two 3-point terms $\tilde{q}^{\nu}$ and $\tilde{q}^{\mu}$ respectively and where S_{ng} corresponds to the source term on the R.H.S. of Eq. (3-36). E^{lk}_{ng} and G^{lk}_{ng} are actually supermatrices with the properties

$$E^{lk}_{ng} \rightarrow \delta^{l}_{n}E^{lk}_{ng} \tag{3-39}$$

$$G^{lk}_{ng} \rightarrow \delta^{k}_{g}G^{lk}_{ng} \tag{3-40}$$

where the first pair of upper and lower indeces indicate the position of an elemental matrix in the supermatrix and where the second pair indicate an element in the elemental matrices. Hence $\underline{\underline{E}}$ and $\underline{\underline{G}}$ have the forms

$$E^{lk}_{ng} = \begin{pmatrix} \begin{pmatrix} x & x & \\ x & x & x \\ & x & x \end{pmatrix}_{NGxNG} & & \\ & \begin{pmatrix} x & x & \\ x & x & x \\ & x & x \end{pmatrix} & \\ & & \begin{pmatrix} x & x & \\ x & x & x \\ & x & x \end{pmatrix}_{NNxNN} \end{pmatrix} \tag{3-41}$$

$$G_{ng}^{lk} = \begin{pmatrix} \begin{pmatrix} x & & \\ & x & \\ & & x \end{pmatrix}\begin{pmatrix} x & & \\ & x & \\ & & x \end{pmatrix} & & \\ & \ddots & \\ & & \begin{pmatrix} x & & \\ & x & \\ & & x \end{pmatrix}\begin{pmatrix} x & & \\ & x & \\ & & x \end{pmatrix} \end{pmatrix}_{NGxNG} \qquad (3\text{-}42)$$

$$\begin{pmatrix} \begin{pmatrix} x & & \\ & x & \\ & & x \end{pmatrix}\begin{pmatrix} x & & \\ & x & \\ & & x \end{pmatrix}\begin{pmatrix} x & & \\ & x & \\ & & x \end{pmatrix} & & \\ & \ddots & \\ & & \begin{pmatrix} x & & \\ & x & \\ & & x \end{pmatrix}\begin{pmatrix} x & & \\ & x & \\ & & x \end{pmatrix}\begin{pmatrix} x & & \\ & x & \\ & & x \end{pmatrix} \end{pmatrix}_{NNxNN}$$

where NG is the number of intervals on the g grid and NN is the number of intervals on the n grid. The supervectors ψ_{lk} and S_{ng} have the forms

$$\psi_{lk} = \begin{pmatrix} \begin{pmatrix} x \\ x \\ x \end{pmatrix}_{NG} \\ \begin{pmatrix} x \\ x \\ x \end{pmatrix} \\ \begin{pmatrix} x \\ x \\ x \end{pmatrix} \end{pmatrix}_{NN} \qquad S_{ng} = \begin{pmatrix} \begin{pmatrix} x \\ x \\ x \end{pmatrix}_{NG} \\ \begin{pmatrix} x \\ x \\ x \end{pmatrix} \\ \begin{pmatrix} x \\ x \\ x \end{pmatrix} \end{pmatrix}_{NN} \qquad (3\text{-}43)$$

The notation of Eq. (3-38) can be simplified somewhat if the index g is taken to be vector index so that it can be rewritten as

$$E\vec{\psi}_n + G_n^l\vec{\psi}_l = \vec{S}_n \qquad (3\text{-}44)$$

This equation merely indicates that each multiplication of a superrow of Eqs. (3-41) and (3-42), by a supercolumn of $\vec{\psi}$, will be treated separately. The following treatment of Eq. (3-44) is based upon a method given by Buzbee, et. al.[4].

In general the matrix E will not be symmetric tridiagonal but a matrix D can be found that will symmetrize E through a similarity transformation $\tilde{E} = DED^{-1}$. If D is allowed to operate on Eq. (3-44) from the left, it then takes the form

$$\tilde{E}D\vec{\psi}_n + G_n^1 D\vec{\psi}_1 = D\vec{S}_n . \tag{3-45}$$

It is easily shown that D has a diagonal form such that it commutes with G_n^1 as indicated.

The symmetric matrix $\tilde{E}$ has a complete set of eigenvectors given by $\tilde{E}\vec{\xi}_\alpha = \lambda_\alpha \vec{\xi}_\alpha$ so that the vectors $D\vec{\psi}$ and $D\vec{S}$ can be expanded as

$$D\vec{\psi}_1 = \sum_\alpha a_{1\alpha}\vec{\psi}_\alpha \tag{3-46}$$

$$D\vec{S}_n = \sum_\alpha b_{n\alpha}\vec{\psi}_\alpha . \tag{3-47}$$

Using these expansions in Eq. (3-45), it is found that it can be rewritten as

$$[G_n^1 + \delta_n^1 \lambda_\alpha]a_{1\alpha} = b_{n\alpha} . \tag{3-48}$$

Eq. (3-48) is recognized to be a tridiagonal system in the coefficients $a_{1\alpha}$ for each index α. This equation can be solved readily by a factorization of the tridiagonal system into upper and lower off-diagonal matrices. This is a standard technique in matrix analysis, the details of which will not be given here. For an excellent presentation of this technique, the reader is refered to Ref. 5.

Once the coefficients $a_{1\alpha}$ are determined, the solution of Eq. (3-45) can be constructed using Eq. (3-46) as

$$\psi_{lg} = \sum_{\alpha} a_{l\alpha} D_g^{-1} \xi_{\alpha g} \quad . \tag{3-49}$$

This is the 'intermediate' distribution function f^* which has been modified for collision effects. It is noted that for the case in which the background plasma remains Maxwellian, the coefficients in Eq. (3-45) remain unchanged such that the eigenvalues and corresponding eigenvectors need be computed only once. But the construction indicated in Eq. (3-49) must be performed at every time step since the $a_{l\alpha}$ will differ as the source term (and therefore the $b_{n\alpha}$) of Eq. (3-45) changes in time. This procedure is carried out for every zone r_i in a given time step.

Eq. (3-37) remains to be solved. This equation is actually equivalent to Eq. (3-18) i.e., the difference approximation except that the collision terms on the R.H.S. are now known as $\tilde{q}^*$ such that

$$\frac{f(r_i, v_g, \mu_n, t_{s+1}) - f_s}{\Delta t_s} + \frac{\mu_n \Delta v_g^4/4}{V_i \Delta v_g^3/3}\left[A_{i+1/2} f_{i+1/2} - A_{i-1/2} f_{i-1/2}\right]$$

$$+ \frac{\Delta v_g^4/4}{V_i \Delta \mu_n \Delta v_g^3/3}\left[\alpha_{n+1/2} f_{n+1/2} - \alpha_{n-1/2} f_{n-1/2}\right] = \tilde{q}^* \quad . \tag{3-50}$$

Eq.(3-50) has the form of the neutron transport equation which has been differenced for S_n treatment and as such, it can be solved as in neutronics. To outline this method, note that Eq. (3-50) is an equation in five unknowns f, $f_{i\pm1/2}$, and $f_{n\pm1/2}$. In general two of these, say $f_{i+1/2}$ and $f_{n-1/2}$, can be determined from boundary conditions or from a previous time step. The other three quantities can be related by some scheme so that a system of three equations in three unknowns can be formed.

The diamond difference relations

$$2f \simeq f_{n+1/2} + f_{n-1/2} \tag{3-51}$$

$$2f \simeq f_{i+1/2} + f_{i-1/2} \tag{3-52}$$

are chosen for this purpose. It is seen in Fig. 1 that these relations linearly interpolate between quantities defined on a topologically rectangular mesh. Using these relations in Eq. (3-50) and solving for f in terms of the known quantities $f_{n-1/2}$ and $f_{i+1/2}$ yields

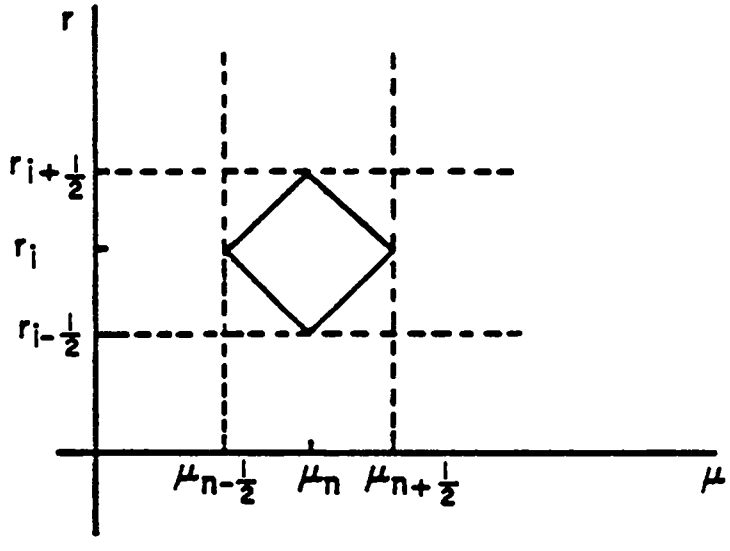

Fig. 1.--The diamond structure of the interpolating procedure shown on a partial r-μ mesh

$$f = \{\tilde{q}^*\Delta t + f_s - \frac{\Delta t\,\mu_n \Delta v_g^4/4}{V_i \Delta v_g^3/3}[A_{i+1/2} + A_{i-1/2}]f_{i+1/2}$$

$$+ \frac{\Delta t\,\Delta v_g^4/4}{V_i \Delta\mu_n \Delta v_g^3/3}[\alpha_{n+1/2} + \alpha_{n-1/2}]f_{n-1/2}\} \qquad (3\text{-}53)$$

$$\{1 + \frac{\Delta t\,\Delta v_g^4/4}{V_i \Delta v_g^3/3}[\frac{1}{\Delta\mu_n}(\alpha_{n+1/2} + \alpha_{n-1/2}) - \mu_n(A_{i+1/2} + A_{i-1/2})]\}\cdot$$

This equation can be used to solve for the updated distribution f for all zones i, starting at the boundary of the sphere by calculating the cell centered distributions f and then extrapolating inward for the cell edged distributions $f_{i-1/2}$. Since the calculation proceeds inward toward the center of the spere, it should only be performed for angles directed inward to avoid the accumulation of numerical error[6] i.e., for the directions μ such that $-1 \leq \mu \leq 0$. A similar equation can be derived for outward directions by considering $f_{i+1/2}$ to be unknown and again using the diamond difference equations in conjunction with Eq. (3-50) to yield

$$f = \{\tilde{q}^*\Delta t + f_s + \frac{\Delta t\,\mu_n \Delta v_g^4/4}{V_i \Delta v_g^3/3}[A_{i+1/2} + A_{i-1/2}]f_{i-1/2}$$

$$+ \frac{\Delta t\,\Delta v_g^4/4}{V_i \Delta\mu_n \Delta v_g^3/3}[\alpha_{n+1/2} + \alpha_{n-1/2}]f_{n-1/2}\} \qquad (3\text{-}54)$$

$$\{1 + \frac{\Delta t\,\Delta v_g^4/4}{V_i \Delta v_g^3/3}[\frac{1}{\Delta\mu_n}(\alpha_{n+1/2} + \alpha_{n-1/2}) + \mu_n(A_{i+1/2} + A_{i-1/2})]\}\cdot$$

The outward integrations can be started by using an isotropy condition at the center of the sphere which is just

$$f_{r=0,n_{outward}} = f_{r=0,n_{inward}}$$

$$n_{outward} = NN+1-n_{inward} \cdot \qquad (3\text{-}55)$$

This integration is done after all of the inward calculations have been performed. In this way, $f(r,v,\mu,t)$ is calculated at the updated time $t = t_{s+1}$ for all zones, speeds, and angles.

Two codes have been developed which perform an integration of the Fokker-Planck transport equation via the methods outlined in this section. The first one, SFTRAN, calculates transport in the system just discussed i.e., in a spherical plasma. The second code CYTRAN calculates transport in a fully symmetric cylindrical plasma but with full velocity space dependence such that $f_a(r,v,\mu,\chi,t)$ is calculated. The methods and results obtained by CYTRAN will be the subject of the last half of this chapter.

In the next section, some results obtained by the spherical code are presented.

Results

The calculation of the energy deposited by fast test ions as they slow down on a background plasma during the collisional transport process is typical of the benchmark problems which have evolved within the literature on charged particle transport. In a pellet plasma, for example, it is of interest to determine how this energy is distributed spatially while being partitioned to the background electrons and ions. It is also of interest to be able to determine the time history of this deposition. Some of the more important applications of these type of calculations include the treatment of fusion product transport and the analysis of injected

charged particle beams. In order to demonstrate the matrix factorization (MF) method of the last sections, the transport of fusion alpha particles and beam deuterons and protons will be considered.

Before proceeding further, it is to be noted that in the transport equation, the factor Γ_{ab} has consistently been kept within the summation over the species 'b'. This is because of the dependence of Γ on the background species through the Coulomb logarithm as

$$\ln\Lambda = \ln(\lambda_d/b_o) = \ln\left[\lambda_d/(Z_a Z_b e^2/4\pi\epsilon_o \mu_{ab} V^2)\right] . \qquad (3\text{-}56)$$

In this work the arguments Λ_i and Λ_e will be approximated as

$$\Lambda_i = \frac{\lambda_d 4\pi\epsilon_o}{Z_a Z_i e^2}\left(\frac{m_i}{m_i + m_a}\right)2E \qquad (3\text{-}57)$$

and

$$\Lambda_e = \frac{\lambda_d 4\pi\epsilon_o}{Z_a e^2} 3\Theta_e \qquad (3\text{-}58)$$

which are valid approximations for cases where the electron thermal velocity $v_{e_{th}}$ is greater than the test ion velocities v, but where $v > v_{i_{th}}$. The test ion energy E in Eq. (3-57) is set to the thermal ion energy to be definite, and the Marshak correction factor[7] is applied in Eq (3-58) when applicable.

The case of 3.5 MeV fusion product alpha particles transporting in a spherical plasma is considered first. In this example, the background electron and hybrid D-T ion densities will be 0.2125×10^3 kg/m^3 while their temperatures are taken to be equal at 50 keV.

Although here the temperatures are set equal, the code does allow for different electron and ion temperatures.

It is chosen to compare the results of the MF calculations with those given by Mehlhorn and Duderstadt in Ref. 1 since their method also allows for velocity space dispersion. In order to match the zoning used in their modified neutronics code TIMEX-FP, 13 radial zones are used while the velocity space variables are discretized by 4 μ directions and an 18 point speed grid. The zone width is taken to be $.7742 \times 10^{-2}$m which is equivalent to $.035\lambda_s$ where λ_s is the range of alpha particles on electrons at the density and temperature given above. Further, in this problem, the arguments of the Coulomb logarithm are not calculated by Eqs. (3-57) and (3-58) but the values of $\ln\Lambda$ are set as $\ln\Lambda_e = 8.25$ and $\ln\Lambda_i = 18.56$ as the were in Ref. 1. The details of the energy deposition calculation are given in Appendix C.

In Figures 2 and 3, the fraction E_d/E_o of the initial alpha particle energy E_o deposited per zone to the background electrons and ions, respectively, is plotted for each zone. It can be seen that the MF method yields results which are in very good agreement with those reported in Ref. 1. In both Figures 2 and 3, the peaks of the spatial deposition profiles occur in the same zones and are nearly identical in magnitude. Similarly, the stopping lengths calculated by the MF method enjoy close agreement to those previously reported. Although small differences occur in the two methods' calculations of the amount of energy deposited in the first few zones to both electrons and ions, the results of the MF method should be reliable since it does not seem to encounter the difficulties near localized sources that the S_n techniques used in TIMEX-FP might[6].

In order to study the effects of the dispersion in velocity space which the alpha particles undergo as they scatter on the plasma, the number of angles NN, used in the calculation was varied. In Figs. 4 and 5 the spatial deposition profiles are again given for electrons and ions separately. It is seen that by increasing the number of directions in which the alpha particle distribution

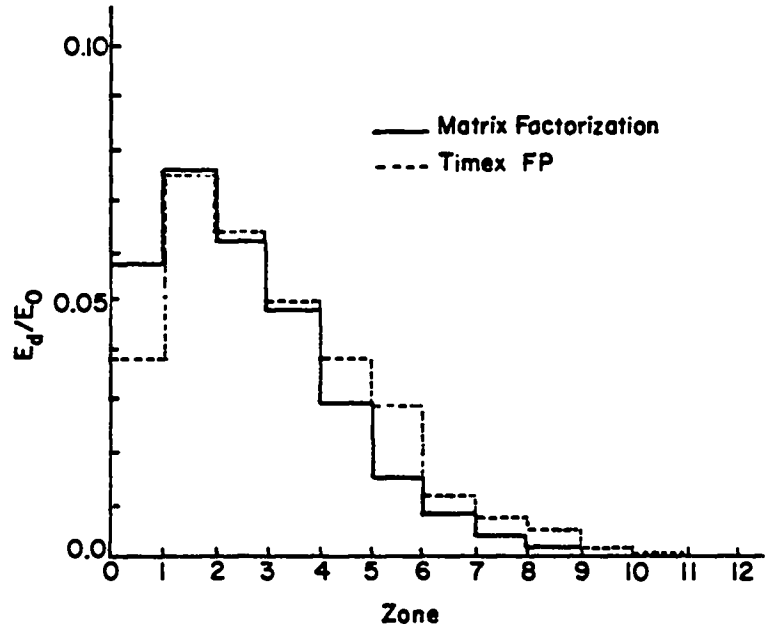

Fig. 2.--Fraction of initial alpha particle energy deposited per zone to electrons

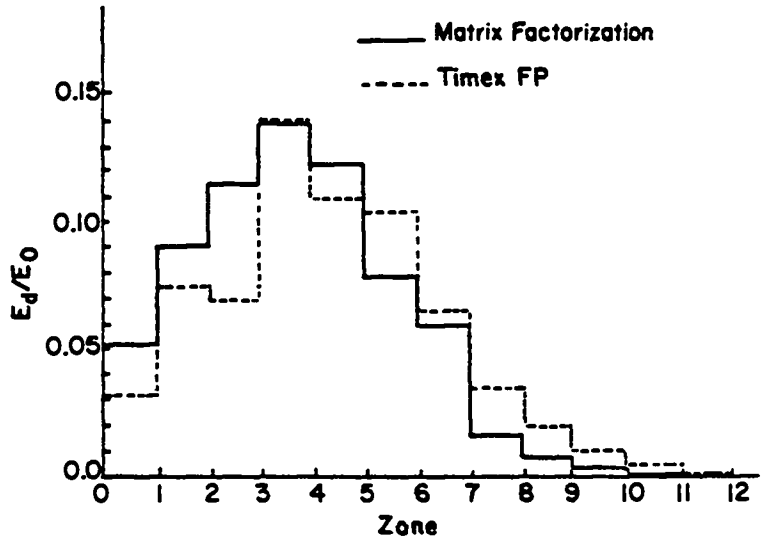

Fig. 3.--Fraction of initial alpha particle energy deposited per zone to ions

function can be defined, for the case of deposition to electrons, the spatial profile's peak is decreased while deposition to the outer zones is increased. In the case of the ions, the peak is also diminished but shifted to the right with the deposition to the outer zones again increasing. This behavior is to be expected for the following reasons. Since the initially isotropic alpha particles are at higher energies than the background electrons and ions, their distribution will depart from the isotropic form as they scatter in an attempt to reach a thermal equilibrium. Although the alpha energy may diminish after the first few collisions in zones near the center of the sphere, the energy is more directed in the outward directions in these zones. They will approach a thermal equilibrium after enough collisions have occurred along their path, so that their distribution will again acquire an isotropic character in the outer zones of the mesh. At this time the particles will have no preferred direction , so that the amount of backscattering will become the same

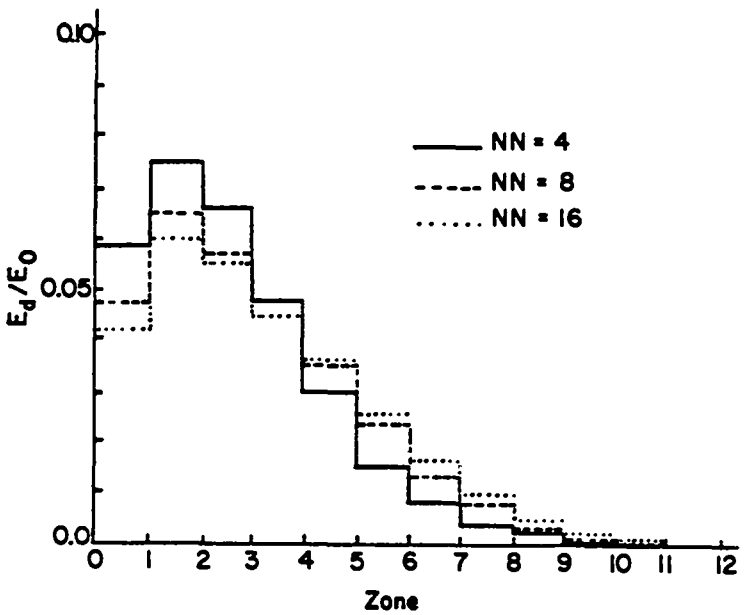

Fig. 4.--Fractional deposition per zone to electrons for an increasing number of directions (NN)

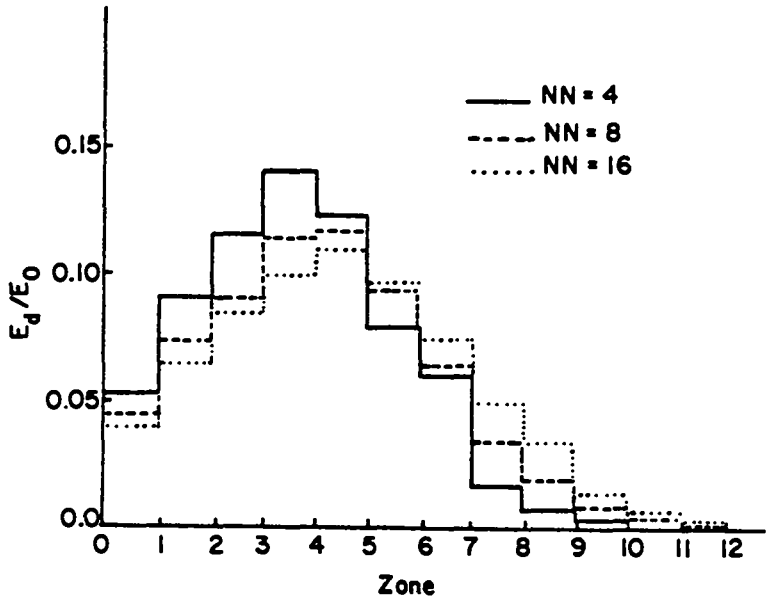

Fig. 5.--Fractional deposition per zone to ions for for an increasing number of directions (nn)

as the amount of forward scattering, thus resulting in higher deposition to these outer zones. That this behavior is indeed the case, is extablished by following the distribution of the cosine (μ) of the alpha particles' velocity vectors with respect to the radial vector as a function of time. In Fig. 6 this spectral information is shown for the center zone at t = 0 while the curves at other times are apprpriate to the third zone on the mesh. It is seen that the distribution (normalized to unity on the abscissa) becomes peaked toward a positive cosine almost instantaneously, showing that the alpha energy is highly directed toward the outer zones. As time (NT) progresses, the particles scatter and lose their energy and the distribution tends toward a Maxwellian at the background temperature. From this information, it can be concluded that by using too few angles in this type of calculation, the results may become biased in showing too much deposition in the first few zones and in ignoring the backscattering effects in the outer zones.

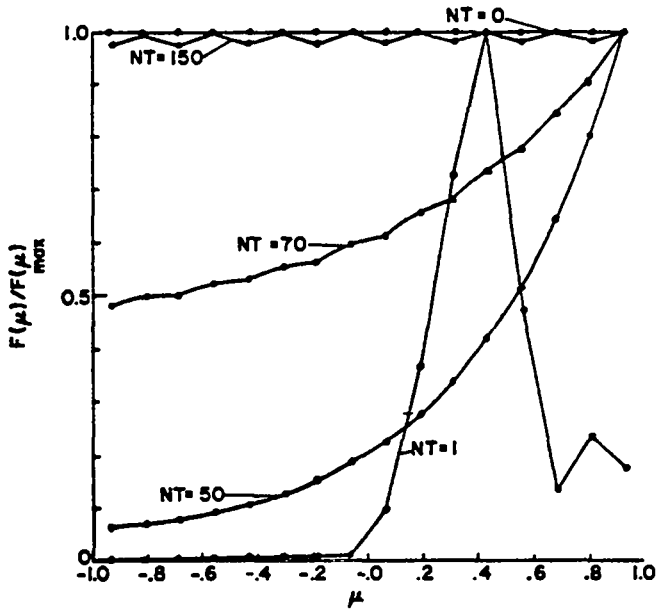

Fig. 6.--Angular spectra of the distribution function at the 3rd position on the zone grid. At the first time step (NT), the spectra is shown for the first zone

It is interesting to note that the plots in Figure 6 contain data points which appear jagged. This is due to the use of a large time step in the algorithm, which gives rise to small fluctuations in the distribution information, a common occurrence in any finite difference scheme. Although this phenomenon could be detrimental in some algorithms, the MF method remained absolutely conservative and convergent.

In Figure 7 the time dependent energy deposition history is shown for both deposition on electrons and on ions. As a check on the accuracy of this method, the curve showing the total energy fraction deposited to both ions and electrons was calculated using the appropriate moment of the L.H.S. of the transport equation, Eq. (3-18). It can be seen that the code remained energy conserving.

It is noted that the total deposition fraction in time tends towards unity but becomes asymptotic at a value less than unity. This is, of course, due to the fact that the alpha particle does not

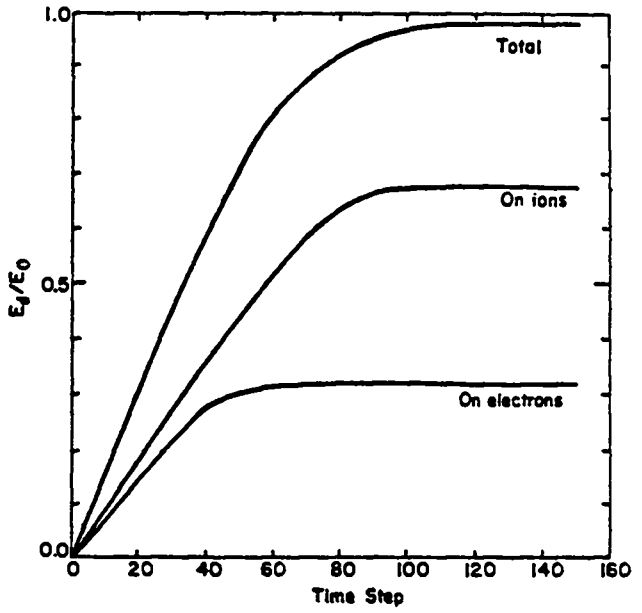

Fig. 7.--Time history of deposition to both electrons and ions

lose all of its kinetic energy but only slows down to an energy defined by the temperature at thermal equilibrium.

The effieciency for the MF method is demonstrated in Figures 8 and 9. The same computations described above for four angles, 13 zones and 18 velocity grid points were performed using 150 time steps (NT) at a time increment of .01 and then carried out again using 1500 time steps at $\Delta t = .001$. Here the time increment Δt is scaled to the slowing-down time of alpha particles due to electrons at 50 keV which is equal to 8.47×10^{-9} sec. It can be seen that very little accuracy is lost by using the larger time step. The calculation using 150 time steps required 5 seconds of CPU time on the CRAY I computer.

The energy deposited to a plasma by an injected beam can be calculated by introducing a distribution function characterizing the beam at the outermost zone of the system. In the examples which follow, the zoning used in the previous examples is retained but a

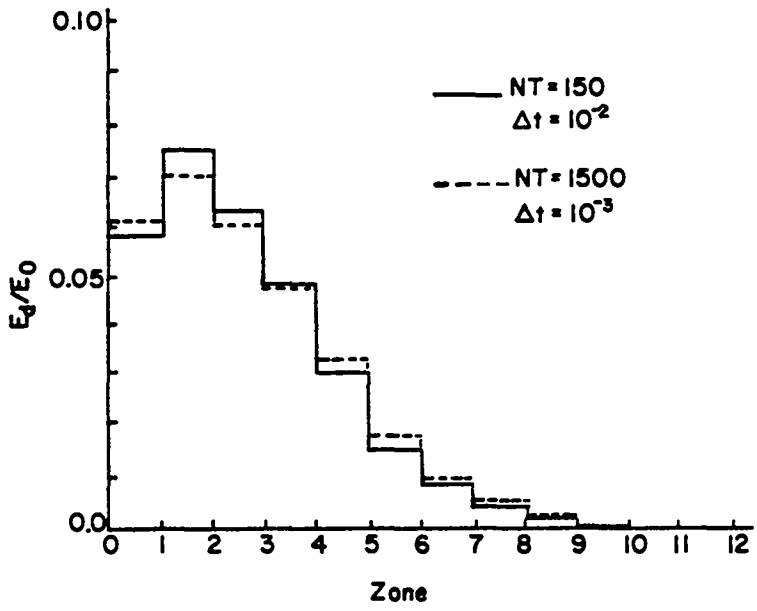

Fig. 8.--Fractional deposition per zone to electrons for two time step sizes and the corresponding number of iterations

delta function distribution (in speed) defined at one ingoing angle is used to simulate a beam entering at the boundary.

In the first example, a beam of 1 MeV deuTerons impinging on D-T plasma (at the same temperature and density as before) at the outermost zone (zone 13) is considered. The delta function is defined at their velocity corresponding to that energy which is $v = 9.823 \times 10^6$ m/sec. In Figs. 10 and 11, the deposition profiles are shown for the case in which the beam consists of an initial burst of ingoing deuterons. Since the beam velocity is much less than the electron thermal velocity in this case, the deuterons should tend to deposit their energy on the background ions in greater proportion. This is seen to be the case.

In Figures 12 and 13, the deposition profiles are shown for an initial burst of 500 keV ingoing protons. Since the proton velocity is the same as above ($v = 9.823 \times 10^6$ m/sec) the same tendency to deposit more energy to the ions should be observed. In addition

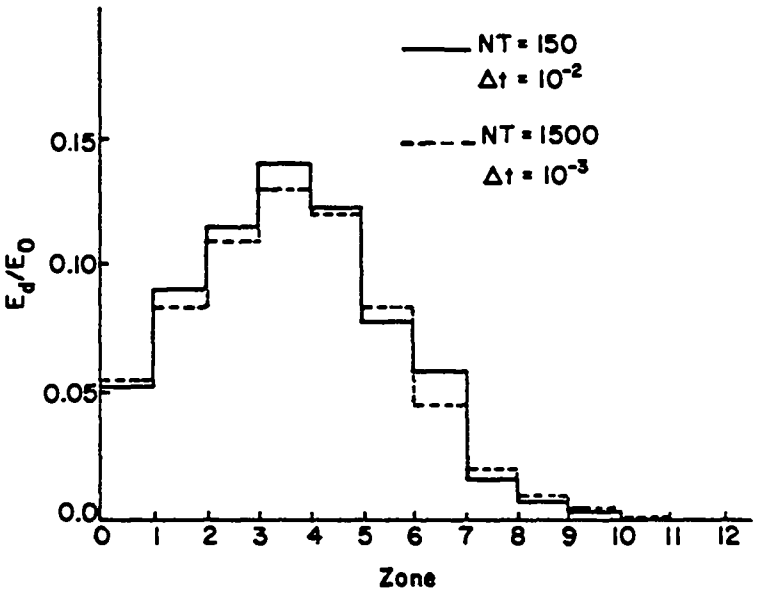

Fig. 9.--Fractional deposition per zone to ions for two time step sizes and the corresponding number of iterations

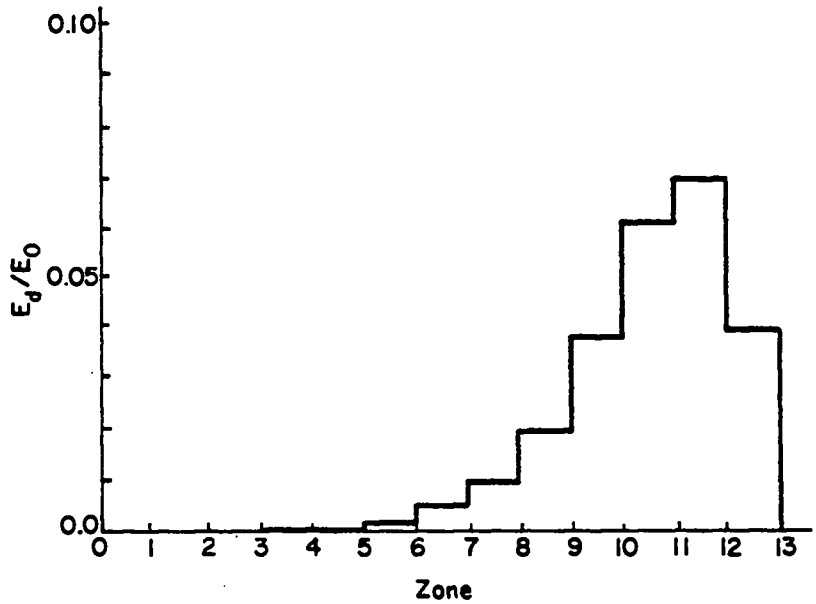

Fig. 10.--Fraction of initial deuteron energy deposited per zone to electrons for a beam entering at zone 13

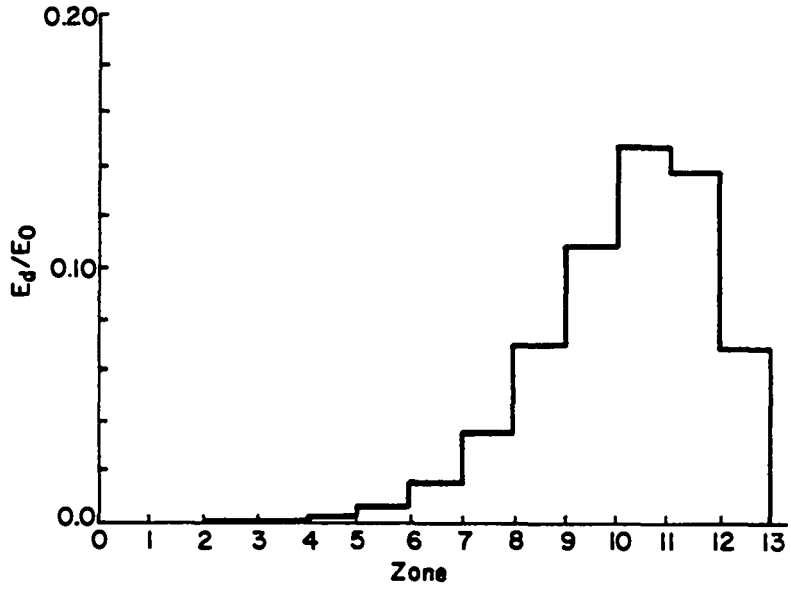

Fig. 11.--Fraction of initial deuteron energy deposited per zone to ions for a beam entering at zone 13

though, since the mass of the protons is less than that of deuterons, they are more easily deflected and so should deposit their energy much more quickly i.e., within the first few zones. Again, this behavior is verified in the figures. Both of the above calculations required about 4.5 seconds of CPU time on the CRAY I.

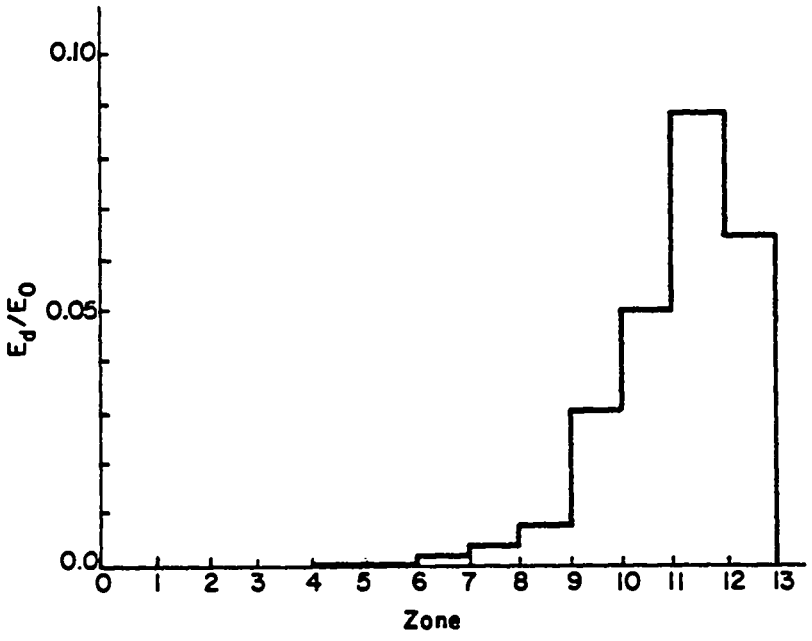

Fig. 12.--Fraction of initial proton energy deposited per zone to electrons for a beam entering at zone 13

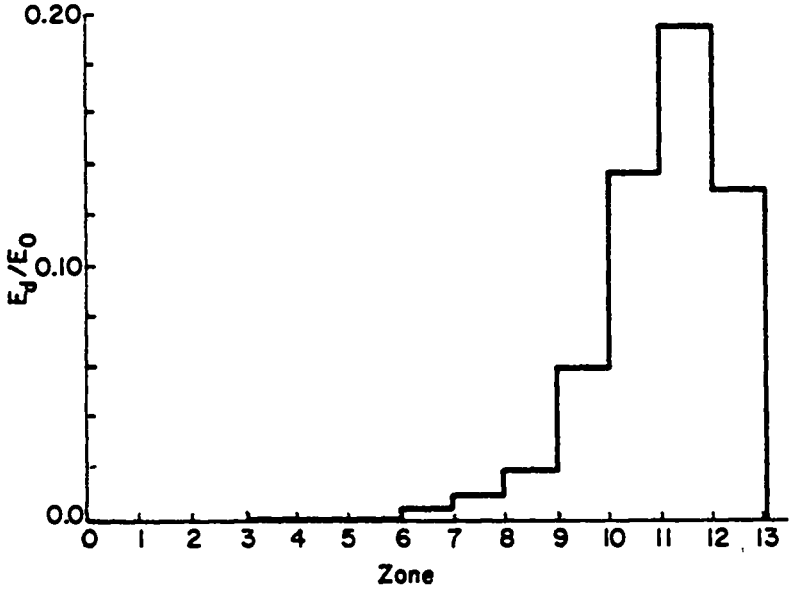

Fig. 13.--Fraction of initial proton energy deposited per zone to ions for a beam entering at zone 13

Solution For A Cylindrical Plasma

In the first sections of this chapter it was shown tnat the Fokker-Planck equation could be solved by the use of a consistent operator splitting technique and the subsequent application of matrix factorization and forward extrapolation to obtain the time dependent distribution function of test particles $f_a(r,v,\mu,t)$. In the following sections it will be shown that these techniques can also be employed to solve for the full 3 dimensional velocity space dependence of the distribution function.

To this end, it is chosen to solve the transport equation for a fully symmetric plasma which is describable in cylindrical coordinates in configuration space and spherical polar coordinates in velocity space such that the time evolution of the distribution function $f_a(r,v,\mu,\chi,t)$ will be sought. In Appendices A and B, the charged particle transport equation, Eq. (2-30), is developed for these geometries as

$$\frac{\partial f_a(r,v,\mu,\chi,t)}{\partial t} + \frac{v(1-\mu^2)^{1/2}\cos\chi}{r}\frac{\partial(rf_a)}{\partial r} - \frac{v}{r}\frac{\partial(f_a(1-\mu^2)^{1/2}\sin\chi)}{\partial\chi} = \frac{\partial f_a}{\partial t}\Big)_c \tag{3-59}$$

where

$$\frac{\partial f_a}{\partial t}\Big)_c = -\left\{\frac{1}{v^2}\frac{\partial}{\partial v}v^2 J^v + \frac{\partial}{\partial\mu}J^\mu + \frac{\partial}{\partial\chi}J^\chi\right\} \tag{3-60}$$

and

$$J^v = \sum_b \Gamma_{ab} \frac{N_o \tau_o Z_b^2}{C_o^3} \left\{ \frac{A_a}{A_b} f_a \frac{\partial L_b}{\partial v} - \frac{1}{2} \frac{\partial f_a}{\partial v} \frac{\partial^2 K_b}{\partial v^2} \right\}, \tag{3-61}$$

$$J^\mu = -\sum_b \Gamma_{ab} \frac{N_o \tau_o Z_b^2}{C_o^3} \left\{ \frac{(1 - \mu^2)}{2v^3} \frac{\partial f_a}{\partial \mu} \frac{\partial K_b}{\partial v} \right\}, \tag{3-62}$$

$$J^X = -\sum_b \Gamma_{ab} \frac{N_o \tau_o Z_b^2}{C_o^3} \left\{ \frac{1}{2v^3(1 - \mu^2)} \frac{\partial f_a}{\partial X} \frac{\partial K_b}{\partial v} \right\} . \tag{3-63}$$

It is again invoked that the background distributions remain Maxwellian for all time and that collisions between particles of species 'a' will not be considered so that the derivatives of K_b and L_b can be evaluated as before in Eqs. (3-6),(3-7) and (3-8). In this case, the Landau-Fokker-Planck components take the simple forms

$$J^v = -4\pi \sum_b \Gamma_{ab} \frac{N_o \tau_o Z_b^2}{C_o^3} \left\{ \frac{A_a}{A_b} f_a \frac{H_{b2}(v)}{v^2} \right.$$

$$\left. + \frac{1}{3} \frac{\partial f_a}{\partial v} \left(\frac{H_{b3}(v)}{v^3} + H_{b1}(v) \right) \right\}, \tag{3-64}$$

$$J^\mu = -4\pi \sum_b \Gamma_{ab} \frac{N_o \tau_o Z_b^2}{C_o^3} \left\{ \frac{(1 - \mu^2)}{2v^3} \frac{\partial f_a}{\partial \mu} \times \right.$$

$$\left. \left(H_{b2}(v) - \frac{H_{b3}(v)}{3v^2} + \frac{2v}{3} H_{b1}(v) \right) \right\} \tag{3-65}$$

$$J\chi = -4\pi\sum_b \Gamma_{ab}\frac{N_o\tau_o}{c_o^3}Z_b^2\left\{\frac{1}{2v^3(1-\mu^2)}\frac{\partial f_a}{\partial \chi}\ x\right.$$

$$\left.\left(H_{b2}(v) - \frac{H_{b3}(v)}{3v^2} + \frac{2v}{3}H_{b1}(v)\right)\right\} \qquad (3\text{-}66)$$

where the definitions of H_{b1},H_{b2}, and H_{b3} given in Eqs. (3-14)-(3-16) have been used.

The Difference Approximation

An operator which discretizes the dependence of f_a on its arguments as $f_a(r_i, v_g, \mu_n, \chi_m, t_s)$ through the transport equation is

$$\kappa = \frac{1}{\beta}\int_{t_s}^{t_{s+1}} dt \int_{r_{i-1/2}}^{r_{i+1/2}} r^2 dr \int_{v_{g-1/2}}^{v_{g+1/2}} v^2 dv \int_{\mu_{n-1/2}}^{\mu_{n+1/2}} d\mu \int_{\chi_{m-1/2}}^{\chi_{m+1/2}} d\chi \qquad (3\text{-}67)$$

where β is now defined as $\Delta t_s(\Delta r_i^2/2)(\Delta v_g^3/3)\Delta\mu_n\Delta\chi_m$ and $\Delta t_s = t_{s+1} - t_s$, $\Delta r_i^2/2 = (r_{i+1/2}^2 - r_{i-1/2}^2)/2$, $\Delta v_g^3/3 = (v_{g+1/2}^3 - v_{g-1/2}^3)/3$, $\Delta\mu = \mu_{n+1/2} - \mu_{n-1/2}$, and $\Delta\chi = \chi_{m+1/2} - \chi_{m-1/2}$. Here again the $\pm$ indices will represent cell edged quantities while the integer indices will represent those that are cell centered and the distribution f_a will always be indexed implicitely i.e, at the advanced time $t = t_{s+1}$ unless specified otherwise.

Applying this operator to the transport equation, Eq. (3-59), yields the difference approximation

$$\frac{f(r_i, v_g, \mu_n, \chi_m, t_{s+1}) - f_s}{\Delta t} + \frac{(1-\mu^2)^{1/2}\cos\chi_m \Delta v_g^4/4}{\Delta r_i^2/2\ \Delta v_g^3/3}\ x$$

$$\left(r_{i+1/2}f_{i+1/2} - r_{i-1/2}f_{i-1/2}\right)$$

$$+ \frac{\Delta v_g^4/4}{\Delta\chi_m \Delta r_i^2/2 \; \Delta v_g^3/3}\left(\alpha_{m+1/2} f_{m+1/2} - \alpha_{m-1/2} f_{m-1/2}\right) \qquad (3\text{-}68)$$

$$= -\left\{-\frac{1}{\Delta v_g^3/3}\left[v_{g+1/2}^2 J_{g+1/2}^v - v_{g-1/2}^2 J_{g-1/2}^v\right]\right.$$

$$\left. + \frac{1}{\Delta\mu_n}\left[J_{n+1/2}^\mu - J_{n-1/2}^\mu\right] + \frac{1}{\Delta\chi_m}\left[J_{m+1/2}^\chi - J_{m-1/2}^\chi\right]\right\}$$

where the alpha coefficients technique of S_n theory[2] has again been used to form the difference approximation of the third term and where the subscript 'a' on the distribution function to be solved for has been dropped. By using the definitions of B_g, C_g, and D_g given in equations (3-19)-(3-21) and by performing the same algebra in the collision terms as before, it is found that they can be written as the sum of three 3-point difference terms so that the R.H.S. of Eq. (3-68) can then be set equal to $\tilde{q}$ as

$$\tilde{q} = \tilde{q}^v + \tilde{q}^\mu + \tilde{q}^\chi \qquad (3\text{-}69)$$

where the three terms are given by

$$\tilde{q}^v = \frac{4\pi}{\Delta v_g^3/3}\left\{f_{g-1}\left[\frac{C_{g-1/2}}{\Delta v_{g-1/2}} - B_{g-1/2}\delta_{g-1/2}\right]\right.$$

$$+ f_g\left[B_{g+1/2}\delta_{g+1/2} - \frac{C_{g-1/2}}{\Delta v_{g-1/2}} - \frac{C_{g+1/2}}{\Delta v_{g+1/2}} - B_{g-1/2}(1 - \delta_{g-1/2})\right]$$

$$\left. + f_{g+1}\left[B_{g+1/2}(1 - \delta_{g+1/2}) + \frac{C_{g+1/2}}{\Delta v_{g+1/2}}\right]\right\}, \qquad (3\text{-}70)$$

$$\tilde{q}^{\mu} = \frac{2\pi}{\Delta\mu_n}\{f_{n-1}\frac{(1 - \mu_{n-1/2}^2)}{\Delta\mu_{n-1/2}} - f_n[\frac{(1 - \mu_{n-1/2}^2)}{\Delta\mu_{n-1/2}} + \frac{(1 - \mu_{n+1/2}^2)}{\Delta\mu_{n+1/2}}]$$

$$+ f_{n+1}\frac{(1 - \mu_{n+1/2}^2)}{\Delta\mu_{n+1/2}}\} , \qquad (3\text{-}71)$$

$$\tilde{q}^{\chi} = \frac{2\pi D_g}{\Delta\chi_m(1 - \mu_n^2)}\{f_{m-1}\frac{1}{\Delta\chi_{m-1/2}} - f_m(\frac{1}{\Delta\chi_{m-1/2}} + \frac{1}{\Delta\chi_{m+1/2}})$$

$$+ f_{m+1}\frac{1}{\Delta\chi_{m+1/2}}\} . \qquad (3\text{-}72)$$

By defining the quantity Λ as

$$\Lambda = \frac{(1 - \mu_n^2)^{1/2}\cos\chi_m \Delta v_g^4/4}{\Delta r_i^2/2\ \Delta v_g^3/3}(r_{i+1/2}f_{i+1/2} - r_{i-1/2}f_{i-1/2})$$

$$+ \frac{\Delta v_g^4/4}{\Delta\chi_m\ \Delta r_i^2/2\ \Delta v_g^3/3}(\alpha_{m+1/2}f_{m+1/2} - \alpha_{m-1/2}f_{m-1/2}) \qquad (3\text{-}73)$$

it is seen that the difference approximation, Eq. (3-68), can now be written in the more concise form

$$f - \tilde{q}\Delta t_s = f_s - \Lambda\Delta t_s . \qquad (3\text{-}74)$$

Solution of the Difference Approximation by Consistent Splitting with Matrix Factorization

Equation (3-74) can be split consistently into two equations of the form

$$\left[f - \tilde{q}\Delta t\right]^* = \left[f_s - \Lambda\Delta t\right]_{t = t_s} \tag{3-75}$$

$$f + \Lambda\Delta t = \tilde{q}^*\Delta t + f_s \quad . \tag{3-76}$$

The solution f^* of Eq. (3-75) will contain the effects of collisions in its velocity space dependence while Eq. (3-76) will use this result as $\tilde{q}^* = \tilde{q}(f^*)$ and can be solved for f, the updated distribution function which will include the effects of streaming in configuration space.

The solution of Eq. (3-75) differs significantly from the solution of its counterpart in spherical coordinates, Eq. (3-36), in the implementation of the matrix factorization technique on an equation that is not fully separable. To see this note that in $\tilde{q}^*$ i.e., Eq. (3-72), there exists a factor $(1 - \mu_n^2)$ in the denominator which gives that term an unwanted dependence on μ. Simple multiplication by this factor will not clear up this problem since it will then introduce the factor into the $\tilde{q}^v$ term (note that simple division by the factor D_g in the $\tilde{q}^\mu$ and $\tilde{q}^\chi$ terms will rid these of any dependence on v). In order to circumvent this problem, a second splitting is introduced such that Eq. (3-75) is itself split into two equations of the form

$$E^{jlk}_{mng}\psi^l_{jlk} + G^{jlk}_{mng}\psi^l_{jlk} = S^l_{mng} \tag{3-77}$$

and

$$E^{jlk}_{mng}\psi^2_{jlk} + F^{jlk}_{mng}\psi^2_{jlk} = S^2_{mng} \quad . \tag{3-78}$$

$$j = m-1,m,m+1$$

$$l = n-1,n,n+1$$

$$k = g-1,g,g+1$$

where the three dimensional supermatrices $\underline{\underline{E}}, \underline{\underline{F}}$, and $\underline{\underline{G}}$ contain the coefficients of the three 3-point terms $\tilde{q}^{\nu}, \tilde{q}^{\mu}$, and $\tilde{q}^{\chi}$ respectively and have the properties $E^{jlk}_{mng} \rightarrow \delta^j_m \delta^l_n E^{jlk}_{mng}$, $F^{jlk}_{mng} \rightarrow \delta^j_m \delta^k_g F^{jlk}_{mng}$, and $G^{jlk}_{mng} \rightarrow \delta^l_n \delta^k_g G^{jlk}_{mng}$. The source terms are now defined as

$$S^1_{mng} = \left[f_s - \Lambda\Delta t\right]_{t = t_s} - \left[\tilde{q}^{\mu}\Delta t\right]_{t = t_s} \tag{3-79}$$

and

$$S^2_{mng} = \left[f_s - \Lambda\Delta t\right]_{t = t_s} - \left[\tilde{q}^{\chi}\Delta t\right]_{t = t_s} \tag{3-80}$$

so that the terms on the L.H.S. of both Eqs. (3-77) and (3-78) are now fully separable.

Both of these equations con now be solved by the matrix factorization method described earlier to yield the two solutions ψ^1_{jlk} and ψ^2_{jlk}. These are subsequently iterated to yield the consistent solution f^* of the original equation, Eq. (3-75).

Eq. (3-76) is solved as in the spherical coordinates case by making use of the diamond difference relations

$$2f \simeq f_{m-1/2} + f_{m+1/2} \tag{3-81}$$

$$2f \simeq f_{i-1/2} + f_{i+1/2} \tag{3-82}$$

to derive inward and outward equations that can be solved by simple forward extrapolation. Here these equations take the form

$$f = \{\bar{q}\Delta t + f_s - \frac{\Delta t\,\Delta v_g^4/4\ (1-\mu_n^2)^{1/2}\cos\chi_m}{\Delta v_g^3/3\ \Delta r_i^2/2} f_{i+1/2}(r_{i+1/2} + r_{i-1/2})$$

$$+ \frac{\Delta t\,\Delta v_g^4/4}{\Delta\chi_m \Delta v_g^3/3\ \Delta r_i^2/2} f_{m-1/2}(\alpha_{m+1/2} + \alpha_{m-1/2})\} \qquad (3\text{-}83)$$

$$\{1 - \frac{\Delta t\,\Delta v_g^4/4}{\Delta v_g^3/3\ \Delta r_i^2/2}[(1-\mu_n^2)^{1/2}\cos\chi_m(r_{i+1/2} + r_{i-1/2})$$

$$- \frac{1}{\Delta\chi_m}(\alpha_{m+1/2} + \alpha_{m-1/2})]\}$$

which is used for the inward integrations i.e., for $\frac{\pi}{2} \leq \chi_m \leq \frac{3\pi}{2}$ and

$$f = \{\tilde{q}^*\Delta t + f_s + \frac{\Delta t\,\Delta v_g^4/4\ (1-\mu_n^2)^{1/2}\cos\chi_m}{\Delta v_g^3/3\ \Delta r_i^2/2} f_{i-1/2}(r_{i+1/2} + r_{i-1/2})$$

$$+ \frac{\Delta t\,\Delta v_g^4/4}{\Delta\chi_m \Delta v_g^3/3\ \Delta r_i^2/2} f_{m-1/2}(\alpha_{m-1/2} + \alpha_{m+1/2})\} \qquad (3\text{-}84)$$

$$\{1 + \frac{\Delta t\,\Delta v_g^4/4}{\Delta v_g^3/3\ \Delta r_i^2/2}[(1-\mu_n^2)^{1/2}\cos\chi_m(r_{i+1/2} + r_{i-1/2})$$

$$+ \frac{1}{\Delta\chi_m}(\alpha_{m+1/2} + \alpha_{m-1/2})]\}$$

which is used for outward integrations.

Results

The methods discussed in the last section can be demonstrated by an energy deposition calculation using the same zoning in r, v, and μ as in the spherical coordinates case i.e., as II = 13, $\Delta r = .7742 \times 10^{-2}$m, NG = 18, and NN = 4. If the same test problem involving an initially isotropic burst of 3.5 MeV alpha particles from the innermost zone is considered, the spatial deposition profiles on the background electrons and ions shown in Figs. 14 and 15 are obtained. Here again the background densities were taken to be 5.12×10^{28}m^{-3} while the ion and electron temperatures were set at 50 keV. The Coulomb logarithms were also set as $\ln\Lambda_e = 8.25$ and $\ln\Lambda_i = 18.5625$ as before. For these examples the number of intervals on the χ grid were varied.

In Figs. 14 and 15 it is seen that by increasing the number of intervals (MM) on the χ grid while keeping the other zoning constant, more deposition occurs in the first zones in both cases. This indicates that a larger number of intervals are necessary to resolve the slight deflection that the particles undergo as they traverse the first few zones. This particle behavior will be verified in the next chapter in which their paths in the plasma is simulated. It can be postulated that if the number of χ_m intervals are increased to a very large number, the deposition profiles will show increased deposition in the first zones and will subsequently drop to zero somewhat faster.

It should be stated that CYTRAN uses considerably more CPU time than SFTRAN for comparable problems. For example, in the above alpha particle slowing down problem where MM was set to 4, CYTRAN comsumed ≈ 300 seconds while the spherical code used only 5 seconds. The main reason for this costly behavior is that in CYTRAN a second splitting was used as explained in the last section. It was found that the

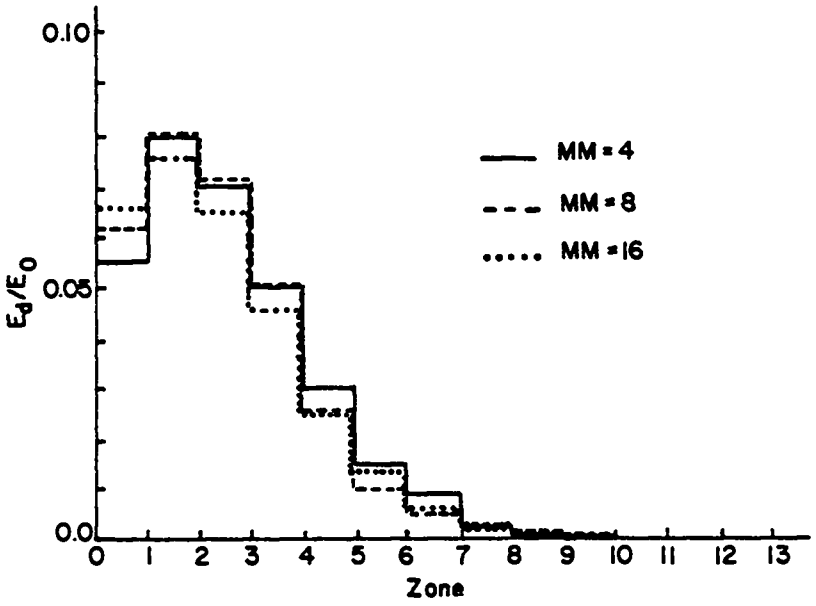

Fig. 14.--Fractional deposition per zone to electrons for an increasing number of intervals on the χ grid

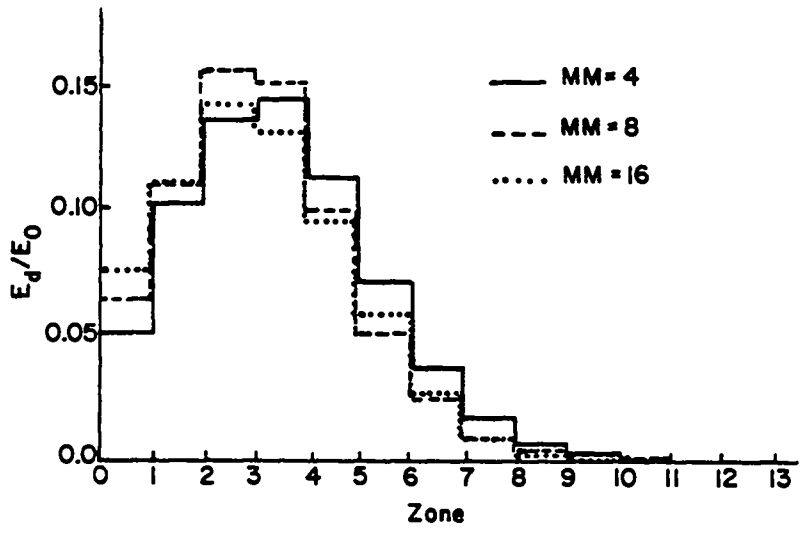

Fig. 15.--Fractional deposition per zone to ions for an increasing number of intervals on the χ grid

solutions obtained in the second splitting had to be iterated to within a very small criterion ($\simeq$ 1/10,000) in order to preserve particle conservation.

It can be concluded that if the $\underline{v}$-space geometry of interest is such that perfect separability cannot be easily achieved, a point of diminishing returns has been reached insofar as the applicability of matrix factorization to a 3-dimensional velocity space problem. Although CYTRAN is still considerably faster than some other transport techniques, it may be well advised to try another method [c.f. Chapter IV] for non-separable geometries.

Note that if perfect separability in Eq. (3-75) does occur for a given n-dimensional velocity space problem, a simple extension of the matrix factorization method in which (n-1) different eigenvector expansions are incorporated can be used to solve the equation rapidly.

Conclusions

It has been shown that the Fokker-Planck charged particle transport equation can be solved in an efficient manner by splitting the difference approximation to yield two fully implicit equations, each of which is solved separately. One split equation contains the collision physics and modifies the distribution of test ions for these effects in its velocity variables v and μ (and/or χ) while the other equation corrects the distribution for spatial transport (streaming). A matrix factorization technique is used to solve the first of these equations ("the collision equation") while a standard forward extrapolation technique is employed to solve the "spatial equation". Using the example of 3.5 MeV alpha particles transporting in a background D-T plasma, it was seen that the combination of these techniques in this algorithm yielded results which were in very good agreement with those previously published. Furthermore, since the algorithm is fully implicit, it was also shown that large time steps

could easily be used to generate accurate results in a minimum of CPU time.

Although the distributions of ions and electrons describing the background plasma were postulated to be fixed Maxwellian distributions, the generalization to time, space and velocity dependent distributions is straightforward within this algorithm. Further, the matrix factorization technique is not restricted to any particular geometry, and here it has been shown to be successfully applicable to the curved geometries of spherical and cylindrical systems.

There are also many other possible extensions of these methods which remain to be investigated. One interesting possibility is the generalization to a two or three dimensional configuration space dependence of the test particle distribution. This appears to be straightforward since the spatial transport effects are solved for separately. Another possibility is the reformulation of the split equations into the more general relativistic forms which would account for the test particle's mass increase at velocities near the speed of light. This extension would be useful for solving transport problems involving test particles at MeV and higher energies and in problems of electron transport in general.

Finally, the inclusion of a magnetic field within this scheme (or even within any other finite difference scheme) remains to be done successfully. Although several differencing procedures were tried, it was found that the acceleration term of the transport equation could not be differenced conservatively i.e., the conservation of particles would be lost for finite sized intervals on the velocity space grids. The work carried out by the author was by no means exhaustive and it remains conceivable that a technique (perhaps similar to the alpha-coefficient technique in S_n theory) can be derived to circumvent this problem.

In the next chapter a different numerical approach is developed to handle Fokker-Planck transport in both field-free and magnetized plasmas.

REFERENCES

1. T.A. Mehlhorn and J.J. Duderstadt, J. of Comp. Phys. 38(1980), 86 and references therein.

2. B.G. Carlson and K.D. Lathrop in "Computing Methods in Reactor Physics", H. Greenspan, C.N. Kelber, and D. Okrent, eds., Gordon and Breach, New York, 1968.

3. J.S. Chang and G. Cooper, J. of Comp. Phys. 6(1970), 1.

4. B.L. Buzbee, G.H. Golub, and C.W. Nielson, SIAM J. Numer. Anal. 7, 4(1970), 637.

5. E. Isaacson and H.B. Keller, "Analysis of Numerical Methods", John Wiley and Sons, New York, 1966.

6. G.I. Bell and S. Glasstone, "Nuclear Reactor Theory", Van Nostrand Reinhold, New York, 1970.

7. L. Spitzer, Jr., "Physics of Fully Ionized Gases", Interscience, New York, 1962.

CHAPTER IV

CHARGED PARTICLE TRANSPORT IN A MAGNETIZED PLASMA: A SIMULATION OF THE FOKKER-PLANCK EQUATION

An Implicit Monte Carlo Technique

In this chapter, a Monte Carlo technique is developed to simulate the behavior of test particles as they collisionally interact with a background plasma. The Monte Carlo procedure is based upon probabilities derived from the Fokker-Planck equation. Most simulations to date have focused on the modeling of collisionless plasmas and the phenomenon associated with them stemming from self-consistent interaction. In this analysis, the test particles will not be allowed to perturb the background plasma and the interaction between them will be ignored such that the results of these simulations will be equivalent to those obtained by integrating the linear Fokker-Planck equation. Also, the methods to be developed here will be applicable to both magnetized and field-free plasmas as will now be shown.

In this Monte Carlo approach, each test particle from an initial sample is allowed to change its velocity and position over a time step according to the collisionless equations of motion. In reality though, during this time step Δt, each particle has experienced some amount of deflection and some amount of energy loss. The exact amounts of deflection and energy loss for each particle would be difficult to obtain since this would mean analyzing each collision in detail. Clearly this is next to impossible since the microfields responsible for each instantaneous encounter would have to be

ascertained. Instead of trying to analyze the slowing down process in this manner. the problem can be approached from the point of view in which the details of each separate collision become unimportant but where the average values of deflection and energy loss acquired by the particles after several collisions becomes of interest.

If these expected values are assigned to each particle at the end of a given time step, then on the average, the particle will slow down and be deflected in much the same way that would occur if each collision was analyzed in detail. Clearly, since the particles are advanced by the collisionless equations of motion, the time steps must be kept small so that the deflections assigned to them at the end of a given time step truly reflect the deflection that they have actually acquired. Oliphant and Nielson[1] first used such an approach in order to calculate the effects of collisions among a single species plasma on the growth of instabilities. In this work, the concern will be on the study of transport of fast ions in a multi-species plasma. In the remainder of this section the equations of motion that are used to advance the particles will be developed.

The collisionless zeroth order motion of a charged particle interacting with a magnetic field can be obtained from the Lorentz equation

$$\frac{d\underline{v}}{dt} = \frac{e}{m}(\underline{v} \times \underline{B}) \quad . \tag{4-1}$$

For a particle streaming in a field-free plasma, Eq. (4-1) can be quickly integrated to yield

$$\underline{v} = \underline{v}_o$$

$$\underline{r} = \underline{v}_o t + \underline{r}_o \tag{4-2}$$

whereas the dynamical equations for a particle in a constant magnetic field are obtained by considering the individual components of Eq. (4-1) in a given coordinate system. If the constant field lies along the $\hat{z}$ direction of an $\hat{x},\hat{y},\hat{z}$ coordinate system and is given by $\underline{B} = B\hat{z}$, the particle will gyrate diamagnetically around field lines with velocities and orbits given by

$$v_x = v_\perp \cos\omega_c t \qquad v_y = v_\perp \sin\omega_c t \qquad v_z = v_{zo} \tag{4-3}$$

$$x - x_o = r_\perp \sin\omega_c t \qquad y - y_o = r_\perp \cos\omega_c t \qquad z = v_{zo} t + z_o$$

where $v_\perp = (v_{xo}^2 + v_{yo}^2)^{1/2}$, ω_c is the cyclotron frequency ZeB/m and $r_\perp = v_\perp/\omega_c$ is the gyroradius.

Hockney[2] first introduced a finite difference approximation of Eq. (4-2) that would insure that the orbits obtained for particles gyrating in a constant magnetic field, projected on a plane perpendicular to the field, would close upon themselves as circles with the correct gyrofrequency. This leap-frog scheme is given as

$$\frac{\underline{v}(t+\Delta t) - \underline{v}(t)}{\Delta t} = \frac{e\alpha}{m}\left[\frac{\underline{v}(t+\Delta t) + \underline{v}(t)}{2} \times \underline{B}\right] \tag{4-4}$$

$$\frac{\underline{r}(t+\Delta t) - \underline{r}(t)}{\Delta t} = \underline{v}(t+\Delta t)$$

where $\alpha = \tan(\omega_c \Delta t/2)/(\omega_c \Delta t/2)$ and Δt is the computer time step.

In the following section, cylindrical configuration space coordinates and spherical velocity space coordinates will be used to

describe a particle's position and velocity. These systems are shown in Fig. 16 from which the components can be seen to be

$$\begin{aligned} x &= r\cos\phi & v_x &= v\sin\theta\cos\omega \\ y &= r\sin\phi & v_y &= v\sin\theta\sin\omega \\ z &= z & v_z &= v\cos\theta \ . \end{aligned} \tag{4-5}$$

In these coordinate sytems Eqs. (4-4) take the component forms

$$\begin{aligned} v_x &= \frac{[1 - (\omega_c \alpha \Delta t/2)^2]v_{xo} + \omega_c \alpha \Delta t v_{yo}}{[1 + (\omega_c \alpha \Delta t/2)^2]} \\ v_y &= \frac{[1 - (\omega_c \alpha \Delta t/2)^2]v_{yo} - \omega_c \alpha \Delta t v_{xo}}{[1 + (\omega_c \alpha \Delta t/2)^2]} \\ v_z &= v_{zo} \end{aligned} \tag{4-6}$$

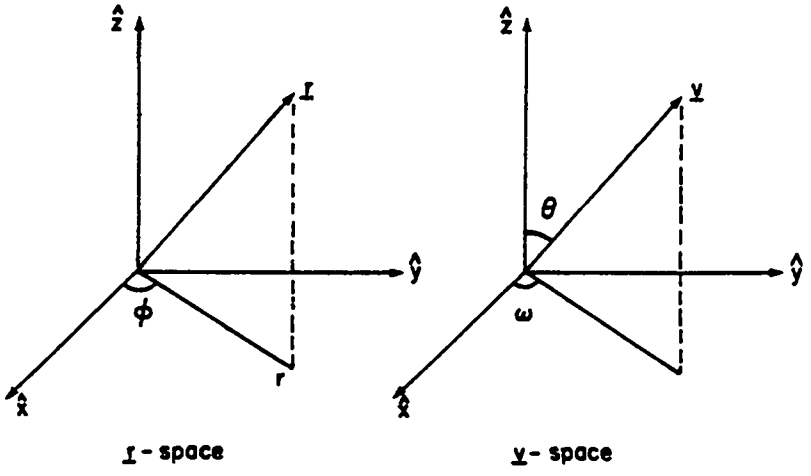

Fig. 16.--Coordinate systems for particle simulation

and

$$x = \Delta t v_x + x_o$$

$$y = \Delta t v_y + y_o \qquad (4\text{-}7)$$

$$z = \Delta t v_z + z_o \quad .$$

Eqs. (4-2), (4-6) and (4-7) constitute the governing dynamical equations which will describe the motion of test particles in between collision events.

Collision Probabilities

The expected time in which a test particle deflects by an angle θ in the laboratory frame can be calculated from the Fokker-Planck equation and in particular, the time in which a test particle deflects by 90^o can be calculated by taking the $v_\perp^2$ moment of the FP equation and then defining

$$\tau_d = v^2 / \left(\frac{\partial v_\perp^2}{\partial t}\right) \quad . \qquad (4\text{-}8)$$

This is the well known "deflection time" where

$$\frac{\partial v_\perp^2}{\partial t} = \int d\underline{v} \left(\frac{\partial f_a}{\partial t}\right)_{F\text{-}P} v_\perp^2 \qquad (4\text{-}9)$$

and where the distribution of test particles at t=0 is assumed to have the form $f_a(\underline{x},\underline{v},t=0) = n_a(\underline{x},t=0)\,\delta(\underline{v} - \underline{v}_o)$ and where the background distributions are taken to be Maxwellian. Montgomery and Tidman[3] give τ_d as

$$\tau_d^{-1} = \frac{2\gamma}{v^3}\frac{\partial}{\partial v}\left\{\sum_b Z_b^2 \ln\Lambda_b \frac{1}{a_b v}\left[\frac{v a_b^{1/2}}{\pi^{1/2}} e^{-a_b v^2}\right.\right.$$

$$\left.\left. + \left(\frac{1}{2} + a_b v^2\right)\mathrm{erf}(a_b^{1/2} v)\right]\right\} \qquad (4\text{-}10)$$

where $\gamma = n_o e^4 Z^2/4\pi\varepsilon_o^2 m^2$ and n_o is the background plasma density and where $a_b = m_b/2kT_b$. If the derivative in this expression is performed, one obtains the working form of the deflection time as

$$\tau_d^{-1} = \frac{2\gamma}{v^3}\sum_b Z_b^2 \ln\Lambda_b \left\{\mathrm{erf}(a_b^{1/2} v)\left(1 - \frac{1}{2a_b v^2}\right)\right.$$

$$\left. + \frac{e^{-a_b v^2}}{\pi^{1/2} a_b^{1/2} v}\right\} \quad . \qquad (4\text{-}11)$$

The relaxation time for an accumulated deflection and Θ ($\theta < 90^o$) is then determined by[4]

$$\tau_\Theta = \tau_d \sin^2\Theta \quad . \qquad (4\text{-}12)$$

The number of times that a test particle is deflected by this expected amount in a given time step is then simply

$$N_\Theta = \Delta t/\tau_\Theta \qquad (4\text{-}13)$$

so that at the end of that time step the particle is forced to change direction by an amount $N_\Theta \cdot \Theta$. Note that the angle Θ can be fixed to be any value between 0^o and 90^o. Note also that the value of N_Θ as

computed from Eq. (4-13) may not be an integer. Integer values of the number of deflections to occur in a time step can be obtained though by a simple Monte Carlo selection which will not bias the results of Eq. (4-13) over many time steps. As is shown in Fig. 17 if I represents an integer just below N_Θ and I+1 one just above, a random number ξ can be used to determine what integer value to use in the calculation as

$$\text{if } \xi < (N_\Theta - I) \quad \text{choose } I+1 \qquad (4\text{-}14)$$

$$\xi > (N_\Theta - I) \quad \text{choose } I \quad .$$

Once the integer number of Θ^o deflections has been determined, each deflection can be performed in a simple velocity space coordinate

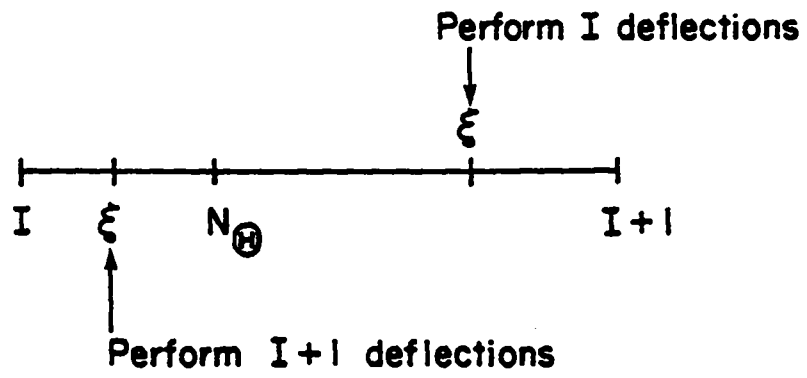

Fig. 17.--Method for determining the integer number of Θ^o deflections to be performed

system $\hat{x}'',\hat{y}'',\hat{z}''$ in which the pre-collision velocity vector $\underline{v}_i$ lies along the $\hat{x}''$ axis (Fig. 18). The transformations from the laboratory system to the double primed coordinate system can be accomplished in two steps. First, the initial velocity is rotated into a frame in which it lies in a plane formed by the $\hat{x}'\hat{y}'$ vectors of an $\hat{x}',\hat{y}',\hat{z}'$ system. This transformation is easily shown to be

$$\begin{aligned} v_x' &= v_x\cos\omega + v_y\sin\omega \\ v_y' &= -v_x\sin\omega + v_y\cos\omega \\ v_z' &= v_z \end{aligned} \tag{4-15}$$

From this system, the velocity can then be transformed easily into an $\hat{x}'',\hat{y}'',\hat{z}''$ system in which it lies along the $\hat{x}''$ axis with the transformation equations

$$\begin{aligned} v_x'' &= v_x'\cos\theta + v_z'\sin\theta \\ v_y'' &= v_y' \\ v_z'' &= -v_z'\sin\theta + v_z'\cos\theta \end{aligned} \tag{4-16}$$

where θ is the angle through which the $\hat{x}',\hat{x}',\hat{z}'$ system would have to be rotated so as to lie along the $\hat{x}'',\hat{y}'',\hat{z}''$ system.

In order to perform the Θ^o deflection in the simple system, the velocity vector is first rotated Θ^o onto the $\hat{x}''\hat{y}''$ plane. Then a random azimuthal direction is chosen as $\beta = 2\pi\xi$ where ξ is a random number. The final velocity's components in that frame are then given by

$$\begin{aligned} v_{xf}'' &= v_{xi}''\cos\Theta \\ v_{yf}'' &= v_{yi}''\sin\Theta\cos\beta \\ v_{zf}'' &= v_{zi}''\sin\Theta\sin\beta \quad . \end{aligned} \tag{4-17}$$

The transformations back to the laboratory system shown in Fig. 16 can easily be accomplished by changing the transformation angles to their negatives so that

$$\begin{aligned} v'_x &= v''_x\cos\theta - v''_z\sin\theta \\ v'_y &= v''_y \\ v'_z &= v''_x\sin\theta + v''_z\cos\theta \end{aligned} \tag{4-18}$$

and finally

$$\begin{aligned} v_x &= v'_x\cos\omega - v'_y\sin\omega \\ v_y &= v'_x\sin\omega + v'_y\cos\omega \\ v_z &= v'_z \quad . \end{aligned} \tag{4-19}$$

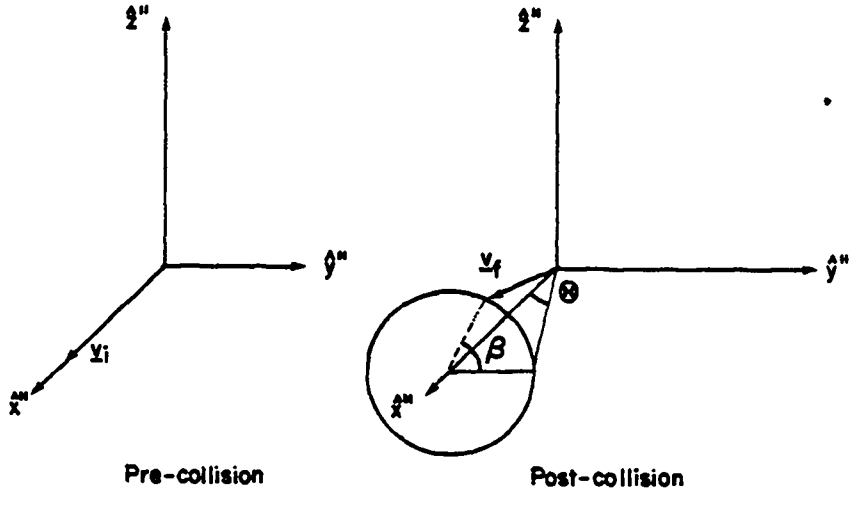

Fig. 18.--The pre and post-collision velocities $\underline{v}_i$ and $\underline{v}_f$

In these calculations, only the direction of the velocity vector is altered according to the amount dictated by Eq. (4-13) while its magnitude is kept constant. The next section describes how this magnitude is changed, again according to an expectation value calculated from the FP equation.

Energy Deposition

The expected amount of energy lost by a test particle as it scatters on a background plasma within a given time step can also be calculated from the Fokker-Planck equation as

$$\Delta E = \Delta t \frac{\partial E}{\partial t} = -E \frac{\Delta t}{\tau_E} \tag{4-20}$$

where τ_E is the "energy exchange" time and is also given in Ref. 3 as

$$\tau_E = -v^2/\gamma \sum_b \ln \Lambda_b Z_b^2 \{2v \frac{\partial}{\partial v}[(1+\frac{m}{m_b})\frac{\mathrm{erf}(a_b^{1/2}v)}{v}]$$

$$+ (\frac{2}{v}\frac{\partial}{\partial v} + \frac{\partial^2}{\partial v^2})[\frac{e^{-a_b v^2}}{\pi^{1/2} a_b^{1/2}} + (\frac{1}{2} + a_b v^2)\frac{\mathrm{erf}(a_b^{1/2}v)}{a_b v}]\} \quad . \tag{4-21}$$

If the derivatives in this expression are taken, the final working form can be shown to be

$$\tau_E = -v^2/\gamma \sum_b \ln \Lambda_b Z_b^2 \{(1+\frac{m}{m_b})\frac{4a_b^{1/2} e^{-a_b v^2}}{\pi^{1/2}}$$

$$- \frac{m2}{m_b v}\mathrm{erf}(a_b^{1/2}v)\} \quad . \tag{4-22}$$

The new velocity magnitude at the end of a time step can then be calculated from the expression for energy conservation as

$$E_{new} = E_{old} - \Delta E \quad . \tag{4-23}$$

As the energy of the test particles is lost to the background plasma in time, it is partitioned to each of the background species present. This partitioning can also be obtained from the energy exchange time since it can written as the sum of a number of terms corresponding to the number of background species present. In the case of slowing down on a two component plasma consisting of electrons and ions

$$\tau_E = \tau_i + \tau_e \tag{4-24}$$

such that the percent energy partitioned to each species can be obtained as

$$\% \text{ to ions} = (1 - \tau_e/\tau_E)\Delta E \tag{4-25}$$

$$\% \text{ to electrons} = (1 - \tau_i/\tau_E)\Delta E \quad . \tag{4-26}$$

In this algorithm the energy deposition calculation is discontinued for a test particle when its velocity has reached the value corresponding to the thermal velocity at the background temperature

$$v_{i_{th}} = \left(\frac{2kT}{m_i}\right)^{1/2} \quad . \tag{4-27}$$

At this velocity, if the particle is still within the system, it is

still allowed to collide (change directions) although it no longer deposits energy.

The spatial zoning increment Δr is fixed at the begining of the program such that the zone in which a particle deposits its energy can be obtained from the expression

$$i = \frac{(x^2 + y^2)^{1/2}}{\Delta r} + 1.0 \quad . \tag{4-28}$$

It is noted that the computer will determine the zone number as an integer with the above expression. If "i" is found to be greater than the total number of zones in the system, the particle is considered lost.

Results

The results obtained for transport problems with the method detailed above can be compared to those obtained with the matrix factorization method for the case of transport in a field-free cylindrical plasma. In order to make this comparison, once again consider the example of an initial burst of 3.5 MeV alpha particles emitted from the origin, slowing down in a D-T plasma at density 5.12 x $10^{28} m^{-3}$ and at a temperature of 50 keV. Again $\Delta r = 7.742 \times 10^{-3} m$. The deposition profiles generated by the Monte Carlo technique are shown in Figs. 19 and 20 and are compared to those obtained by CYTRAN. In the MC method the scattering angle was set to be $\Theta = 5^{o}$ and 500 particles were generated in random directions at t=0 at the origin in order to simulate an initially isotropic delta distribution function. It was found that the results obtained by the MC method were fairly insensitive to the choice of scattering angle Θ as long as it was kept to within small values ($\Theta < 10^{o}$). In all of the examples to follow Θ will be set to 5^{o}.

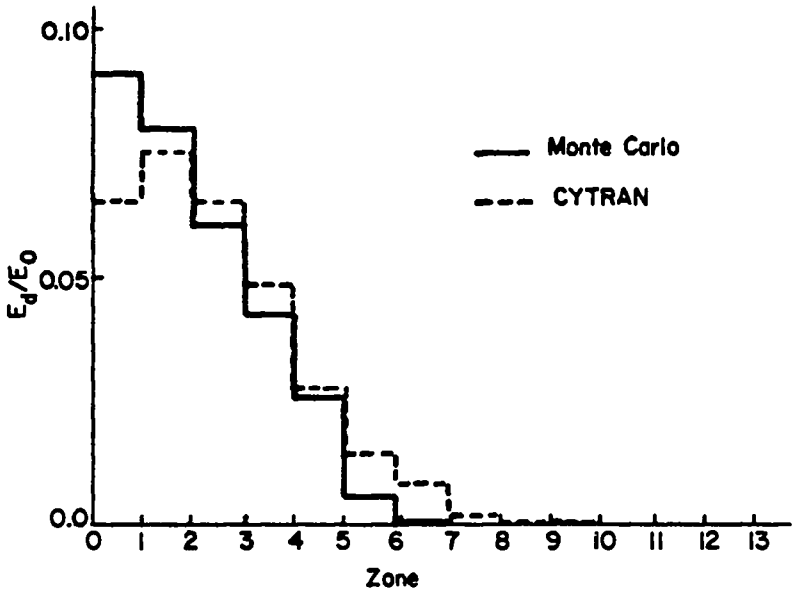

Fig. 19.--Fractional deposition per zone to electrons as calculated by Monte Carlo and CYTRAN

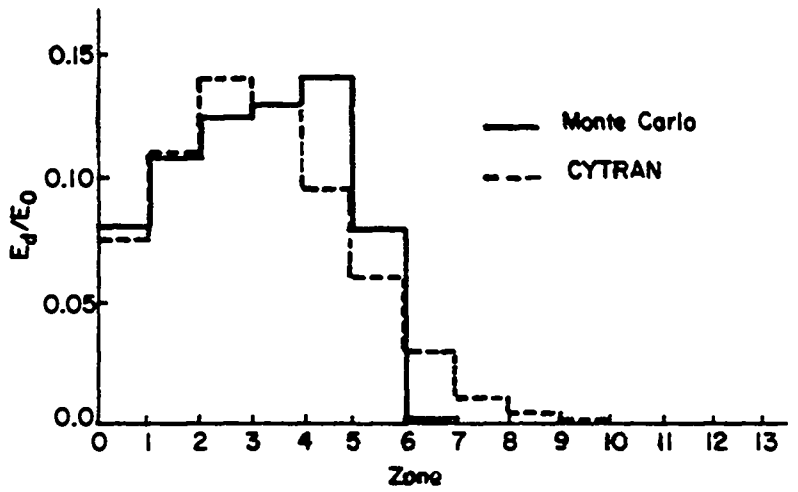

Fig. 20.--Fractional deposition per zone to ions as calculated by Monte Carlo and CYTRAN

For the case of deposition to electrons [Fig. 19] it is seen that the results are in good agreement except for the deposition in the first zone. The MC method predicts higher deposition there but it should be remembered, as was shown in Figs. 16 and 17, that many χ angle intervals are necessary in CYTRAN to predict the particle behavior correctly. In Fig. 16 as these intervals were increased, so did the deposition in the first zone. In the case of deposition to ions, the results are again in roughly good agreement [Fig. 20]. In Fig. 15, as the number of χ intervals in CYTRAN is increased to 16 it is seen that the deposition in the first zones increases and that the deposition in the peak zones diminishes to values near those predicted by MC. In both cases of deposition to electrons and ions, the MC method brings the particles to an abrupt halt before CYTRAN does. It is believed that the slight tails on the profiles generated by CYTRAN are a result of the smoothing that occurs in the finite difference approach.

Fig. 21 shows the tracks of the first 50 alpha particles that were followed in the example described above. Each dot represents the position of a given particle at the end of a time step projected onto the x-y plane at $z = 0$. It can be seen that the dots on a given path grow closer together as the particles slow down and deflect while they scatter on the background plasma. From the same figure, it is noted that the RMS deflection during their initial flight is very small and the appreciable deflection does not occur until the particles are almost thermal. From this information it is verified that the discrete mesh in χ space of CYTRAN would indeed need many intervals in order to resolve these slight deflections.

In Fig. 22 the time history of the deposition to each of the species is shown. Note that the deposition rate is greater on electrons initially and that not until the alpha particles have slowed somewhat do they begin to lose more energy to the background ions. In the examples above the time step Δt was initially set to $\tau_s \times 10^{-2}$ where τ_s is the slowing down time for 3.5 MeV alpha particles on 50 keV electrons (8.47×10^{-9}sec) but it was adjusted such that Δt

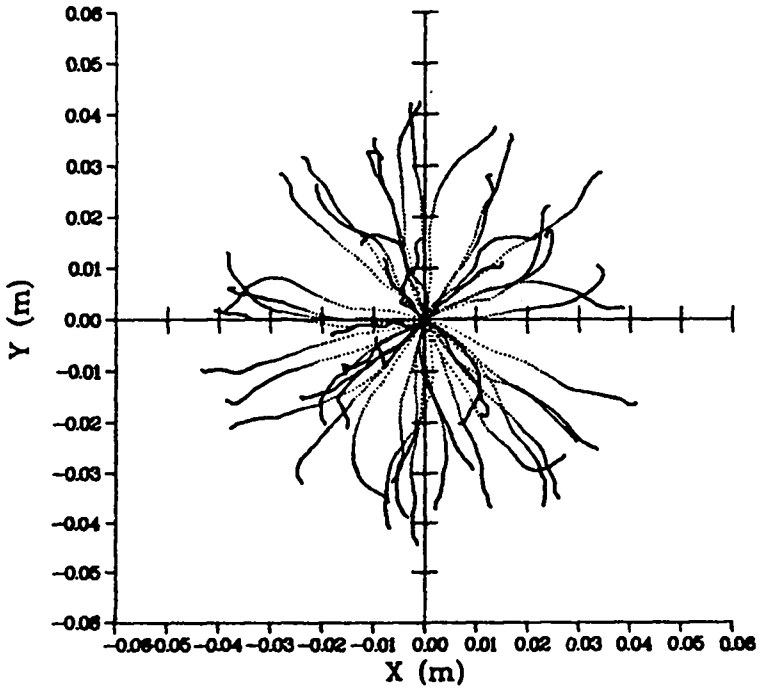

Fig. 21.--Alpha particle tracks after transporting from the origin in the field-free case

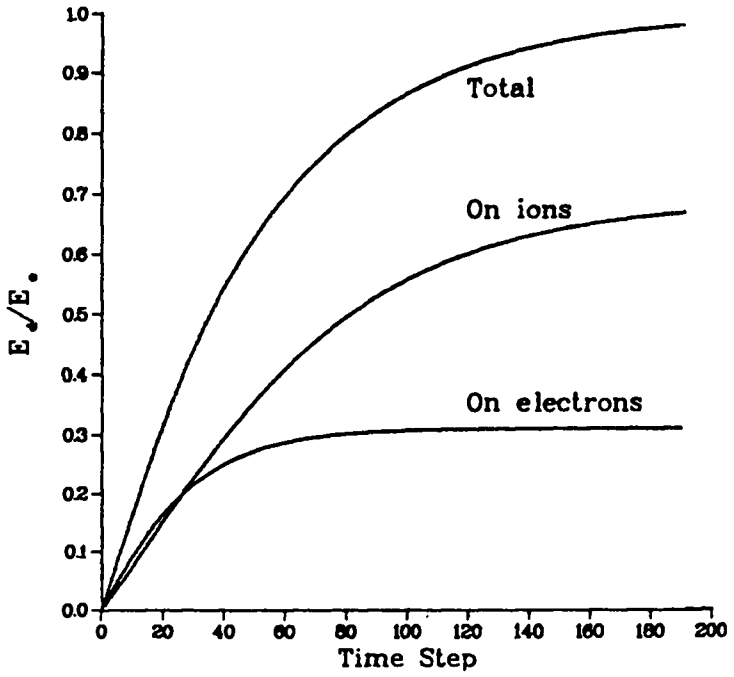

Fig. 22.--Time history of deposition to background ions and electrons

was always $\leq \tau_E/50$. In this way, the amount of energy deposited per time step would always be tractable and the number of collisions per time step per particle would remain small. As was explained earlier, this time step control is also necessary in order to show the true amount of deflection for each particle on the scatter plots. Although the deposition information in the plots above were obtained for an initial sample of 500 particles, the computer runs consumed only about 1 minute of CPU time. It was found that good results could be obtained with samples as low as 100 particles in which case only about 10 secs. of CPU time was needed.

In the following examples the same test problem described above (3.5 MeV alpha particles born at the origin) is used as a basis for cases in which an external magnetic field is activated. Here the field will always lie along the z axis. In Fig. 23, the orbits of the first ten (out of 500) particles are shown for a case in which the magnetic induction was set as b = 20 tesla but for which the plasmas were made collisionless. Here the paths of the test particles are just the orbit solutions of Hockney's equations Eqs. (4-6) and (4-7). It is seen that the particles retrace their circular paths without deflection with a maximum gyroradius $v_\perp/\omega_c$ = 0.01347m as can be verified in the figure. The smaller circular orbits are, of course, the projections on the x-y plane of the orbits of particles that had higher initial velocity components along the $\hat{z}$ direction. When collisions are allowed to occur, these orbits should deviate from their circular paths and furthermore, the gyroradii of the particles should decrease in time since their perpendicular velocity is being reduced as they lose energy to the background. Fig. 24 shows the same orbits of particles as in Fig. 23 but with collisions being allowed to occur. It is seen that the circular orbits degenerate as the particles lose their energy and that the radii of curvature indeed become extremely small and distorted as they near thermalization. The magnetic field should inhibit the flight of particles out of the system so that their energy is more locally deposited in the zones about their orbits. This is verified

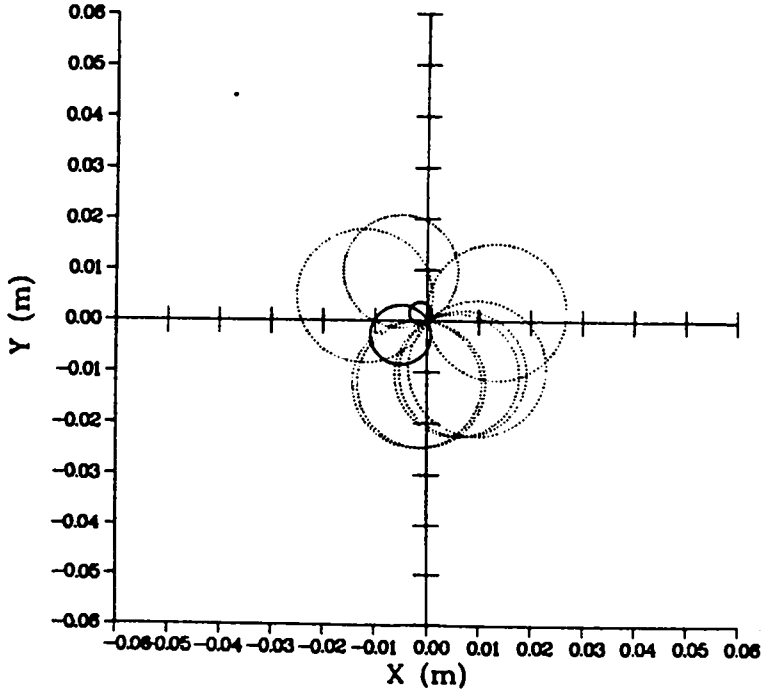

Fig. 23.--Free streaming orbits of 3.5 MeV alpha particles for B=20 tesla

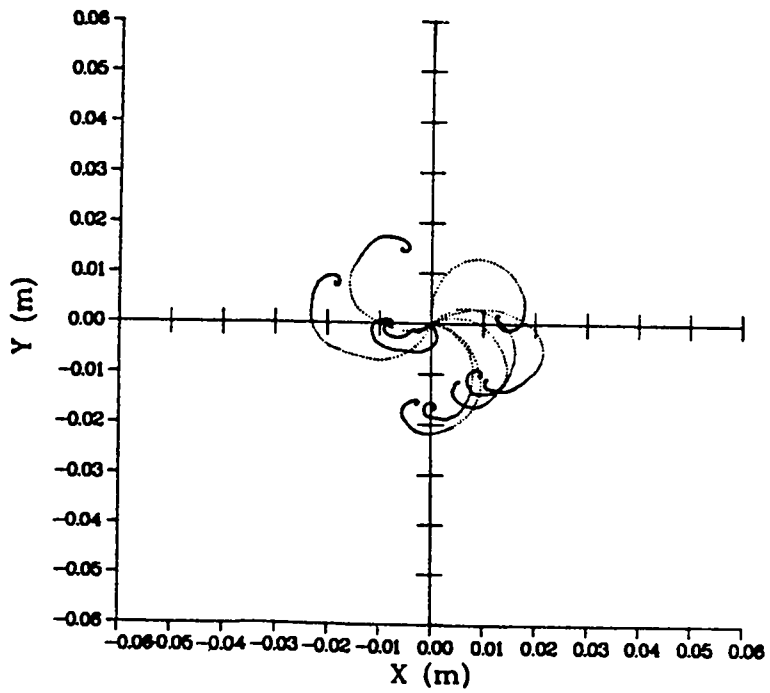

Fig. 24.--Orbits of alpha particles as they collisionally slow down with B=20 tesla

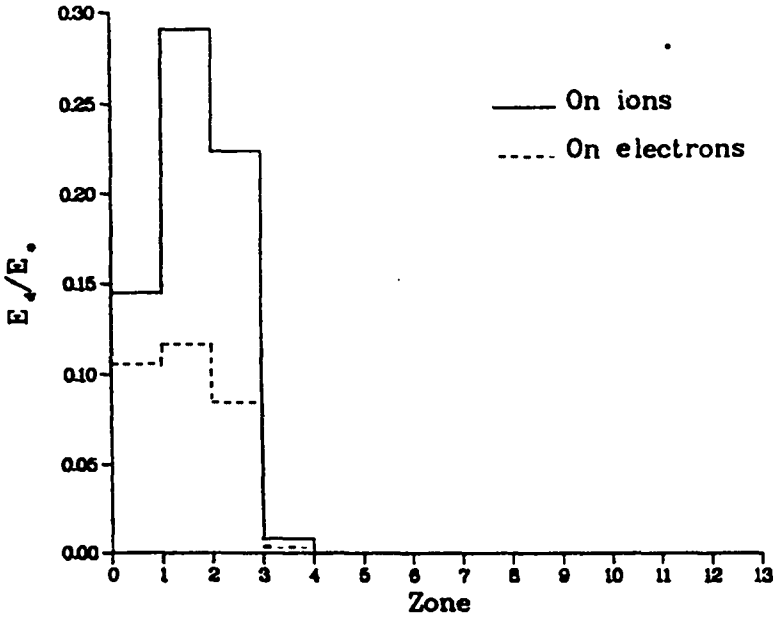

Fig. 25.--Fractional deposition per zone to ions and electrons with B=20 tesla

in Fig. 25 which shows much higher deposition to both electrons and ions in the first zones. In Figs. 26, 27, 28, and 29, the same graphs are shown for the cases in which the induction as set as B=10 tesla and B=.01 tesla. It is seen that the deposition profiles expand as the field strength decreases and that in the case of a weak field (B=.01 tesla) the results are almost identical to the field-free case. In all of these examples the initial time step was also taken to be $\tau_s \times 10^{-2}$ and each consumed approximately 1 minute of CPU time.

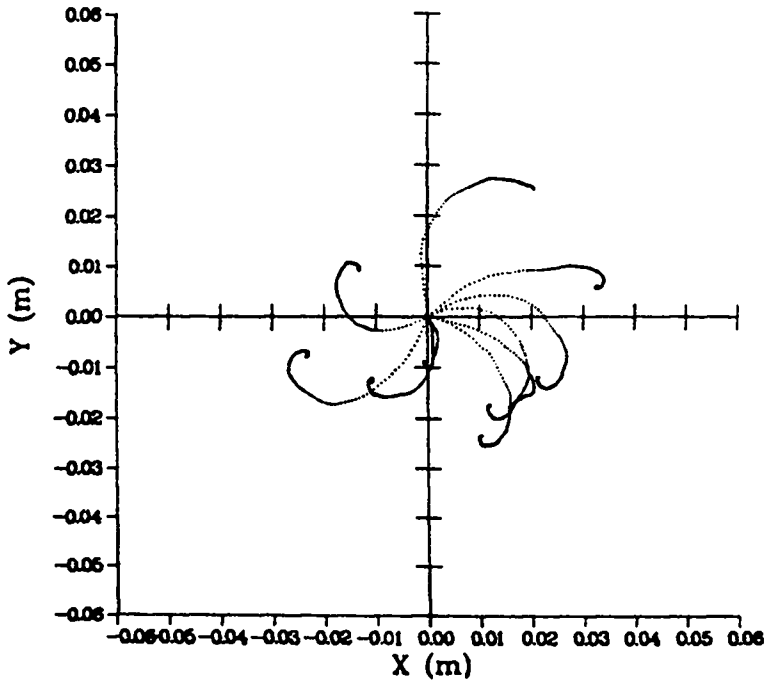

Fig. 26.--Orbits of alpha particles as they collisionally slow down with B=10 tesla

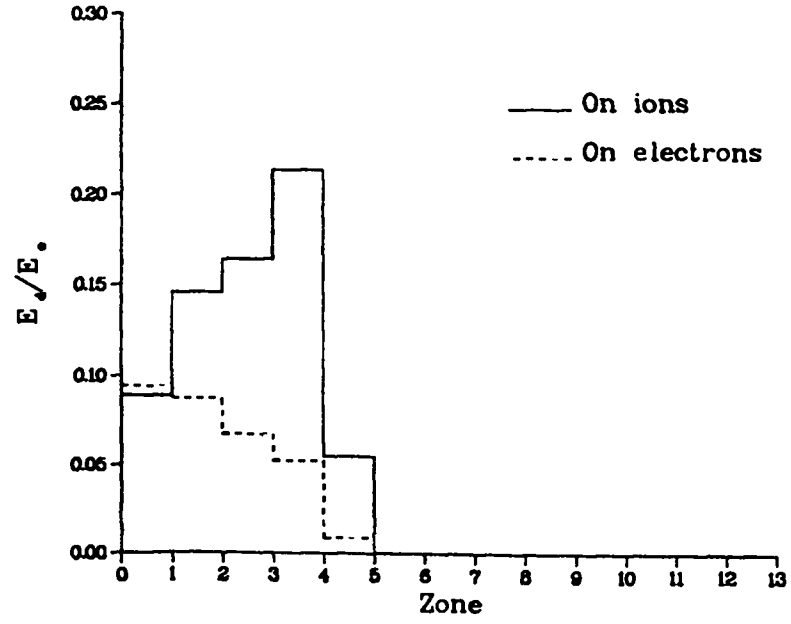

Fig. 27.--Fractional deposition per zone to ions and electrons with B=10 tesla

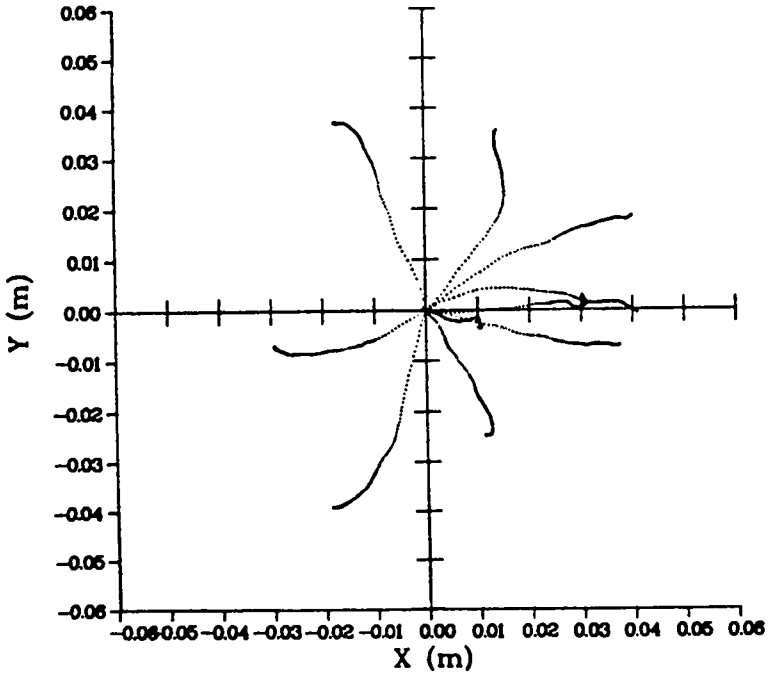

Fig. 28.--Orbits of alpha particles as they collisionally slow down with B=.01 tesla

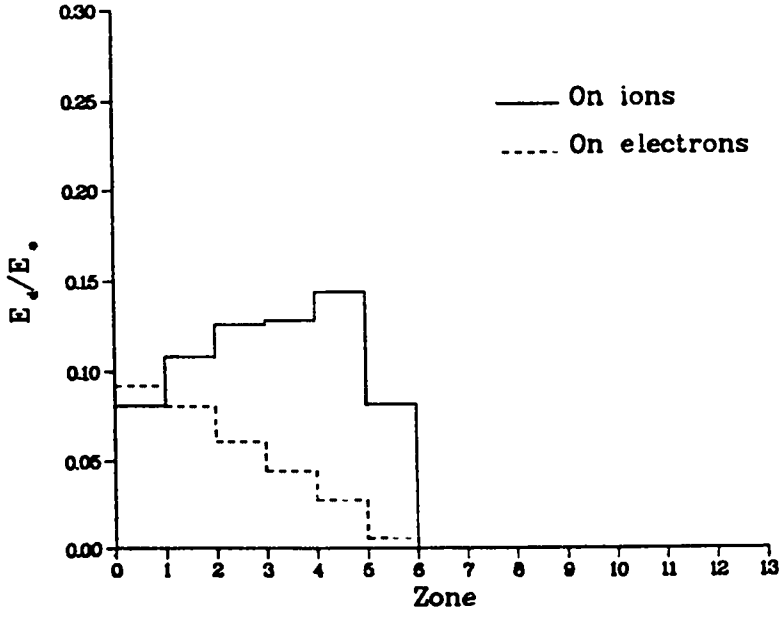

Fig. 29.--Fractional deposition per zone to ions and electrons with B=.01 tesla

A Treatment of Nuclear Scattering

As an energetic ion transports through a background plasma, it deflects and loses energy primarily as the result of many small angle collisions i.e., encounters with the fluctuating microfields of the background particles in its vicinity. The amount of energy that it transfers to either the background ions or electrons depends on the velocity of the test particle relative to the background particles' velocities. In any case, although the amount of energy lost by the test particle in a given period of time is a statistical quantity, an average or expected amount of energy lost in this process can be calculated for that period of time. As was shown in the last section, this energy exchange time and other characteristic interaction times can be used to predict the dynamical behavior of the test particles.

A phenomenon which also occurs in the collisional transport process is the direct binary interaction between the test ions and the background ions which result in the test particle's deflection through large laboratory angles. For this case, the amount of energy lost by a test particle can take on a wide range of values which depend on the details of the collision. As such, characteristic times cannot be used to predict the dynamical state of a particle at the end of a given time period and only a detailed analysis of each large angle collision occuring in that time step will suffice to determine that state.

The probability that a test ion suffers a large angle collision in a given computer time step, Δt, can be determined from the following analysis. If P(dt) is the probability that a test particle enters a large angle collision in a time interval dt, then

$$P(dt) = \frac{dt}{t_c} \qquad (4\text{-}29)$$

where dt will be restricted as $dt \leq t_c$ and where t_c is defined as the large angle collision time by

$$t_c = \frac{1}{v\Sigma_{total}} \quad . \tag{4-30}$$

Here v is the pre-collision velocity of the test particle and Σ_{total} is the macroscopic cross section $n_i\sigma(E)$ where n_i is the background ion density and where $\sigma(E)$ is the center of mass angle integrated cross section for large angle scattering at energy E. The energy E in $\sigma(E)$ is the energy available for a nuclear reaction to take place i.e, $E = E_{cm} + Q$ where E_{cm} is the total kinetic energy in the center of mass and Q is difference between the final and initial laboratory kinetic energies. Since the processes to be considered here will always be elastic collisions, Q will always be identically equal to zero. In order to determine $E = E_{cm}$, a collision partner will always be sampled for from the background Maxwellian ion distribution such that $E_{cm} = \frac{1}{2}\mu_{ab}v_{rel}^2$ can be calculated.

The cross section $\sigma(E)$ is given by

$$\sigma(E) = 2\pi\int_{\theta_o}^{\pi} \sigma(E,\theta)\sin\theta \, d\theta \tag{4-31}$$

where θ_o is the cutoff angle which will define the onset of large angle scattering. In this work θ_o will be set to 5^o. Note that the upper limit on the integral of Eq. (4-31) will be $\pi/2$ instead of π for collisions occuring between identical particles[5].

The probability that the test ion will survive without collision in the first time interval is then $[1 - P(dt)]$. Hence, the probability that it survives without collision during n time intervals is $[1 - P(dt)]^n$. Here $t = n \cdot dt$ so that this probability can be rewritten in the form

$$[1 - P(dt)]^n = \left[1 - \frac{t}{nt_c}\right]^n \quad . \tag{4-32}$$

If the quantities $l=-t/t_c$ and $m=n/l$ are defined, Eq. (4-32) takes the form

$$[1 - P(dt)]^n = \left[\left(1 + \frac{1}{m}\right)^m\right]^l \quad . \tag{4-33}$$

Now if the limit of small time intervals is taken i.e., $dt \to 0$, since $t=n \cdot dt$, n must approach ∞ for t to remain the same. From the definition of m, this limit also implies that $m \to \infty$. Recall that the base e of the natural logarithm is defined as

$$e = \lim_{m \to \infty} \left(1 + \frac{1}{m}\right)^m \tag{4-34}$$

so that the probability that no collision occurs in time t can now be obtained from Eq. (4-33) as

$$e^l = e^{-t/t_c} \quad . \tag{4-35}$$

From this expression then, the probability R(t) that a test particle does suffer a large angle collision during time t is then simply given by

$$R(t) = 1 - e^{-t/t_c} \quad . \tag{4-36}$$

The time t in this equation can be set equal to the computer time step Δt such that it will give the probability that a test ion

suffers a large angle collision in Δt. Note that if it is agreed from here on that the maximum number of large angle (l.a.) collisions per test ion per time step is to be limited to one, then Eq. (4-36) can be used to determine whether or not a collision occurs. This is done by sampling the interval $0 \leq R(t) < 1$ with a random number. The reason for limiting the number of collisions to one is that again, the equations of collisionless motion are used to move the particles through a distance $\underline{\Delta r}$ in the time step Δt after which a new velocity is assigned to them. This new velocity is the post collision velocity which may have a vastly different direcion and magnitude than the pre-colision velocity. In order for this type of analysis to be realistic, the distance traveled in the time Δt must be kept small. In order to insure that this is the case, the ratio of $\Delta t/t_c$ is kept small throughout the calculation. Normally this ratio itself would give the expected number of l.a. collisions per time step but since this number is being restricted here to a maximum of unity, sampling for the occurance of a l.a. collision in the interval $0 \leq \Delta t/t_c < 1$ is equivalent to sampling in the interval $0 \leq R(t) < 1$ as will be done in this work (to see this, merely expand the exponential in Eq. (4-36)).

If it has been determined that a test ion does indeed collide with its collision partner, its energy and direction are modified most conveniently in the center of mass (c.m.) system. In this system the c.m. scattering angle θ of the test ion is the only quantity that need be obtained since it is known that the recoil particle's final c.m. velocity will be oppositely directed. The c.m. scattering angle can be sampled for from its distribution function as

$$\xi = \frac{2\pi}{\sigma(E)} \int_{\theta_o}^{\theta} \sigma(E,\theta) \sin\theta \, d\theta \qquad (4\text{-}37)$$

where ξ is a random number and E is now the energy available for reaction i.e., $\frac{1}{2}\mu_{ab}V_{rel}^2$. This expression implicitly determines the

scattering angle since $\xi\sigma(e)$ is now the integrated cross section for scattering through angles between θ_o and θ. In reality though, since the cross sections are tabulated in various bins θ_i for a given reaction energy as

$$2\pi\int_{\theta_i}^{\pi} \sigma(E,\theta)\ \sin\theta\ d\theta \tag{4-38}$$

the scattering angle can be sampled for by the formula

$$2\pi\int_{\theta}^{\pi} \sigma(E,\theta)\ \sin\theta\ d\theta = \sigma(e)(1 - \xi)\ . \tag{4-39}$$

The L.H.S. of Eq. (4-39) is recognized as the cross section for scattering into c.m. angles greater that or equal to θ. Once this random cross section is determined, it can be compared to the tabulated cross sections. It will usually lie between those tabulated at some θ_i and θ_{i+1}. A simple linear interpolation is then used to obtain the final c.m. scattering angle. In the c.m. system, the initial and final magnitudes of the test particles velocity with respect to the c.m. are not affected by an elastic collision but its direction is changed through the c.m. angles θ and β. The c.m. scattering angle θ determined previously is the angle between the initial and final lines of flight of the test particle in the c.m. system while β is the c.m. azimuthal scattering angle.

The deflection of the test particle in the c.m. system can be performed in the more convenient coordinate system referred to earlier in which the pre-collision c.m. velocity is allowed to lie along an $\hat{x}''$ axis [Fig. 18]. This velocity is then rotated onto the $\hat{x}''\hat{y}''$ plane by the amount θ. A random azimuthal c.m. angle $\beta = 2\pi\xi$ is then chosen in order to place the final c.m. velocity randomly on the θ cone centered along the x'' axis. After this velocity is transformed back into the original velocity space system, the c.m. velocity v_{cm} is added to it to give the final velocity in the

laboratory system. This is the velocity that is assigned to the test particle at the end of a time step.

As in the case of transport with only small angle scattering, a particle which leaves the boundaries of the system is considered lost. Otherwise, it is allowed to deposit the amount of energy lost in the collision to the recoil particle. This recoil energy is usually non-negligible and as such, a proper treatment of charged particle transport for cases in which these nuclear elastic processes are taken into account, should provide for the transport of the recoil particles also. In the method used here, all of the recoil particles are transported from their point of origin along with the original particles, begining at the time step after the one in which they were created. The method is kept efficient though, by ignoring the lowest energy recoil particles. This is done by discriminating against those collisions which produce only slight test particle laboratory scattering angles. In this way only those recoil particles whose energies may significantly affect the deposition rates and profiles are followed in time. In all of the examples to follow, this angle discriminator will be set to allow the transport of recoil particles only if the original projectile is deflected by more than 10^{o} in the laboratory system.

Results

In the first few examples to follow, the transport of 4.5 MeV deuterons in a field free spherical system will be considered. A spherical background deuterium plasma will be taken to have a density of $1.28 \times 10^{28} m^{-3}$ and varying electron temperatures. The background ion temperatures will be set to values 50% greater than the electron temperatures in order to be able to compare the results with those obtained by Evans in Reference 6. In Ref. 6, the transport of charged particles in field free spherical deuterium plasmas is treated by an explicit Monte Carlo method i.e., by a method which transports one particle at a time until it either leaves the system

or until it thermalizes and becomes uninteresting. In order to match the zoning used in Ref. 6, the spherical shell zone widths in the first example will be set as $\Delta r=.02m$. In Fig. 30 the fraction of initial energy deposited per zone to both the background ions and electrons (total) is given as a function of radius for a case in which the electron temperature was taken to be 75 keV. It is seen that the inclusion of Coulomb-nuclear scattering (Monte Carlo) in this high temperature plasma has a significant effect on the deposition profile when compared to the profile generated by considering only small angle scattering (Rutherford). The results obtained here are seen to be in very good agreement with those obtained by Evans who also included Coulomb-nuclear processes in his calculation. The initial sample was comprised of 200 4.5 MeV deuterons originating from the center of sphere at t=0 in random directions. It was found that this 200 particle initial sample was usually sufficient to reproduce published results for cases in which

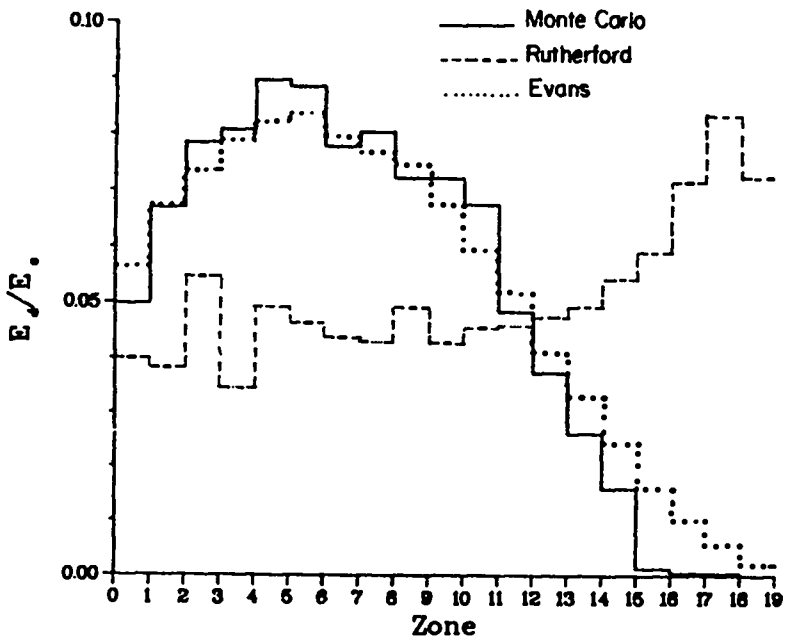

Fig. 30.--Fractional energy loss per zone for both small and large angle scattering in a 75 keV plasma

only small angle scattering is accounted for [c.f. Ref. 6]. It should be recalled though, that for runs in which the large angle scattering is activated, many recoil particles are created which are also transported along with the original sample. These additional knock-ons should then be expected to help improve the statistics of the problem. The fact that the results obtained by Evans, who used a 10,000 particle initial sample, are in good agreement with this method's results, seems to verify this.

In Figs. 31 and 32, the fractional deposition profiles are given for the cases in which the background electron temperatures are taken to be 25 and 10 keV respectively. In Fig. 31 the zone width was set as 7.5×10^{-3}m while in Fig. 32 the zone width is equal to 2.5×10^{-3}m. From these figures it can be seen that as the plasma temperatures are lowered while keeping the initial test deuteron's energy constant (4.5 MeV), the effects from large angle scattering processes diminish. In the case where Te=10 keV, the profiles given for small and large angle scattering are seen to converge. From this information it can be surmised that in low temperatures deuterium plasmas, one can ignore the l.a. scattering processes and that the dominant form of collisional energy loss will come from Rutherford scattering which is treatable by Fokker-Planck methods. For high temperature plasmas, the l.a. scattering mechanism for energy loss is seen to be extremely important. The change in the shape of the deposition profiles for these cases as compared to cases in which only small angle scattering is accounted for is attributable to higher partitioning of the original sample's energy to the background ions. This is, of course, due to the fact that many lower energy particles are created after large angle collisions which subsequently collide more frequently with the background ions that have lower thermal velocities than the background electrons.

In the following examples the transport of 4.5 MeV deuterons on a background plasma at a density of $5.12 \times 10^{28} m^{-3}$ and at T_e=75 keV will again be considered but with the configuration geometry now being taken to be cylindrical. The zone size in the remaining

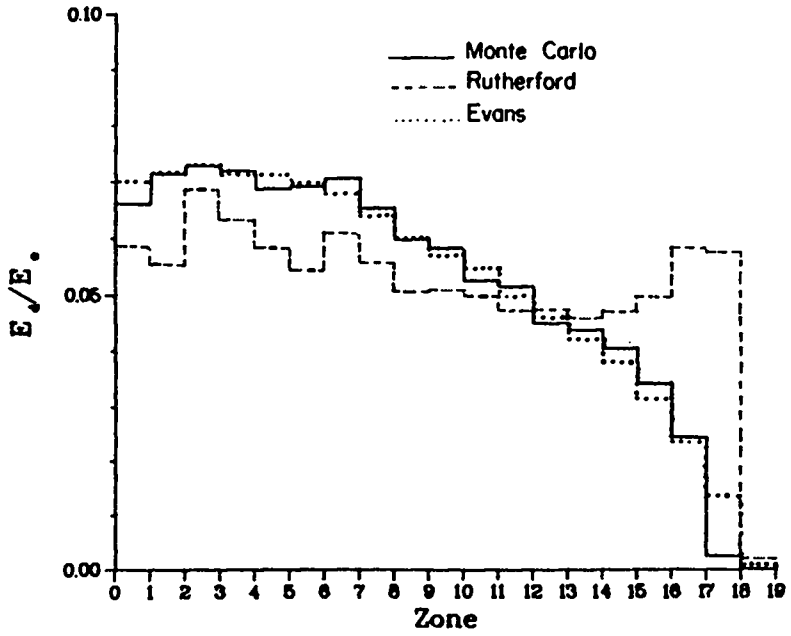

Fig. 31.--Fractional energy loss per zone for both small and large angle scattering in a 25 keV plasma

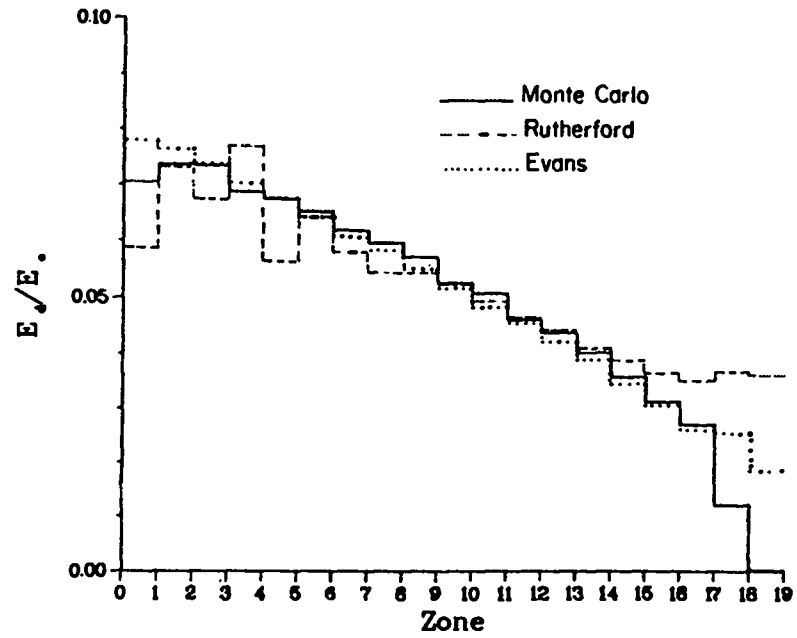

Fig. 32.--Fractional energy loss per zone for both small and large angle scattering in a 10 keV plasma

examples will be $\Delta r = .02m$. In Figs. 33 and 34, the deposition profiles are shown for the case of field free transport in an infinite cylindrical plasma. Fig. 33 shows the partitioning of the fraction of initial deuteron energy per zone to the background electrons and ions as a function of radius for a case in which only small angle scattering is considered. From the experience with the previous examples though, it can be expected that the inclusion of l.a. scattering should have a significant effect on the deposition profile. In Fig. 34 the fractional deposition per zone to both ions and electrons is shown for a computer run in which the l.a. scattering was included. The deposition profile is seen to be shifted to the left with a maximum occuring in the first few zones, indicating large energy losses in the accompanying l.a. scatter events occuring early on as the test particles move along their paths. This trend was also seen in the examples of transport in spherical systems. If an externally generated magnetic field is now

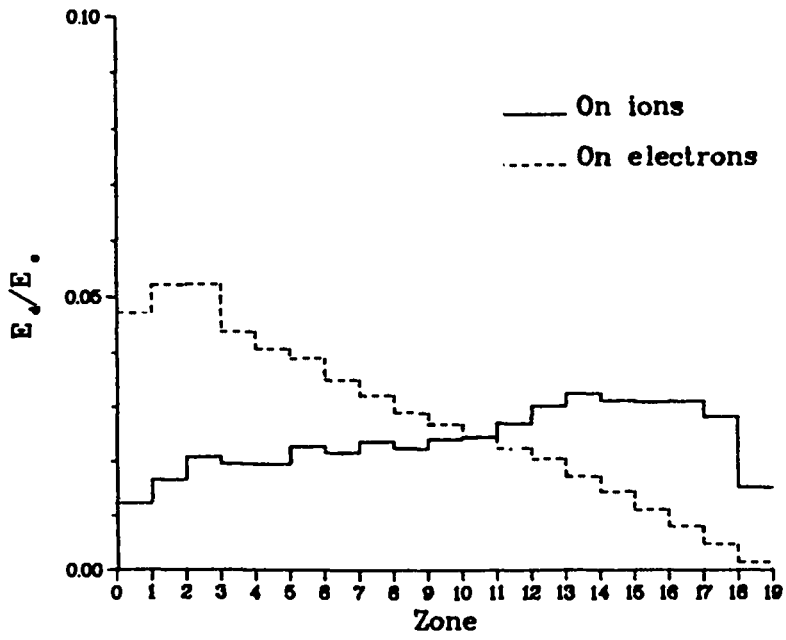

Fig. 33.--Fractional deposition per zone on ions and electrons for small angle scattering in a 75 keV plasma

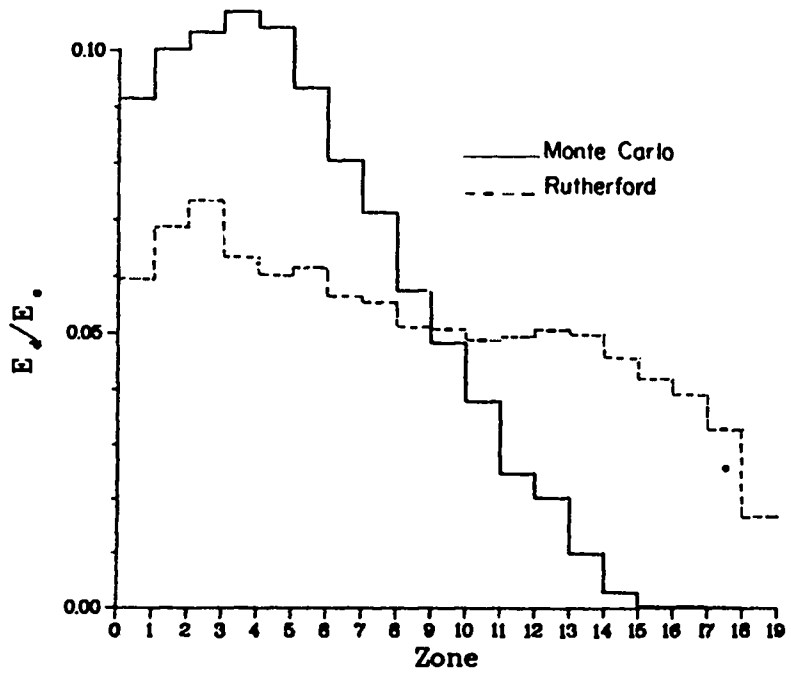

Fig. 34.--Fractional deposition per zone for both small and large angle scattering in a 75 keV plasma

imposed on this cylindrical system such that it lies uniformly along the $\hat{z}$ direction, the test particles will then gyrate about the field lines as they scatter and lose energy by both small angle (s.a.) and l.a. collisions in the 75 keV plasma. When the s.a. and l.a. collision routines are turned off, the particles gyrate in closed circular paths as shown in Fig. 35 for a case in which the magnetic induction was taken to be 5 tesla. Here the orbits of the first ten out of an initial 200 particle sample are shown. When the small angle scattering routines are reactivated, the particle tracks shown in Fig. 36 are obtained. It is seen that the deterioration of the orbits as the particle loses small amounts of energy in these collisions, is gradual. For this example, it is seen that noticeable deflection does not occur even through almost half of a gyroperiod. Eventually, though, when the particles begin to lose more energy to the ions, the orbits are seen to degenerate more quickly as the particles tend toward equilibrium. Fig. 37 shows that the deposition profiles for this case are much more localized, as would be expected

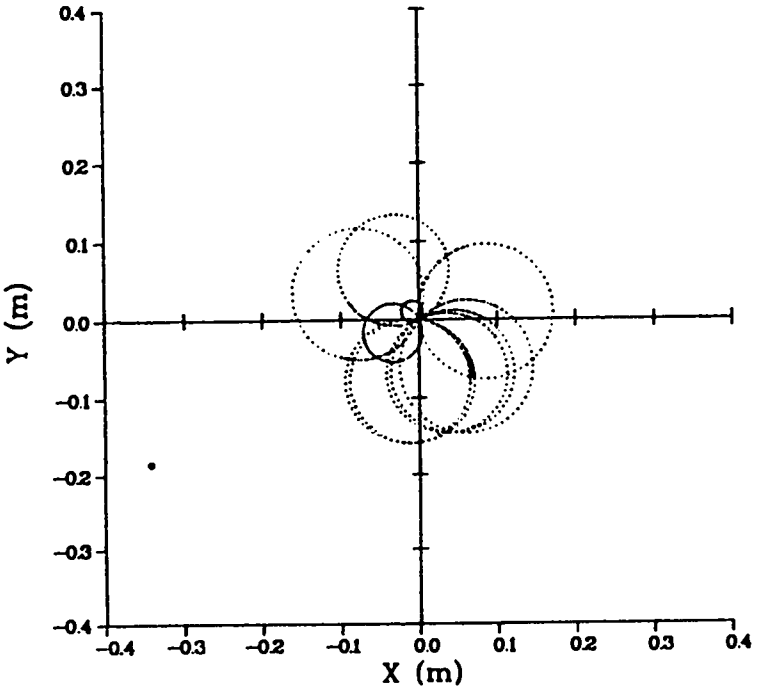

Fig. 35.--Orbits of 4.5 MeV deuterons for B=5 tesla

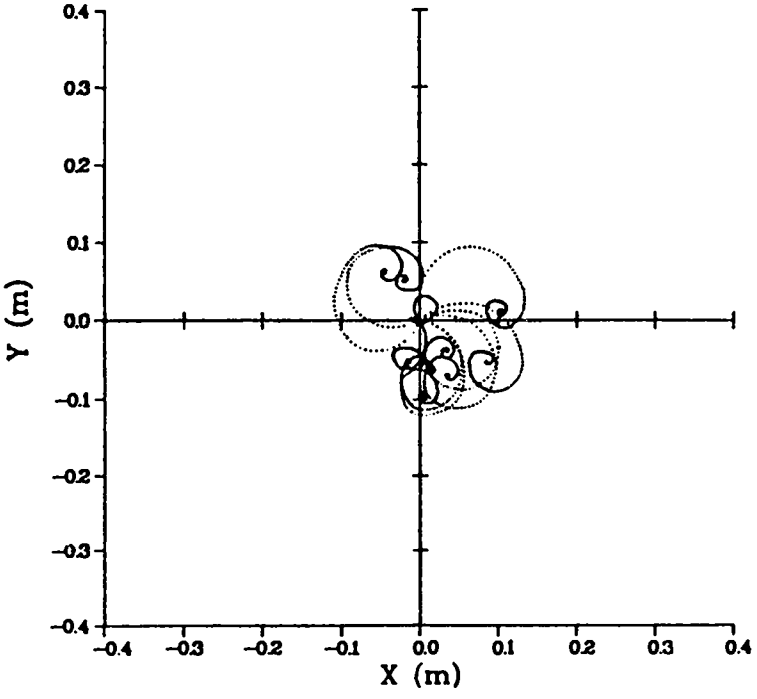

Fig. 36.--Orbits of 4.5 MeV deuterons for B=5 tesla as they slow down with small angle scattering

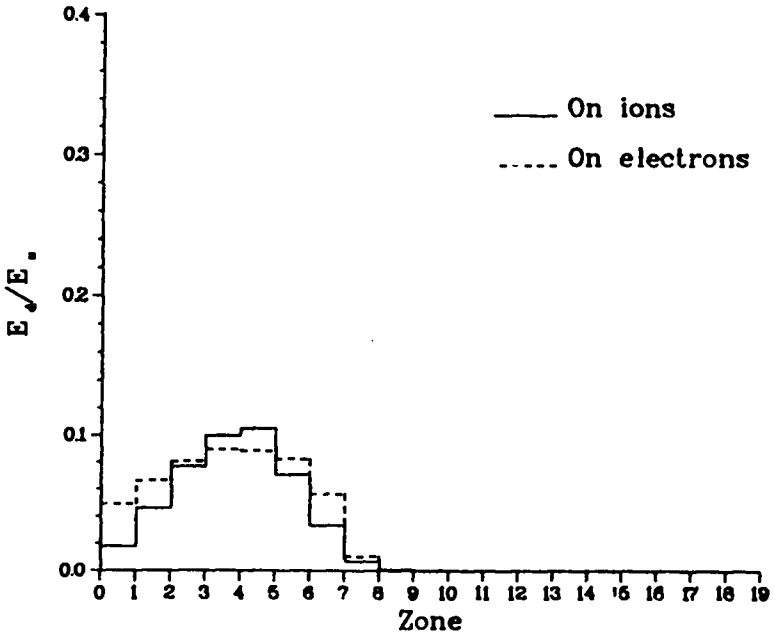

Fig. 37.--Fractional deposition per zone on ions and electrons for small angle scattering with B=5 tesla

for cases in which magnetic fields are used to confine particles. If the l.a. scattering routines are now activated along with the s.a. routines, the particle tracks shown in Fig. 38 are obtained. It is seen that the orbits degenerate much more quickly. This is possible because each of the test particles can now lose large amounts of perpendicular (and parallel) energy in the l.a. collsions that they encounter. The corresponding deposition profiles showing the partitioning of the fraction of initial energy per zone to the background ions and electons is shown in Fig. 39.

Conclusions

For the case of Fokker-Planck slowing down i.e., for collisional transport in the small angle scattering approximation, it has been shown that a Monte Carlo treatment of the collsions physics based on the expected values of the energy exchange and deflection times yields results which are in good agreement with those obtained by a

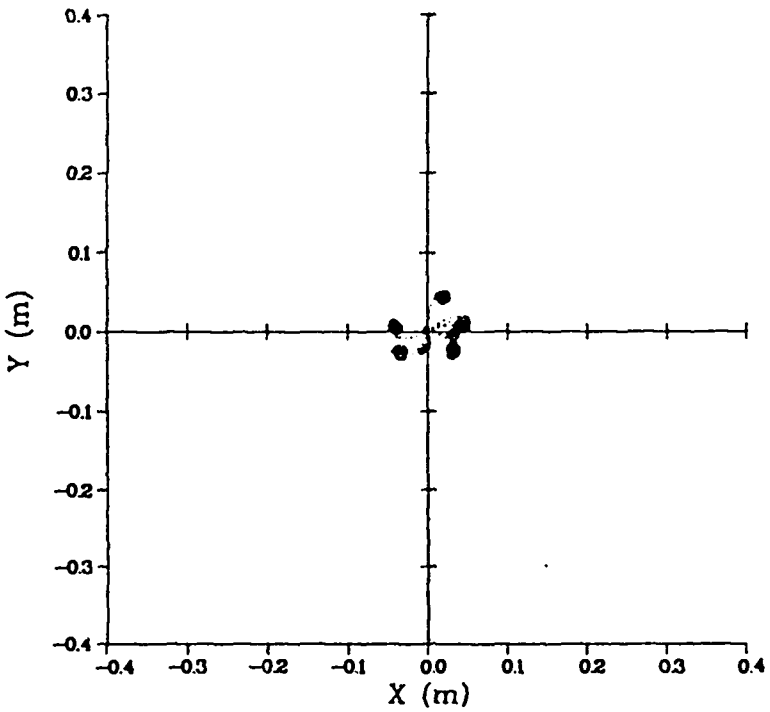

Fig. 38.--Orbits of 4.5 MeV deuterons for B=5 tesla as they slow down with large angle scattering

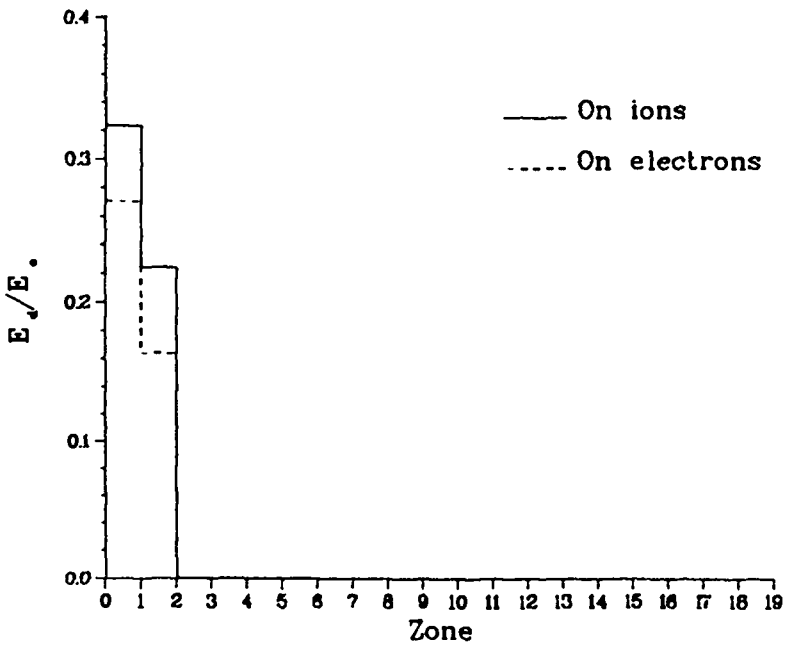

Fig. 39.--Fractional deposition per zone on ions and electrons for large angle scattering with B=5 tesla

finite difference technique. This Monte Carlo treatment allows the calculation of transport processes in both field free and magnetized plasmas.

The results of the transport of alpha particles in a magnetic field are verified by their agreement with those obtained in a field free mode in the limit of weak magnetic induction. For the case of transport in strong magnetic fields, it has been shown that the fast ions deposit their energy almost entirely in regions near their original orbits as expected, due to the confining effect of the magnetic field. In both cases of field free and magnetized transport, the calculations were carried out in a minimum of CPU time. This makes this method attractive for use both as a code in itself to determine deposition profiles and stopping lengths and also as a package which may be installed in larger time dependent magnetohydrodynamic codes in which charged particle heating effects are often needed.

It has also been shown that the inclusion of Coulomb-nuclear elastic scattering processes is of vital importance in the analysis of transport in high temperature plasmas. For plasma temperatures above approximately 10 keV, the effects from these large angle scattering events become noticeable and at higher temperatures, they may become a dominant mechanism for energy loss.

Various possibilities exist for the extension of these methods. One straightforward application would be found in the study of diffusion phenomenon in field free and magnetized plasmas. For this case, transport coefficients could be obtained which could then be compared to those calculated analytically and further, they may also be obtained in domains of temperatures and densities in which analytic results are scarce. Another possibility lies in the extension of this linear method to a form which is self-consistent. Again, since the particle advancement here is implicit, at the end of a given time step, the self-consistent fields generated by the particles themselves could be calculated. This extension would then

perhaps be a basis for the study of the effects of collisions on instabilities and other collective phenomenon.

ACKNOWLEDGMENTS

I would like to express my sincere gratitude to my advisor Professor Terry Kammash for his guidance throughout my graduate career, for his invaluable advice during my dissertation research, and for making plasma physics such a pleasure to learn. I would also like to thank my on-site advisor Thomas A. Oliphant of the Los Alamos National Laboratory for his insightful suggestions and advice during even the most trying times in the preparation of this thesis. I am indebted to T.R. Hill and E.W. Larsen of the Theoretical Division for many helpful discussions on the fine points of the discrete ordinates transport technique and to F. Evans of the Applied Theoretical Physics Division for providing me with the large angle Coulomb-nuclear scattering cross sections. I am also grateful to R.W. Selden, J.C. Porter, P.C. White and J.H. Brownell for making it possible for me to conduct my thesis research within the Applied Theoretical Physics Division of the Los Alamos National Laboratory.

REFERENCES

1. T.A. Oliphant and C.W. Nielson, Phys. Fluids 11,8 (1970), 2103.

2. R.W. Hockney, "Computer Simulation of Anomalous Plasma Diffusion and Numerical Solution of Poisson's Equation," Stanford University Technical Report SUIPR-53, (May,1966).

3. D.C. Montgomery and D.A. Tidman, "Plasma Kinetic Theory", McGraw-Hill, New York, 1964.

4. L. Spitzer, Jr., "Physics of Fully Ionized Gases", Interscience, New York, 1962.

5. W.E. Meyerhof, "Elements of Nuclear Physics", McGraw-Hill, New York, 1967.

6. F. Evans, Phys. Fluids 16, 7(1973), 1011.

APPENDIX A

THE LANDAU-FOKKER-PLANCK TERM IN SPHERICAL VELOCITY SPACE

In Chapter II the Landau-Fokker-Planck collision term is given by Eqs. (2-30) and (2-31) as

$$\left(\frac{\partial f_a}{\partial t}\right)_c = -\nabla_{\underline{v}} \cdot \underline{J} \tag{A-1}$$

where

$$J^i = \sum_b \Gamma_{ab} \frac{N_o \tau_o}{C_o^3} Z_b^2 \left\{ \frac{A_a}{A_b} f_a a^{i\alpha} L_{b,\alpha} - \frac{1}{2} a^{i\alpha} a_{aj\beta} \times \right.$$

$$\left. \left[f_{a,j} K_{b,\beta\alpha} + f_a R^{\gamma}_{.\beta\alpha j} K_{b,\gamma} \right] \right\} \quad . \tag{A-2}$$

Eq. (A-2) can be used to calculate the velocity space components of the collision term in any geometry once the metric tensor a_{ij} which defines the space of interest is specified. The square of the linear element in a given space defines the metric tensor as

$$ds^2 = a_{ij} dx^i dx^j \quad . \tag{A-3}$$

From Fig. 40 the lengths of the sides of the volume element $d\underline{v}$ in a spherical velocity space are easily seen to be dv, $vd\mu/(1-\mu^2)^{1/2}$. and $v(1-\mu^2)^{1/2}d\omega$ so that the metric tensor takes the form

$$\begin{pmatrix} 1 & 0 & 0 \\ 0 & v^2(1-\mu^2)^{-1} & 0 \\ 0 & 0 & v^2(1-\mu^2) \end{pmatrix} \qquad \text{(A-4)}$$

The only non-trivial relations needed to calculate the J^i are the expressions for the second covarient derivatives of $K_b(\underline{v})$ and for the Riemann-Christoffel tensor $R^{\gamma}_{.\beta\alpha j}$. These are given by

$$K_{b,ji} = K_{b,ij} = \partial^2_{ij}K_b - \frac{a^{mn}}{2}(\partial_j a_{in} + \partial_i a_{jn} - \partial_n a_{ij})K_{b,m} \qquad \text{(A-5)}$$

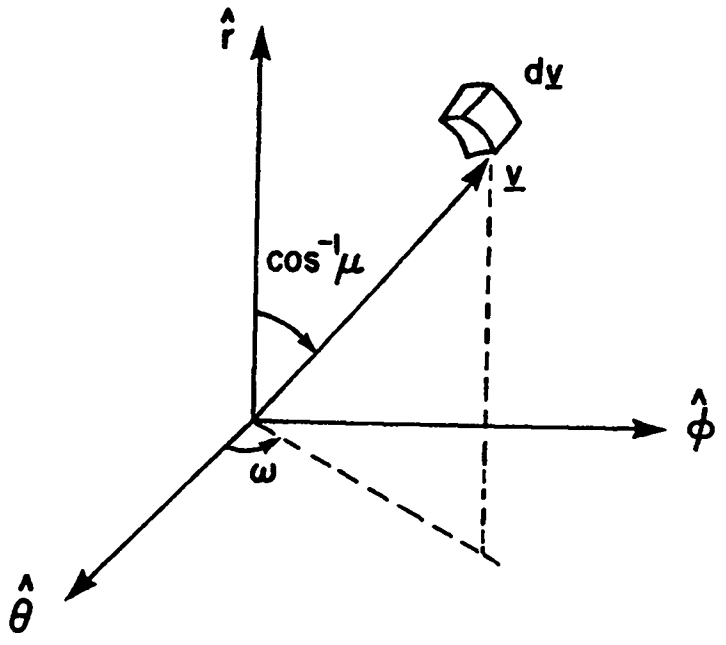

Fig. 40.--The volume element for a spherical velocity space

and

$$R^{l}_{.jnp} = \partial_n \frac{a^{lm}}{2}(\partial_p a_{jm} + \partial_j a_{pm} - \partial_m a_{jp})$$

$$- \partial_p \frac{a^{lm}}{2}(\partial_n a_{jm} + \partial_j a_{nm} - \partial_m a_{jn})$$

$$+ \frac{a^{lm}}{2}(\partial_s a_{nm} + \partial_n a_{sm} - \partial_m a_{ns})\frac{a^{so}}{2}(\partial_p a_{jo} + \partial_j a_{po} - \partial_o a_{jp}) \quad \text{(A-6)}$$

$$- \frac{a^{lm}}{2}(\partial_s a_{pm} + \partial_p a_{sm} - \partial_m a_{ps})\frac{a^{so}}{2}(\partial_n a_{jo} + \partial_j a_{no} - \partial_o a_{jn}) \quad .$$

Here ∂_j means the partial derivative with respect to the j^{th} component. Although Eq. (A-6) appears to be cumbersome, it is easily evaluated for this geometry (or any geometry with a diagonal metric tensor) since $a_{ij} \rightarrow \delta_{ij} a_{ij}$. A useful property of the RC tensor is that $R^{l}_{.lnp} = 0$. With these relations, the elements of Eq. (A-2) can be calculated to yield

$$K_{,11} = \frac{\partial^2 K}{\partial v^2}, \qquad K_{,12} = \frac{\partial^2 K}{\partial v \partial \mu} - \frac{1}{v}\frac{\partial K}{\partial \mu},$$

$$K_{,13} = \frac{\partial^2 K}{\partial v \partial \omega} - \frac{1}{v}\frac{\partial K}{\partial \omega}, \quad K_{,22} = \frac{\partial^2 K}{\partial \mu^2} + \frac{v}{(1-\mu^2)}\frac{\partial K}{\partial v} - \frac{\mu}{(1-\mu^2)}\frac{\partial K}{\partial \mu} \quad \text{(A-7)}$$

$$K_{,23} = \frac{\partial^2 K}{\partial \mu \partial \omega} + \frac{\mu}{(1-\mu^2)}\frac{\partial K}{\partial \omega}, \quad K_{,33} = \frac{\partial^2 K}{\partial \omega^2} + v(1-\mu^2)\frac{\partial K}{\partial v} - \mu(1-\mu^2)\frac{\partial K}{\partial \mu} \quad .$$

For this geometry the elements of the RC tensor are easily shown to all be identically zero. Hence, using Eqs. (A-2) and (A-7), the first component of $\underline{J}$ can be written down as

$$J^{v} = \sum_{b}\Gamma_{ab}\frac{N_o\tau_o Z_b^2}{C_o^3}\{\frac{A_a}{A_b}f_a a^{11}L_{b,1}$$

$$- \frac{a^{11}}{2}[a^{j\beta}f_{a,j}K_{b,\beta 1}]\} \qquad \text{(A-8)}$$

and by performing the indicated sums over the repeated indices

$$J^{v} = \sum_{b}\Gamma_{ab}\frac{N_o\tau_o Z_b^2}{C_o^3}\{\frac{A_a}{A_b}f_a\frac{\partial L_b}{\partial v} - \frac{1}{2}[\frac{\partial f_a}{\partial v}\frac{\partial^2 K_b}{\partial v^2}$$

$$+ \frac{(1-\mu^2)}{v^2}\frac{\partial f_a}{\partial \mu}(\frac{\partial^2 K_b}{\partial v\partial \mu} - \frac{1}{v}\frac{\partial K_b}{\partial \mu}) + \frac{1}{v^2(1-\mu^2)}\frac{\partial f_a}{\partial \omega}(\frac{\partial^2 K_b}{\partial v\partial \omega} - \frac{1}{v}\frac{\partial K_b}{\partial \omega})]\}. \qquad \text{(A-9)}$$

Similarly, the μ and ω components can be calculated to be

$$J^{\mu} = \sum_{b}\Gamma_{ab}\frac{N_o\tau_o Z_b^2}{C_o^3}\{\frac{A_a}{A_b}f_a\frac{(1-\mu^2)}{v^2}\frac{\partial L_b}{\partial \mu} - \frac{(1-\mu^2)}{2v^2}[$$

$$\frac{\partial f_a}{\partial v}(\frac{\partial^2 K_b}{\partial v\partial \mu} - \frac{1}{v}\frac{\partial K_b}{\partial \mu}) + \frac{(1-\mu^2)}{v^2}\frac{\partial f_a}{\partial \mu}(\frac{\partial^2 K_b}{\partial \mu^2} + \frac{v}{(1-\mu^2)}\frac{\partial K_b}{\partial v} - \frac{\mu}{(1-\mu^2)}\frac{\partial K_b}{\partial \mu})$$

$$+ \frac{1}{v^2(1-\mu^2)}\frac{\partial f_a}{\partial \omega}(\frac{\partial^2 K_b}{\partial \mu\partial \omega} + \frac{\mu}{(1-\mu^2)}\frac{\partial K_b}{\partial \omega})]\} \qquad \text{(A-10)}$$

$$J^{\omega} = \sum_{b}\Gamma_{ab}\frac{N_o\tau_o Z_b^2}{C_o^3}\{\frac{A_a}{A_b}f_a\frac{1}{v^2(1-\mu^2)}\frac{\partial L_b}{\partial \omega} - \frac{1}{2v^2(1-\mu^2)}[$$

$$\frac{\partial f_a}{\partial v}\left(\frac{\partial^2 K_b}{\partial v \partial \omega} - \frac{1}{v}\frac{\partial K_b}{\partial \omega}\right) + \frac{(1-\mu^2)}{v^2}\frac{\partial f_a}{\partial \mu}\left(\frac{\partial^2 K_b}{\partial \mu \partial \omega} + \frac{\mu}{(1-\mu^2)}\frac{\partial K_b}{\partial \omega}\right)$$

$$+ \frac{1}{v^2(1-\mu^2)}\frac{\partial f_a}{\partial \omega}\left(\frac{\partial^2 K_b}{\partial \omega^2} + v(1-\mu^2)\frac{\partial K_b}{\partial v} - \mu(1-\mu^2)\frac{\partial K_b}{\partial \mu}\right)\Big]\Big\} \ . \qquad \text{(A-11)}$$

When the Rosenbluth potentials $K_b(\underline{v})$ and $L_b(\underline{v})$ are isotropic i.e., when the background distributions f_b are isotropic, the components simplify to

$$J^v = \sum_b \Gamma_{ab} \frac{N_o \tau_o}{C_o^3} Z_b^2 \left\{\frac{A_a}{A_b} f_a \frac{\partial L_b}{\partial v} - \frac{1}{2}\left[\frac{\partial f_a}{\partial v}\frac{\partial^2 K_b}{\partial v^2}\right]\right\} \qquad \text{(A-12)}$$

$$J^\mu = \sum_b \Gamma_{ab} \frac{N_o \tau_o}{C_o^3} Z_b^2 \left\{-\frac{(1-\mu^2)}{2v^2}\left[\frac{1}{v}\frac{\partial f_a}{\partial \mu}\frac{\partial K_b}{\partial v}\right]\right\} \qquad \text{(A-13)}$$

$$J^\omega = \sum_b \Gamma_{ab} \frac{N_o \tau_o}{C_o^3} Z_b^2 \left\{-\frac{1}{2v^2(1-\mu^2)}\left[\frac{1}{v}\frac{\partial f_a}{\partial \omega}\frac{\partial K_b}{\partial v}\right]\right\} \ . \qquad \text{(A-14)}$$

APPENDIX B

THE TRANSPORT EQUATION IN SPHERICAL AND CYLINDRICAL GEOMETRIES

In order to use Eq. (2-30) in curved geometries, the appropriate forms of $\underline{v}\cdot\nabla f$ must be used. Although these forms are available in a variety of texts, their derivation is often omitted. In this appendix a somewhat non-conventional derivation of the form of $v\cdot\nabla f$ is given for both spherical and cylindrical coordinates.

Since in an Eulerian desciption of a system the observer is not confined to move with a particle but rather chooses his own vantage point, $\underline{v}\cdot\nabla f = \nabla\cdot vf$ i.e., $\underline{v}$ is not related to $\underline{r}$ as $\dot{\underline{r}}$. One complicating aspect of curved geometries is that the coordinates of v with respect to its basis vectors in velocity space change as the particle streams in coordinate space thus giving the appearance that $\underline{v}$ is related to $\underline{r}$.

$\underline{v}\cdot\nabla f$ in Spherical Coordinates

In Fig. 41 the orthonormal basis vectors $\hat{x},\hat{y},\hat{z}$ in configuration space and the $\theta,\hat{\phi},\hat{r}$ basis vectors in velocity space are shown for a spherical coordinate system in both configuration and velocity space. Here ω is the angle between the $\hat{r}\theta$ and $\Omega\hat{r}$ planes while $\cos^{-1}\mu$ defines the angle between the $\hat{r}$ and Ω vectors. It is easily seen that as a particle streams in the direction Ω, the $\theta,\hat{\phi},\hat{r}$ triple will continuously change its attitude with respect to Ω if the vector r follows the path of that particle. Hence, both μ and ω will change as θ and ϕ change. In order to account for this in the gradient term, the partial derivatives are written as

$$\underline{v}\cdot\nabla f = v\Omega\cdot\{\hat{r}\frac{\partial}{\partial r} + \theta[\frac{\partial}{\partial\theta} + \frac{\partial\mu}{\partial\theta}\frac{\partial}{\partial\mu} + \frac{\partial\omega}{\partial\theta}\frac{\partial}{\partial\omega}]$$

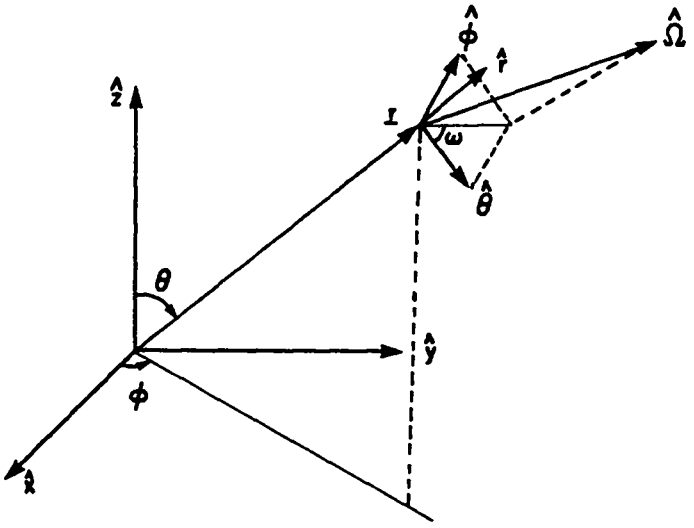

Fig. 41.--The spherical coordinate systems for a particle described by the vectors r in configuration space and $\underline{v}$ in velocity space

$$+ \hat{\phi}\left[\frac{\partial}{\partial\phi} + \frac{\partial\mu}{\partial\phi}\frac{\partial}{\partial\mu} + \frac{\partial\omega}{\partial\phi}\frac{\partial}{\partial\omega}\right]\Big\}f \quad . \tag{B-1}$$

The problem of obtaining $\underline{v}\cdot\nabla f$, then, is in obtaining the quantities $\frac{\partial\mu}{\partial\theta}$, $\frac{\partial\omega}{\partial\theta}$, $\frac{\partial\mu}{\partial\phi}$, and $\frac{\partial\omega}{\partial\phi}$. In order to obtain these the following analysis can be performed.

The unit vector Ω in Fig. 41 can be decomposed in terms of its components along the $\theta, \hat{\phi}, \hat{r}$ basis vectors by defining the projections along these as

$$\eta = \theta\cdot\Omega = (1-\mu^2)^{1/2}\cos\omega \tag{B-2}$$

$$\xi = \hat{\phi}\cdot\Omega = (1-\mu^2)^{1/2}\sin\omega \tag{B-3}$$

$$\mu = \hat{r} \cdot \Omega \quad . \tag{B-4}$$

Note from the same figure that the components of the $\theta, \hat{\phi}, \hat{r}$ vectors along the $\hat{x}, \hat{y}, \hat{z}$ vectors are given by

$$\theta = \cos\theta \cos\phi \hat{x} + \cos\theta \sin\phi \hat{y} - \sin\theta \hat{z} \tag{B-5}$$

$$\hat{\phi} = -\sin\phi \hat{x} + \cos\phi \hat{y} + 0\hat{z} \tag{B-6}$$

$$\hat{r} = \sin\theta \cos\phi \hat{x} + \sin\theta \sin\phi \hat{y} + \cos\theta \hat{z} \quad . \tag{B-7}$$

Further, if the direction cosines of Ω along the $\hat{x}, \hat{y}, \hat{z}$ were known to be ε_1, ε_2, and ε_3, the projections of η, ξ, and μ along these axes would then be

$$\eta = \varepsilon_1 \cos\theta \cos\phi + \varepsilon_2 \sin\phi \cos\theta - \varepsilon_3 \sin\theta \tag{B-8}$$

$$\xi = -\varepsilon_1 \sin\phi + \varepsilon_2 \cos\phi \tag{B-9}$$

$$\mu = \varepsilon_1 \sin\theta \cos\phi + \varepsilon_2 \sin\theta \sin\phi + \varepsilon_3 \cos\theta \tag{B-10}$$

Taking differentials of these last three expressions leads to the relations

$$d\eta = \xi \cos\theta \, d\phi - \mu d\theta \tag{B-11}$$

$$d\xi = -(\varepsilon_1 \cos\phi + \varepsilon_2 \sin\phi) d\phi \tag{B-12}$$

$$d\mu = \eta d\theta + \xi \sin\theta \, d\phi \tag{B-13}$$

and by using the definitions of η and ξ given in Eqs. (B-2) and (B-3), it is found that

$$\frac{d\mu}{d\theta} = \eta = (1-\mu^2)^{1/2}\cos\omega \tag{B-14}$$

$$\frac{d\mu}{d\phi} = \xi\sin\theta = (1-\mu^2)^{1/2}\sin\omega\,\sin\theta \tag{B-15}$$

$$\frac{d\omega}{d\theta} = \frac{\mu\sin\omega}{(1-\mu^2)^{1/2}} \tag{B-16}$$

$$\frac{d\omega}{d\phi} = -\left[\cos\theta + \frac{\mu\cos\omega\,\sin\theta}{(1-\mu^2)^{1/2}}\right] . \tag{B-17}$$

One further item to be noted is that whenever an operator in a given space S acts on quantities defined in another space T, the physical components of those T quantities in the space S must be determined. In this case, the operation is the dot product of Ω and ∇. The physical components of Ω are given by

$$\Omega^r = \mu \tag{B-18}$$

$$\Omega^\theta = (1-\mu^2)^{1/2}\cos\omega/r \tag{B-19}$$

$$\Omega^\phi = (1-\mu^2)^{1/2}\sin\omega/r\sin\theta \tag{B-20}$$

where the definition of the physical components of the velocity vector Ω in configuration space has been used. This definition has the form

$$\Omega^i_{\underline{r}\text{-space}} = \frac{\Omega^i_{\underline{v}\text{-space}}}{(a_{ii})^{1/2}} \tag{B-21}$$

where a_{ii} is the well known metric tensor of a spherical configuration space and is given by

$$\underline{\underline{a}} = \begin{pmatrix} 1 & 0 & 0 \\ 0 & r^2 & 0 \\ 0 & 0 & r^2\sin^2\theta \end{pmatrix} . \qquad \text{(B-22)}$$

Using Eqs. (B-14)-(B-17) and (B-15)-(B-20) in Eq. (B-1), $\Omega\cdot\nabla f$ can be shown to be

$$\Omega\cdot\nabla f = \mu\frac{\partial f}{\partial r} + (1-\mu^2)^{1/2}\frac{\cos\omega}{r}\frac{\partial f}{\partial\theta} + (1-\mu^2)^{1/2}\frac{\cos^2\omega}{r}\frac{\partial f}{\partial\mu}$$

$$+ \mu\frac{\cos\omega}{r}\sin\omega\frac{\partial f}{\partial\omega} + (1-\mu^2)^{1/2}\frac{\sin\omega}{r\sin\theta}\frac{\partial f}{\partial\phi} + (1-\mu^2)^{1/2}\frac{\sin^2\omega}{r}\frac{\partial f}{\partial\mu}$$

$$- \cot\theta(1-\mu^2)^{1/2}\frac{\sin\omega}{r}\frac{\partial f}{\partial\omega} - \mu\sin\omega\frac{\cos\omega}{r}\frac{\partial f}{\partial\omega} . \qquad \text{(B-23)}$$

By further using the relations

$$\frac{1}{r}\frac{\partial(1-\mu^2)f}{\partial\mu} = \frac{(1-\mu^2)}{r}\frac{\partial f}{\partial\mu} - \frac{2\mu f}{r} \qquad \text{(B-24)}$$

$$\frac{(1-\mu^2)^{1/2}\cos\omega}{r\sin\theta}\frac{\partial(f\sin\theta)}{\partial\theta} = \frac{(1-\mu^2)^{1/2}\cos\omega}{r}\frac{\partial f}{\partial\theta}$$

$$+ \frac{(1-\mu^2)^{1/2}\cos\omega}{r}f\cot\theta \qquad \text{(B-25)}$$

and

$$\frac{\cot\theta}{r}\frac{\partial[f(1-\mu^2)^{1/2}\sin\theta]}{\partial\theta} = \frac{\cot\theta(1-\mu^2)^{1/2}\sin\omega}{r}\frac{\partial f}{\partial\omega}$$

$$+ \frac{\cot\theta(1-\mu^2)^{1/2}}{r}\frac{}{}f\cos\omega, \qquad \text{(B-26)}$$

$\underline{v}\cdot\nabla f$ can be computed in its conservative form as

$$\underline{v}\cdot\nabla f = \frac{v\mu\alpha\partial r^2 f}{r^2\partial r} + \frac{v(1-\mu^2)^{1/2}\sin\omega\partial f}{r\sin\theta\partial\phi} + \frac{v(1-\mu^2)^{1/2}\cos\omega\partial(f\sin\theta)}{r\sin\theta\partial\theta}$$

$$+ \frac{1\partial[(1-\mu^2)f]}{r\partial\mu} - \frac{\cot\theta\partial[f(1-\mu^2)^{1/2}\sin\omega]}{r\partial\omega} . \qquad \text{(B-27)}$$

$v\cdot\nabla f$ in Cylindrical Coordinates

The orthonormal triple $\hat{x},\hat{y},\hat{z}$ and $\hat{r},\hat{\phi},\hat{z}$ for cylindrical geometry with a spherical velocity space are shown in Fig. 42 for a particle located at $\underline{r}$ having unit velocity Ω. Here χ is the angle between the $\hat{r}\hat{z}$ and $\Omega\hat{z}$ planes and $\cos^{-1}\mu$ is the angle between the $\hat{z}$ and Ω vectors. It can be seen that as a particle streams in configuration space, the angle χ will change as the angle ϕ changes. Hence,

$$v\cdot\nabla f = v\Omega\cdot\{\hat{r}\frac{\partial}{\partial r} + \hat{\phi}[\frac{\partial}{\partial\phi} + \frac{\partial\chi}{\partial\phi}\frac{\partial}{\partial\chi}] + \hat{z}\frac{\partial}{\partial z}\}f \quad . \qquad \text{(B-28)}$$

In this case, $\frac{\partial\chi}{\partial\phi}$ must be calculated. Following a procedure similar to the one used in the last section, the projections of Ω on the $\hat{r},\hat{\phi},\hat{z}$ vectors are written as

$$\xi = \Omega\cdot\hat{r} = (1-\mu^2)^{1/2}\cos\chi \qquad \text{(B-29)}$$

$$\eta = \Omega\cdot\hat{\phi} = (1-\mu^2)^{1/2}\sin\chi \qquad \text{(B-30)}$$

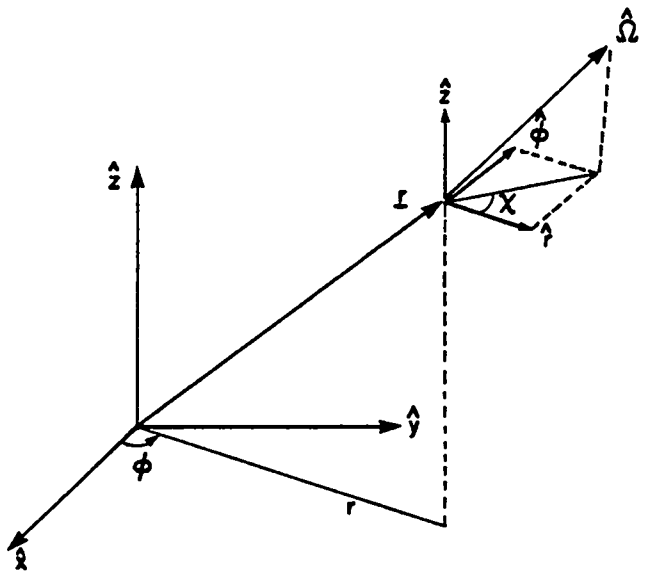

Fig. 42.--A cylindrical coordinate system in configuration space wi4h a spherical system in velocity space

$$\mu = \Omega \cdot \hat{z} \quad . \tag{B-31}$$

From Fig. 42 it is also seen that the components of the $\hat{r}, \hat{\phi}, \hat{z}$ vectors on the $\hat{x}, \hat{y}, \hat{z}$ vectors are

$$\hat{r} = \cos\phi\ \hat{x} + \sin\phi\ \hat{y} + 0\ \hat{z} \tag{B-32}$$

$$\hat{\phi} = -\sin\phi\ \hat{x} + \cos\phi\ \hat{y} + 0\ \hat{z} \tag{B-33}$$

where $\hat{z}$ remains the sme in both systems. If α and β are the direction cosines of Ω on the $\hat{x}$ and $\hat{y}$ vectors then the projections of ξ and η along these axes would be

$$\xi = \alpha\cos\phi + \beta\sin\phi \tag{B-34}$$

$$\eta = -\alpha\sin\phi + \beta\cos\phi \quad . \tag{B-35}$$

Taking differentials in Eqs. (B-34) and (B-35) yields

$$d\xi = \eta d\phi \tag{B-36}$$

$$d\eta = -\xi d\phi \quad . \tag{B-37}$$

By using the definitions of η and ξ in Eqs. (B-36) and (B-37), after some algebra, it can be shown that

$$\frac{\partial\phi}{\partial\chi} = -1 \quad . \tag{B-38}$$

The physical components of Ω in r space are

$$\Omega^r = (1-\mu^2)^{1/2}\cos\chi \tag{B-39}$$

$$\Omega^\phi = (1-\mu^2)^{1/2}\sin\chi/r \tag{B-40}$$

$$\Omega^z = \mu \tag{B-41}$$

so that from Eq. (B-26)

$$\Omega\cdot\nabla f = (1-\mu^2)^{1/2}\cos\chi\frac{\partial f}{\partial r} + \frac{(1-\mu^2)^{1/2}\sin\chi\partial f}{r\quad\partial\phi}$$

$$- (1-\mu^2)^{1/2}\frac{\sin\chi\partial f}{r\ \partial\chi} + \mu\frac{\partial f}{\partial z} \tag{B-42}$$

and with the relations

$$\frac{1}{r}\frac{\partial[f(1-\mu^2)^{1/2}\sin\chi]}{\partial\chi} = \frac{(1-\mu^2)^{1/2}\sin\chi}{r}\frac{\partial f}{\partial\chi} + \frac{f(1-\mu^2)^{1/2}\cos\chi}{r} \qquad \text{(B-43)}$$

$$\frac{(1-\mu^2)^{1/2}\cos\chi}{r}\frac{\partial(rf)}{\partial r} = \frac{(1-\mu^2)^{1/2}\cos\chi}{r}f + (1-\mu^2)^{1/2}\cos\chi\frac{\partial f}{\partial r} \qquad \text{(B-44)}$$

$\underline{v}\cdot\nabla f$ can be written in its conservative form as

$$\underline{v}\cdot\nabla f = \frac{v(1-\mu^2)^{1/2}\cos\chi}{r}\frac{\partial(rf)}{\partial r} - \frac{v}{r}\frac{\partial[f(1-\mu^2)^{1/2}\sin\chi]}{\partial\chi}$$

$$+ \frac{(1-\mu^2)^{1/2}\sin\chi}{r}\frac{\partial f}{\partial\phi} + \mu\frac{\partial f}{\partial z} \quad . \qquad \text{(B-45)}$$

APPENDIX C

CALCULATION OF ENERGY DEPOSITION

The time history of the amount of energy deposited by the fast ions to each component of the background plasma can be obtained by taking the v^2 moment of the Fokker-Planck term of Eq. (3-1). Note that the terms in the sum on the background species 'b' will yield the deposition rate for each of the species individually.

Consider the definition of the v^2 moment of f_a given as

$$\langle v^2 \rangle = \frac{4\pi}{n_a} \int_0^\infty f_a v^4 dv \tag{C-1}$$

where

$$n_a = 4\pi \int_0^\infty f_a v^2 dv \ . \tag{C-2}$$

If f_a is a Maxwellian distribution given in scaled variables as

$$f_a = \frac{n_a}{\pi^{3/2} v_{oa}^3} \exp(-v^2/v_{oa}^2) \tag{C-3}$$

where $v_{oa} \equiv (T_a/A_a)^{1/2}$, then Eq. (C-1) can be calculated as

$$\langle v^2 \rangle = \frac{3}{2} v_{oa}^2 = \frac{3}{2} (T_a/A_a)^{1/2} \tag{C-4}$$

so that

$$T_a = \frac{2}{3}A_a\langle v^2\rangle \quad . \tag{C-5}$$

Since the average kinetic energy of the particles in this distribution is defined as $E_a = 3T_a/2$ (in scaled variables),

$$E_a = A_a\langle v^2\rangle \quad . \tag{C-6}$$

With this result, the time rate of energy deposited to the background plasma can be written as

$$\frac{\partial E_a(r,t)}{\partial t} = -A_a\int v^2\left(\frac{\partial f}{\partial t}\right)_c d\underline{v} \tag{C-7}$$

where the minus sign indicates that the energy lost by species 'a' is gained by the background plasma. From Eqs. (3-3) and (3-4), it can be seen that only the J^v component term of $\left(\frac{\partial f}{\partial t}\right)_c$ will contribute to the integral in Eq. (C-7) such that

$$\frac{\partial E_a(r,t)}{\partial t} = -A_a\int \frac{1}{v^2}\frac{\partial}{\partial v}v^2J^v\ v^4 dv d\mu d\chi \quad . \tag{C-8}$$

This expression can be solved numerically as

$$\frac{\partial E_a(r,t)}{\partial t} = -A_a\int v^4 dv d\mu d\chi\ \left[\frac{1}{\Delta v_g^3/3}\left(v^2_{g+1/2}J^v_{g+1/2} - v^2_{g-1/2}J^v_{g-1/2}\right)\right] \tag{C-9}$$

By using the expressions for $J^v_{g+1/2}$ and $J^v_{g-1/2}$ given in Eqs. (3-22) and (3-23), the above equation becomes

$$\frac{\partial E_a(r,t)}{\partial t} = 4\pi A_a \int_0^{2\pi} d\chi \int_{-1}^{1} d\mu \sum_g v_g^2 \, x$$

$$\{f_{g-1}\left[\frac{C_{g-1/2}}{\Delta v_{g-1/2}} - B_{g-1/2}\delta_{g-1/2}\right] + f_g\left[B_{g+1/2}\delta_{g+1/2} - \frac{C_{g-1/2}}{\Delta v_{g-1/2}}\right.$$

$$\left. - \frac{C_{g+1/2}}{\Delta v_{g+1/2}} - B_{g-1/2}(1-\delta_{g-1/2})\right] + f_{g+1}\left[B_{g+1/2}(1-\delta_{g+1/2})\right.$$

$$\left. + \frac{C_{g+1/2}}{\Delta v_{g+1/2}}\right]\} \qquad \text{(C-10)}$$

where the integral over speed has been approximated by $\int v^4 dv = \sum_g v_g^2 \Delta v_g^3/3$. In the computer codes SFTRAN and CYTRAN, the integrals over μ and χ are also done numerically.

☆U.S. GOVERNMENT PRINTING OFFICE: 1981-0-777-022/133

Printed in the United States of America
Available from
National Technical Information Service
US Department of Commerce
5285 Port Royal Road
Springfield, VA 22161

Microfiche $3.50 (A01)

Page Range	Domestic Price	NTIS Price Code	Page Range	Domestic Price	NTIS Price Code	Page Range	Domestic Price	NTIS Price Code	Page Range	Domestic Price	NTIS Price Code
001-025	$ 5.00	A02	151-175	$11.00	A08	301-325	$17.00	A14	451-475	$23.00	A20
026-050	6.00	A03	176-200	12.00	A09	326-350	18.00	A15	476-500	24.00	A21
051-075	7.00	A04	201-225	13.00	A10	351-375	19.00	A16	501-525	25.00	A22
076-100	8.00	A05	226-250	14.00	A11	376-400	20.00	A17	526-550	26.00	A23
101-125	9.00	A06	251-275	15.00	A12	401-425	21.00	A18	551-575	27.00	A24
126-150	10.00	A07	276-300	16.00	A13	426-450	22.00	A19	576-600	28.00	A25
									601-up	†	A99

†Add $1.00 for each additional 25-page increment or portion thereof from 601 pages up.